Dijet Production as a Probe of the Initial State of Hadronic Collisions with the ATLAS Detector

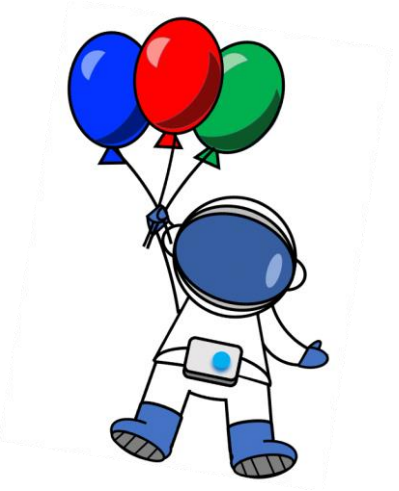

Ben Gilbert
On behalf of the ATLAS Collaboration

ATLAS-CONF-2022-021
ATLAS-HION-2023-05, arXiv:2309.00033

ATLAS EXPERIMENT

COLUMBIA UNIVERSITY
IN THE CITY OF NEW YORK

Introduction: Nuclear PDFs

- The kinematic coverage of world data constraining nuclear Parton Distribution Functions (nPDFs) has expanded massively with contributions from the LHC.

- Gaps still remain in the data determining nPDFs, leaving large stretches of phase space un-constrained.
  - We must currently rely on interpolation and miss the finer details of their evolution.

- The EIC will provide more coverage, but it is years away.
  - It still will not extend as high in Q^2 as measurements from the LHC.

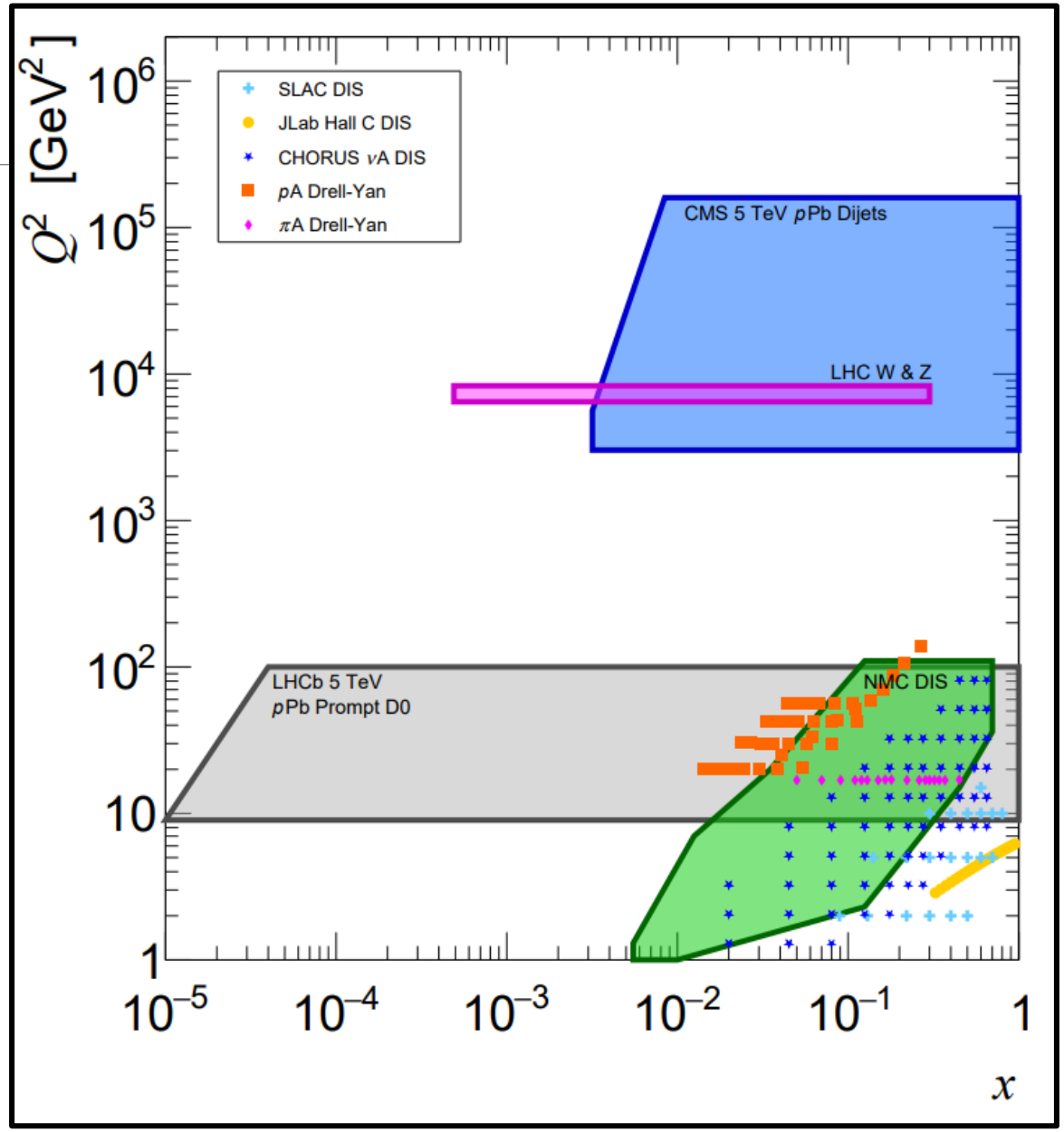

Figure inspired by arXiv:2112.12462

Introduction: Nuclear PDFs

- The kinematic coverage of world data constraining nuclear Parton Distribution Functions (nPDFs) has expanded massively with contributions from the LHC.

- Gaps still remain in the data determining nPDFs, leaving large stretches of phase space un-constrained.
  - We must currently rely on interpolation and miss the finer details of their evolution.

- The EIC will provide more coverage, but it is years away.
  - It still will not extend as high in Q^2 as measurements from the LHC.

- Two recent ATLAS measurements will help to constrain a large region of this phase-space:
  - 5.02 TeV UPC dijets
  - 8.16 TeV p+Pb dijets

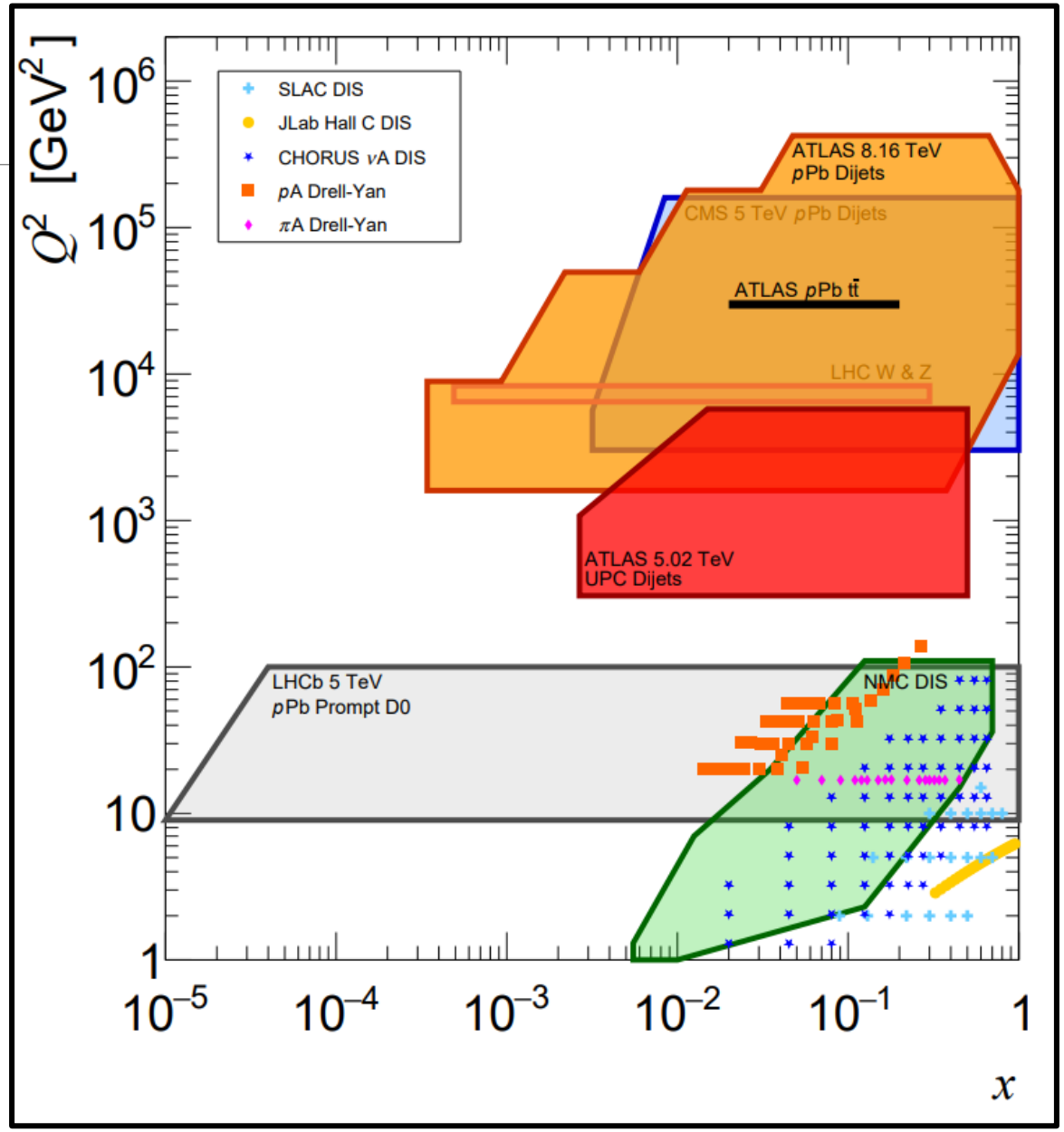

Figure inspired by [arXiv:2112.12462]

Introduction: Nuclear PDFs

- The kinematic coverage of world data constraining nuclear Parton Distribution Functions (nPDFs) has expanded massively with contributions from the LHC.

- Gaps still remain in the data determining nPDFs, leaving large stretches of phase space un-constrained.
  - We must currently rely on interpolation and miss the finer details of their evolution.

- The EIC will provide more coverage, but it is years away
  - It still will not extend as high in Q^2 from the LHC.

- Two recent ATLAS measurements will help to constrain a large region of this phase-space:
  - 5.02 TeV UPC dijets
  - 8.16 TeV p+Pb dijets

What about the initial state of the probe?

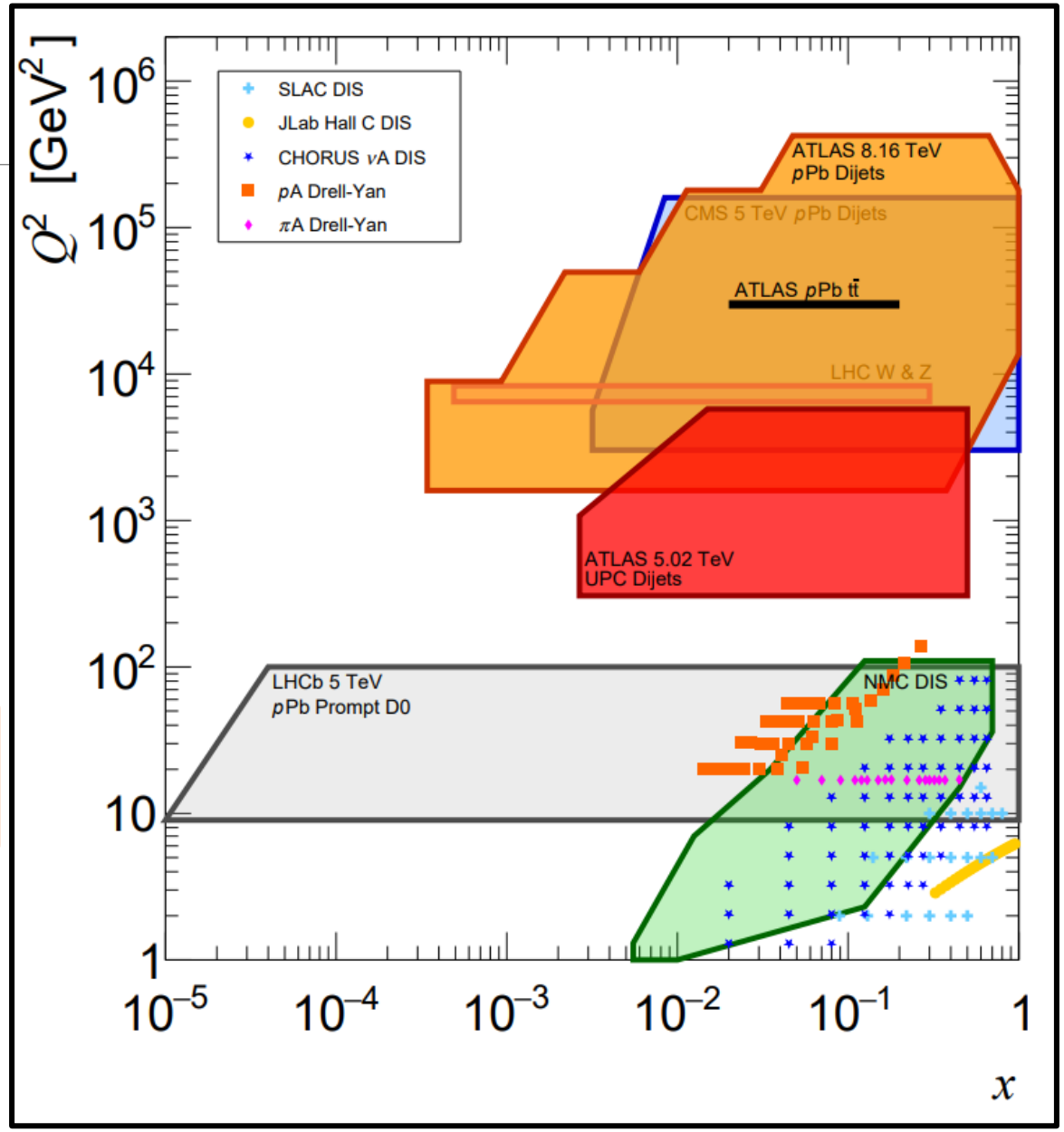

Figure inspired by arXiv:2112.12462

Introduction: Centrality-Dependence in p+Pb

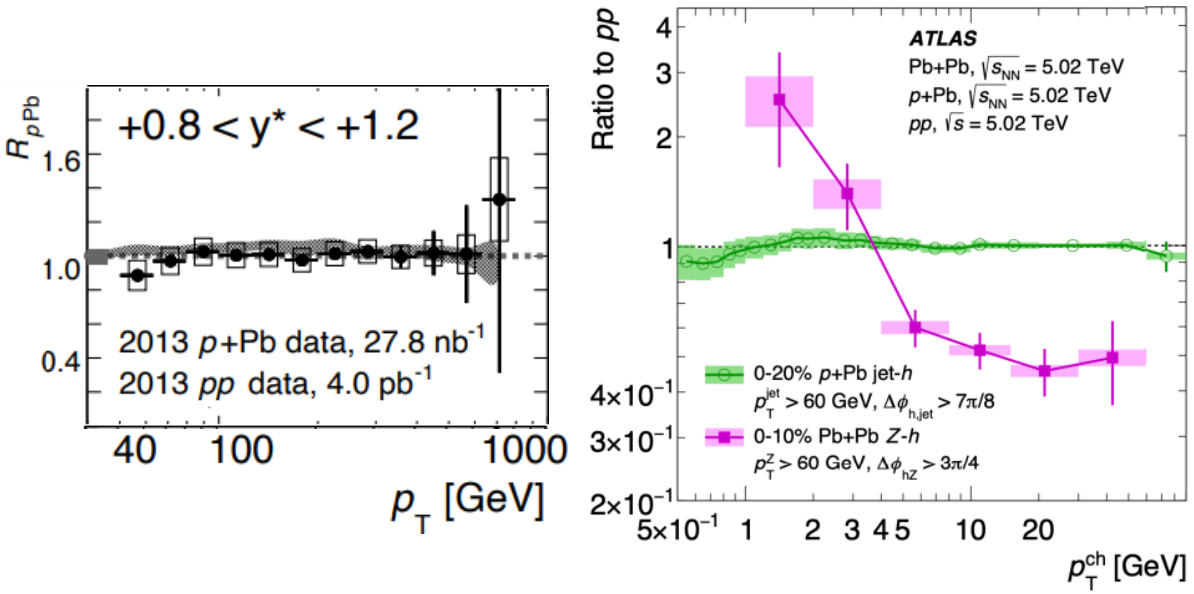

- Strong evidence supports the claim there is no jet quenching p+Pb collisions.
  - New constraints from ATLAS, arXiv:2206.01138
- Variation with centrality is an initial, not final state effect!

Introduction: Centrality-Dependence in p+Pb

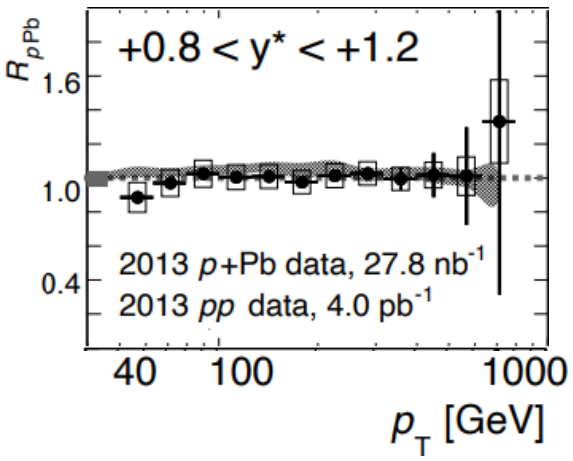

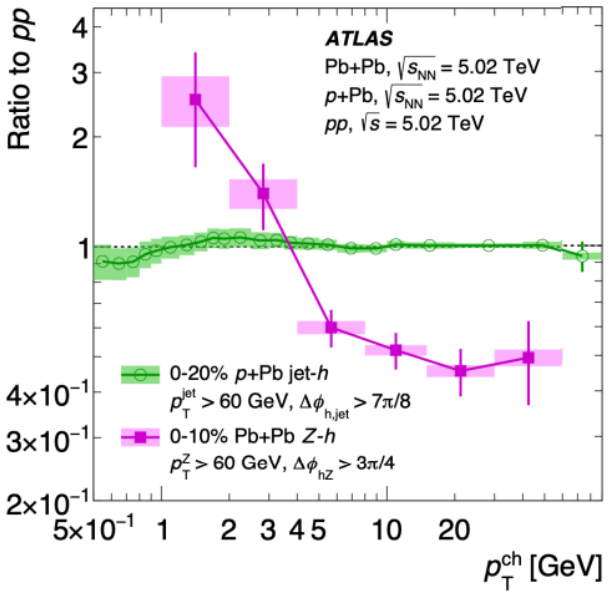

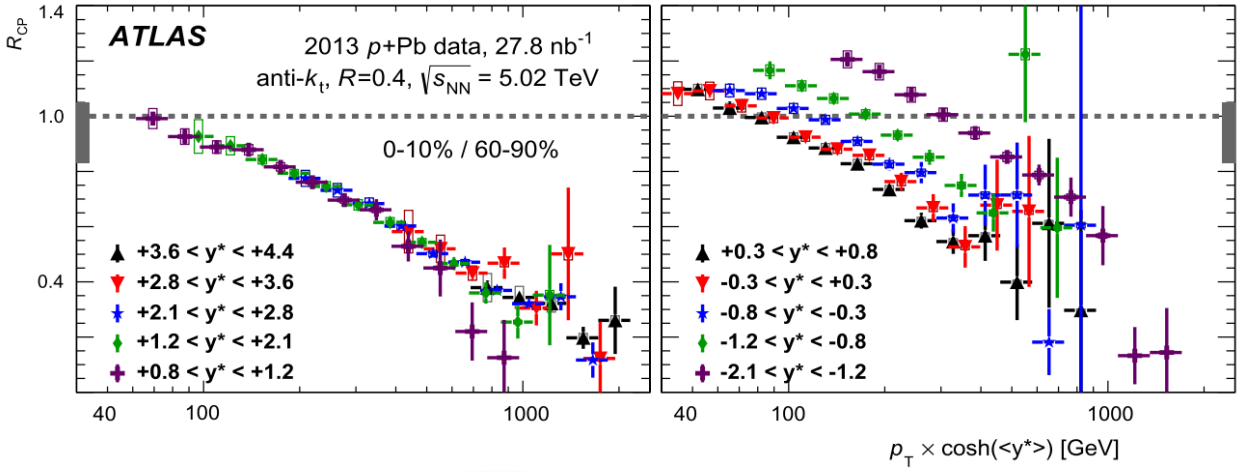

- Strong evidence supports the claim there is no jet quenching p+Pb collisions.
  - New constraints from ATLAS, arXiv:2206.01138
- Variation with centrality is an initial, not final state effect!

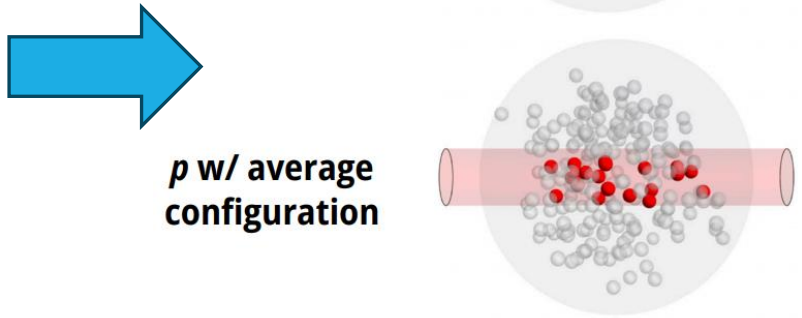

This effect has been quite successfully described through a framework of color fluctuations.

Proton probes containing a high-x parton have smaller than average size (color transparency).

Sketch from Alvioli et al., arXiv:1709.04993

Introduction: Centrality-Dependence in p+Pb

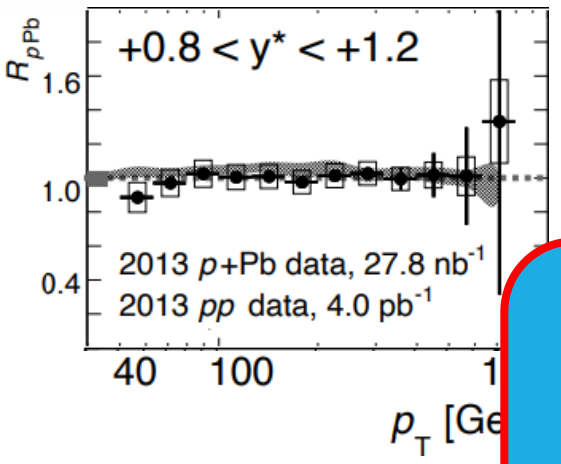

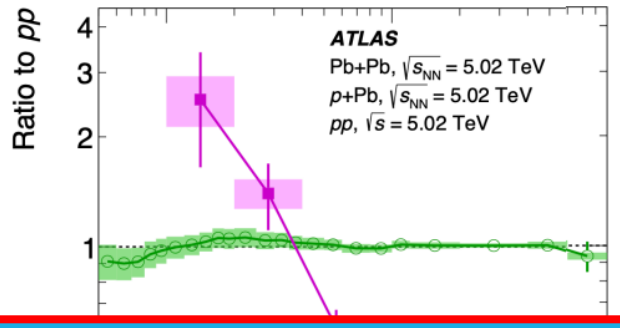

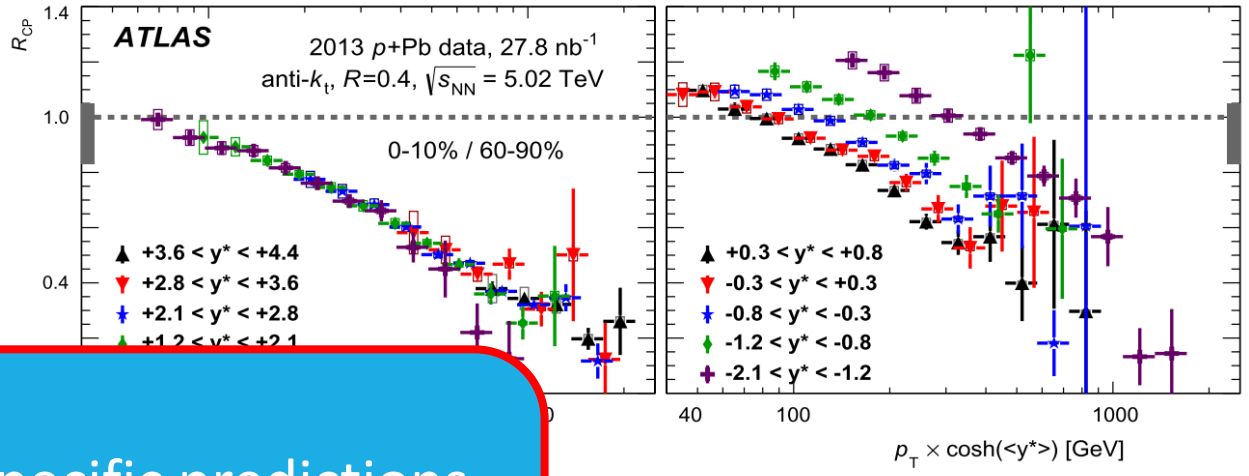

Color transparency makes specific predictions about dependence on x_p, not x_{Pb}. Dijets can probe this effect in unprecedented detail!

- Strong evidence supp
  quenching p+Pb collisions.
  - New constraints from ATLAS, arXiv:2206.01138
- Variation with centrality is an initial, not final state effect!

This effect has been quite successfully described through a framework of color fluctuations.

Proton probes containing a high-x parton have smaller than average size (color transparency).

Sketch from Alvioli et al., arXiv:1709.04993

Dijet Measurements in Two Collision Systems

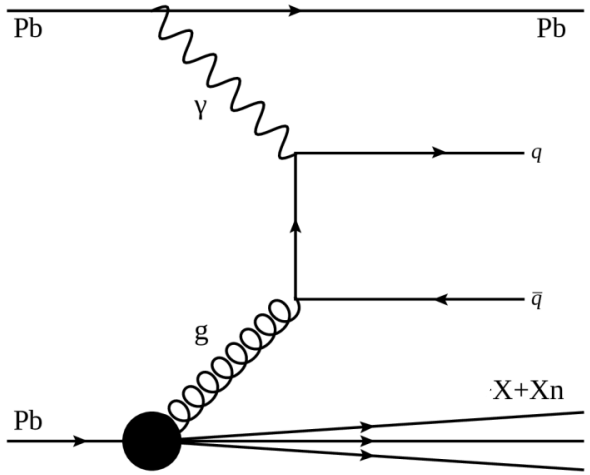

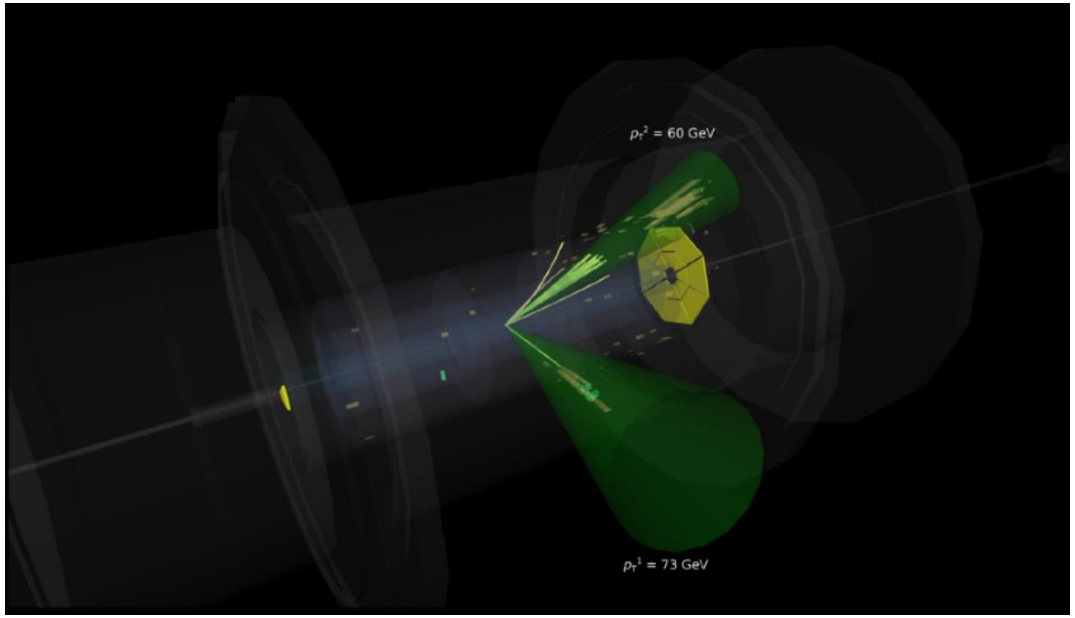

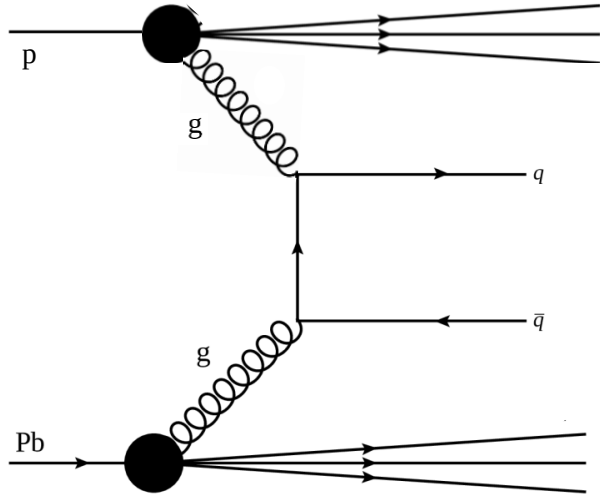

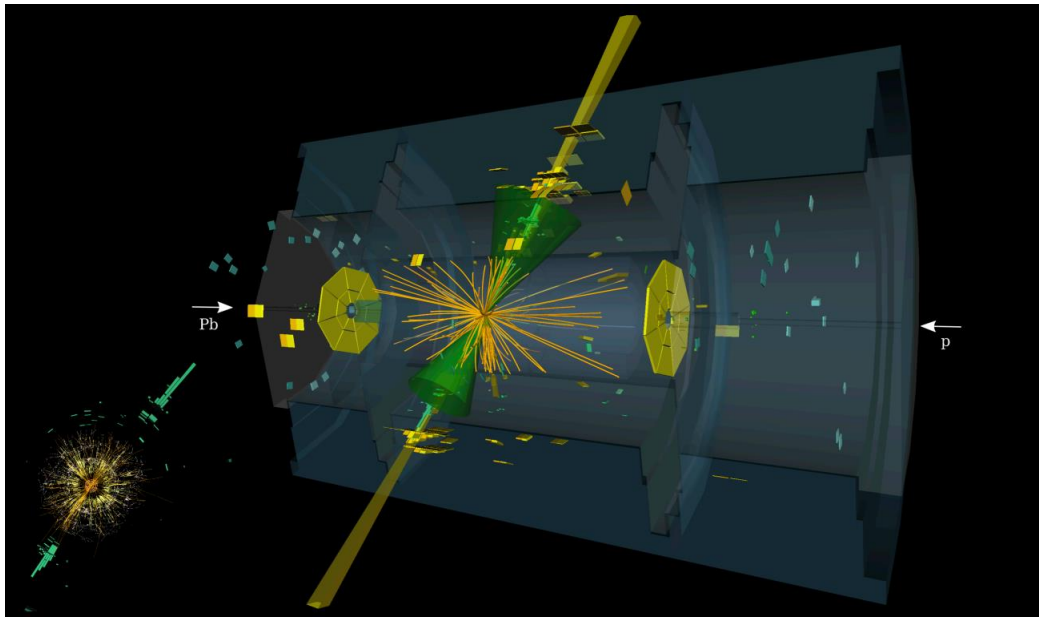

Dijet Measurements in Two Collision Systems

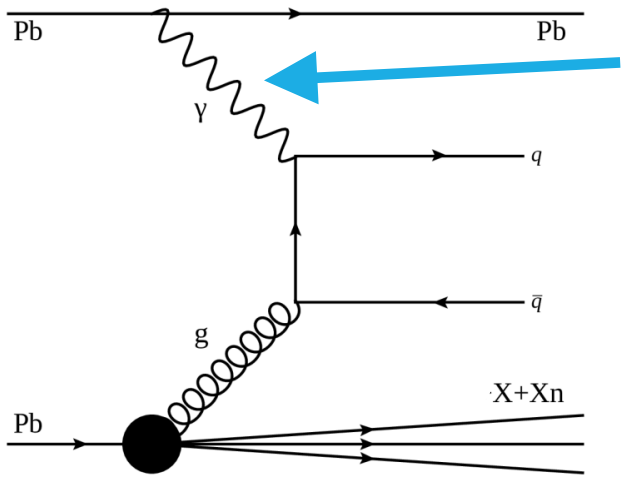

In ultra-relativistic heavy ion collisions, the intense electromagnetic fields provide a flux of quasi-real photons.

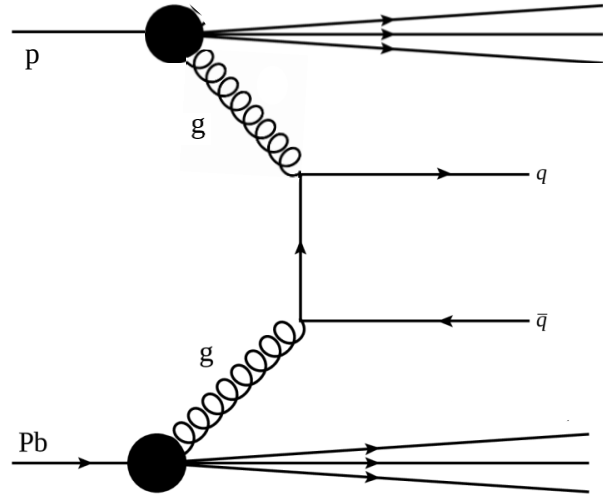

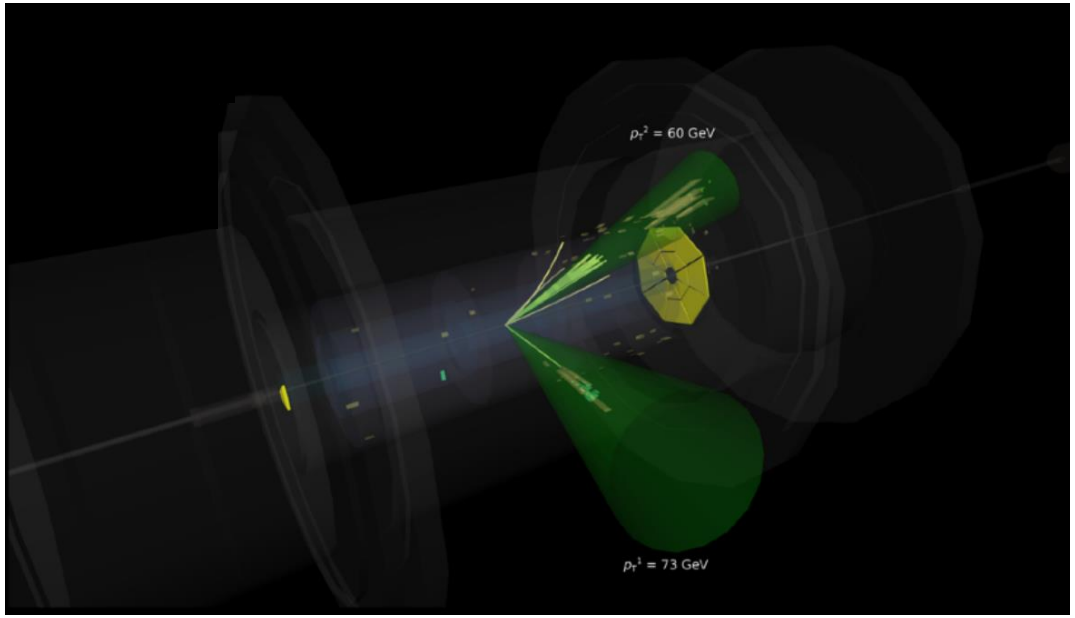

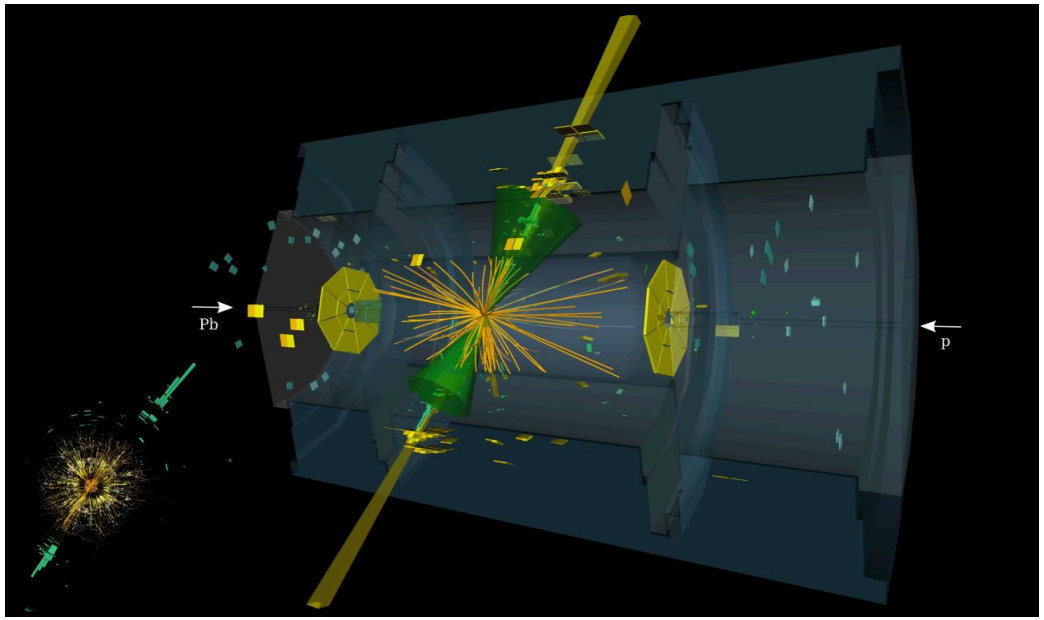

Dijet Measurements in Two Collision Systems

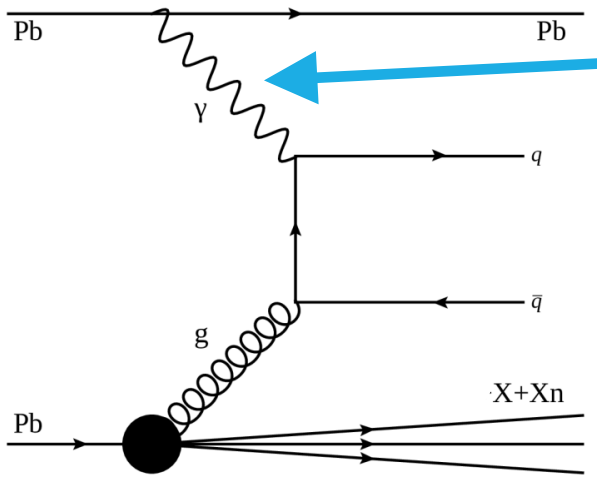

In ultra-relativistic heavy ion collisions, the intense electromagnetic fields provide a flux of quasi-real photons.

In p+Pb collisions, a partonic constituent from the proton strikes the Pb nucleus.

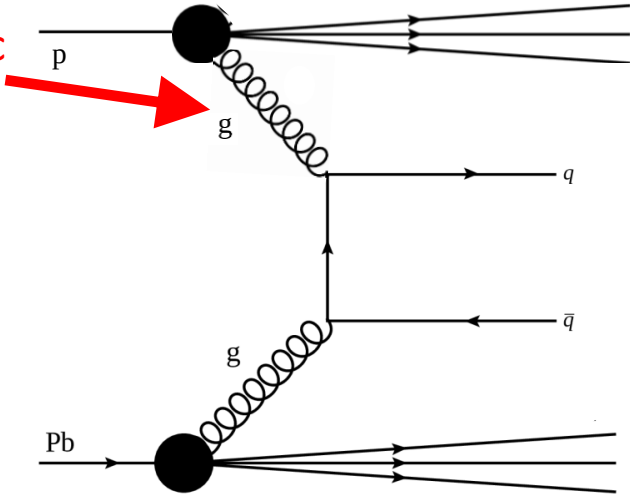

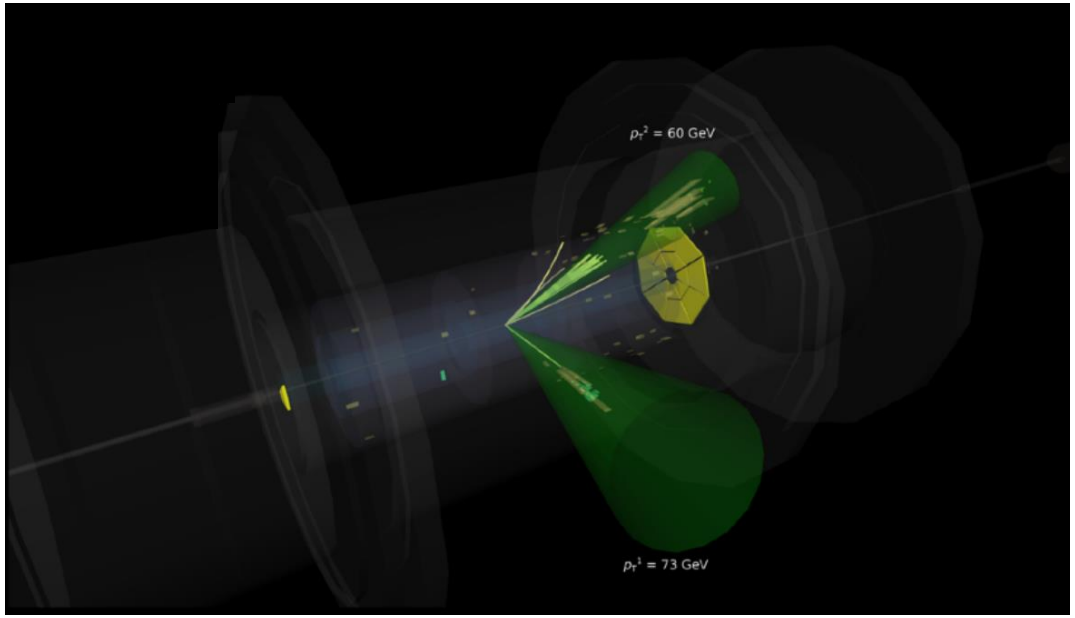

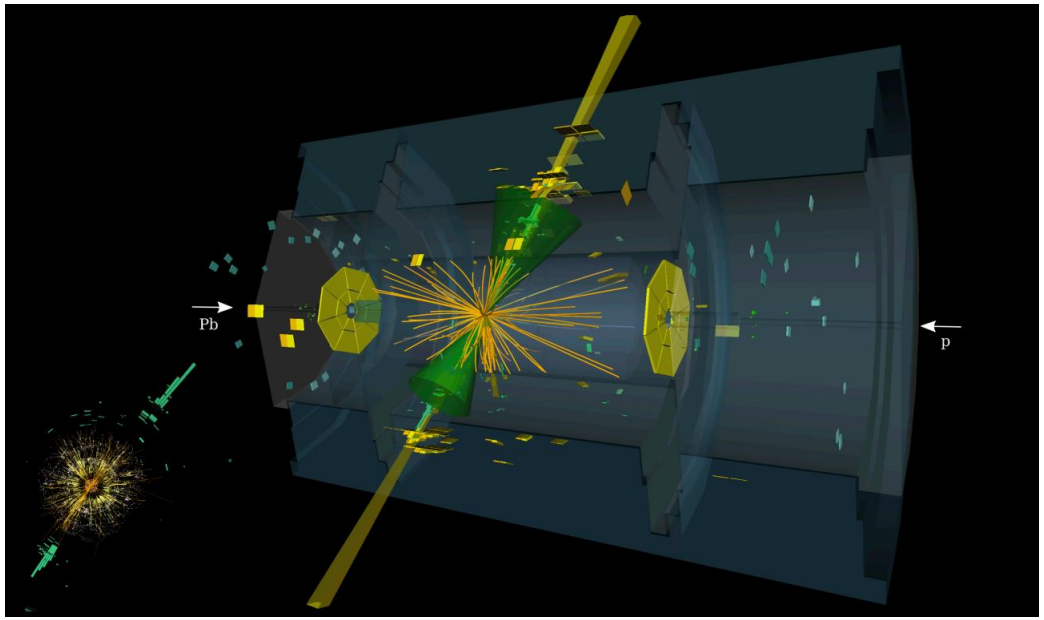

Dijet Measurements in Two Collision Systems

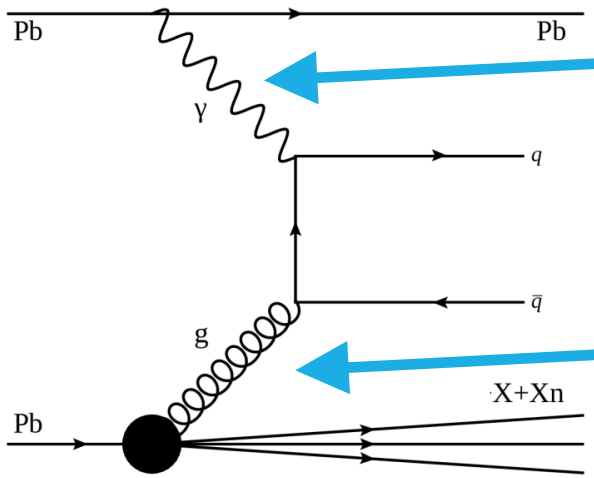

In ultra-relativistic heavy ion collisions, the intense electromagnetic fields provide a flux of quasi-real photons.

In p+Pb collisions, a partonic constituent from the proton strikes the Pb nucleus.

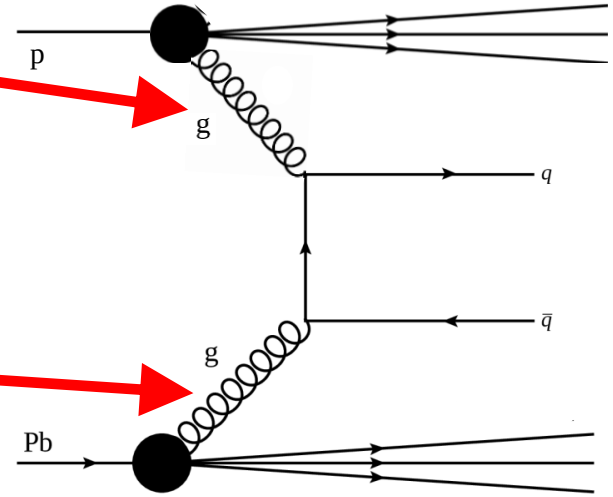

In both cases, they scatter from a parton in the Pb target, probing its nPDF.

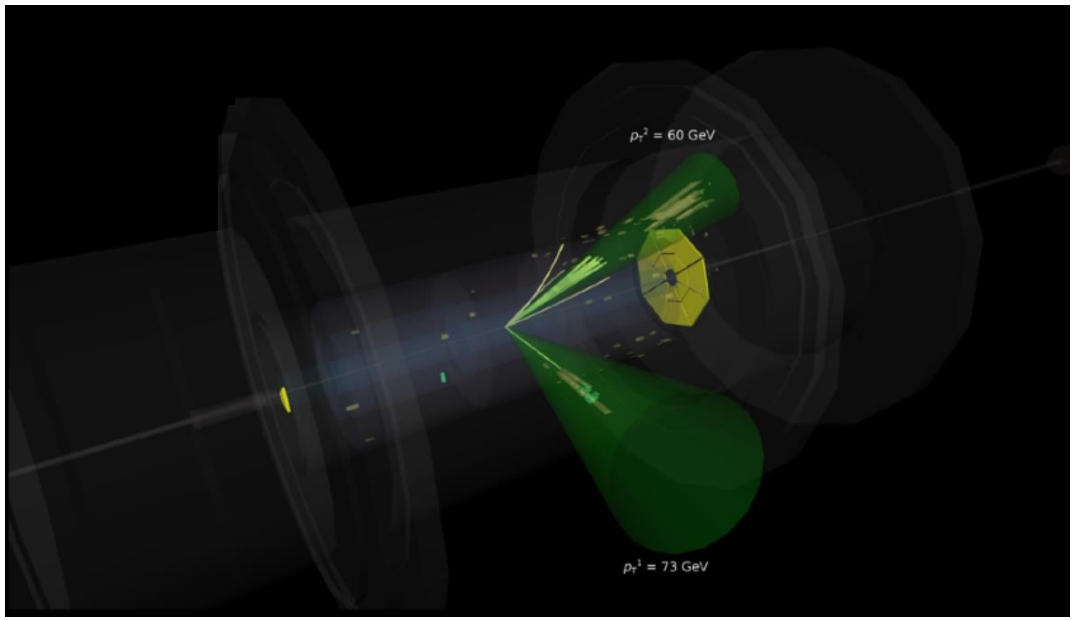

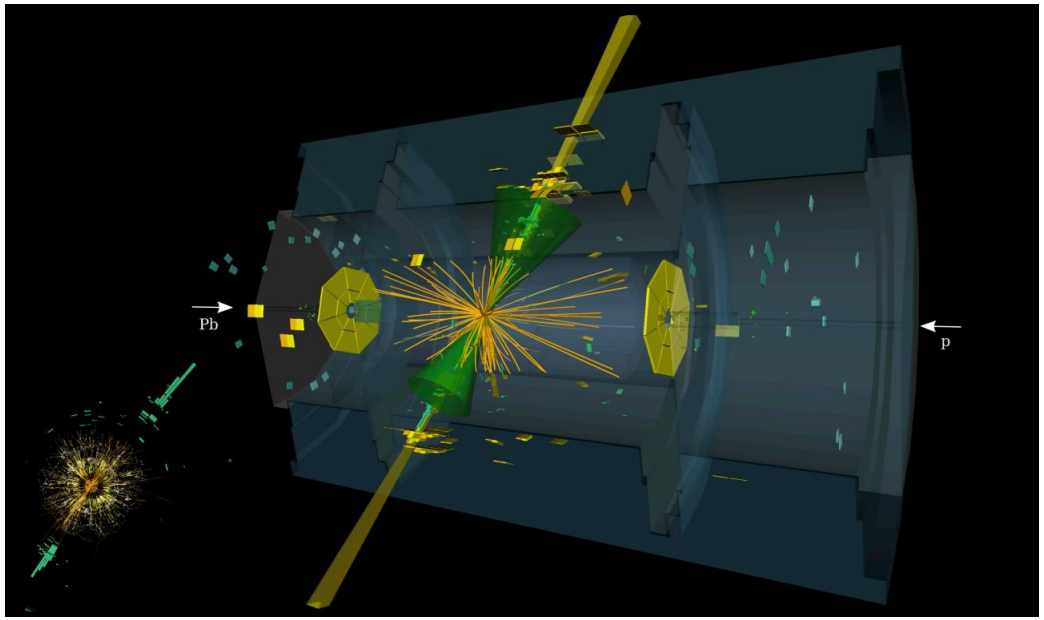

Dijet Measurements in Two Collision Systems

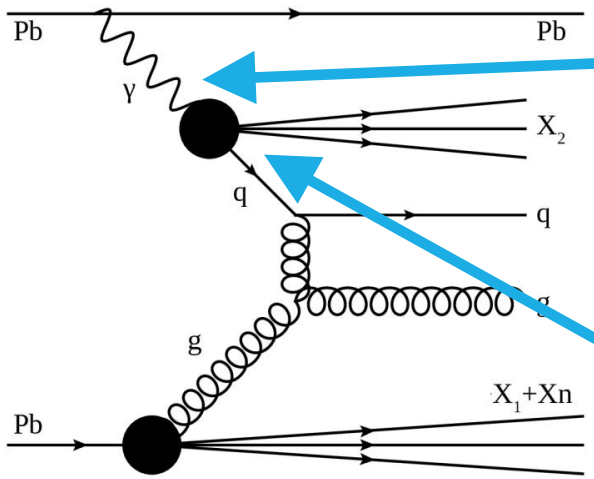

In ultra-relativistic heavy ion collisions, the intense electromagnetic fields provide a flux of quasi-real photons.

In resolved processes, the photon can fluctuate to some hadronic state.

In p+Pb collisions, a partonic constituent from the proton strikes the Pb nucleus.

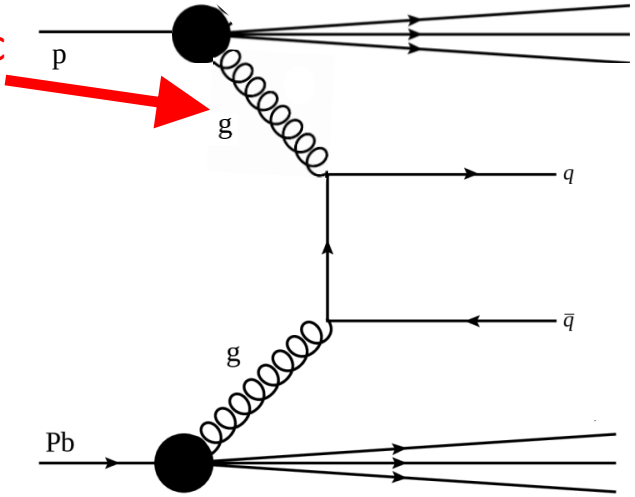

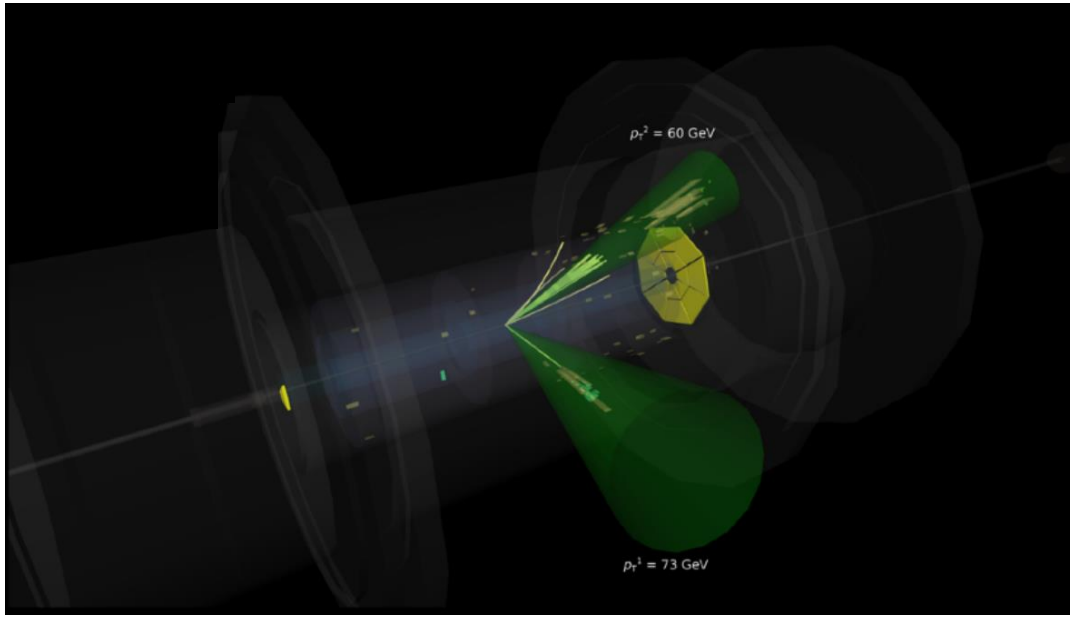

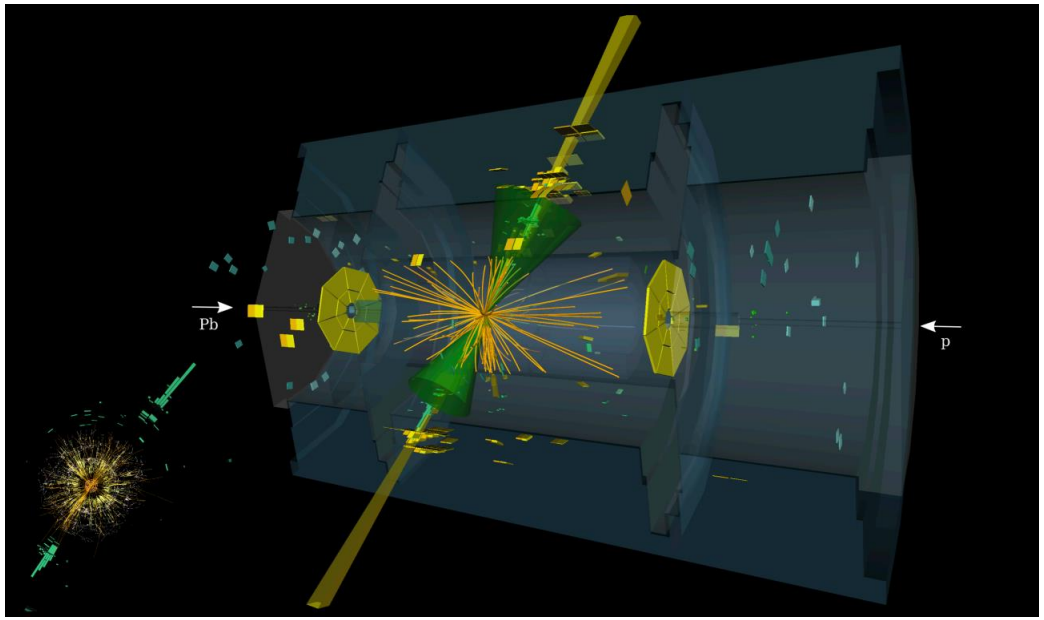

Dijet Measurements in Two Collision Systems

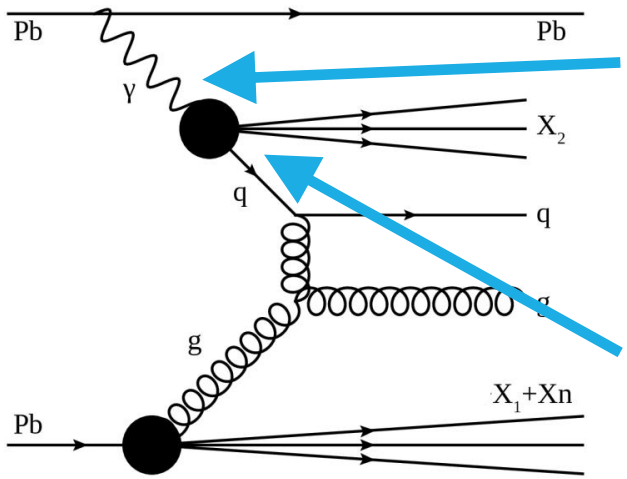

In ultra-relativistic heavy ion collisions, the intense electromagnetic fields provide a flux of quasi-real photons.

In resolved processes, the photon can fluctuate to some hadronic state.

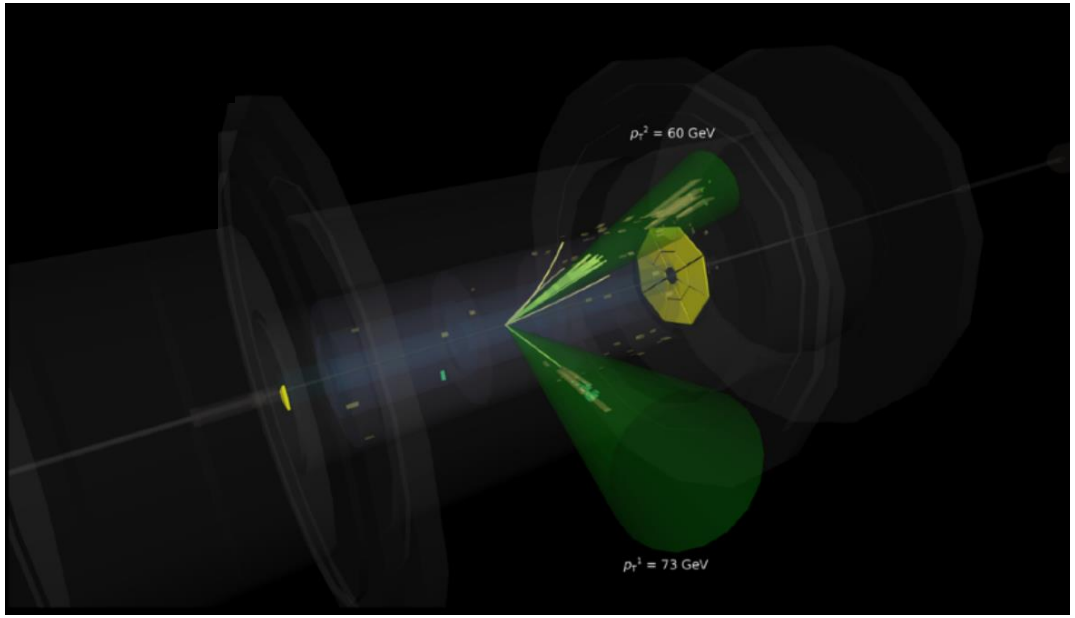

In p+Pb collisions, a partonic constituent from the proton strikes the Pb nucleus.

The probe in p+Pb collisions always has a more complex hadronic structure.

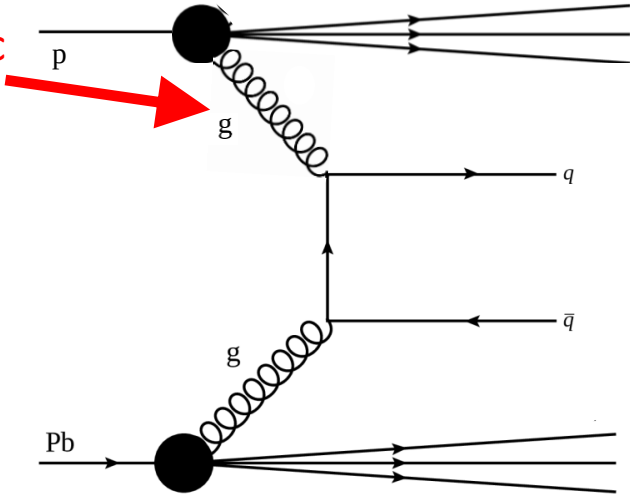

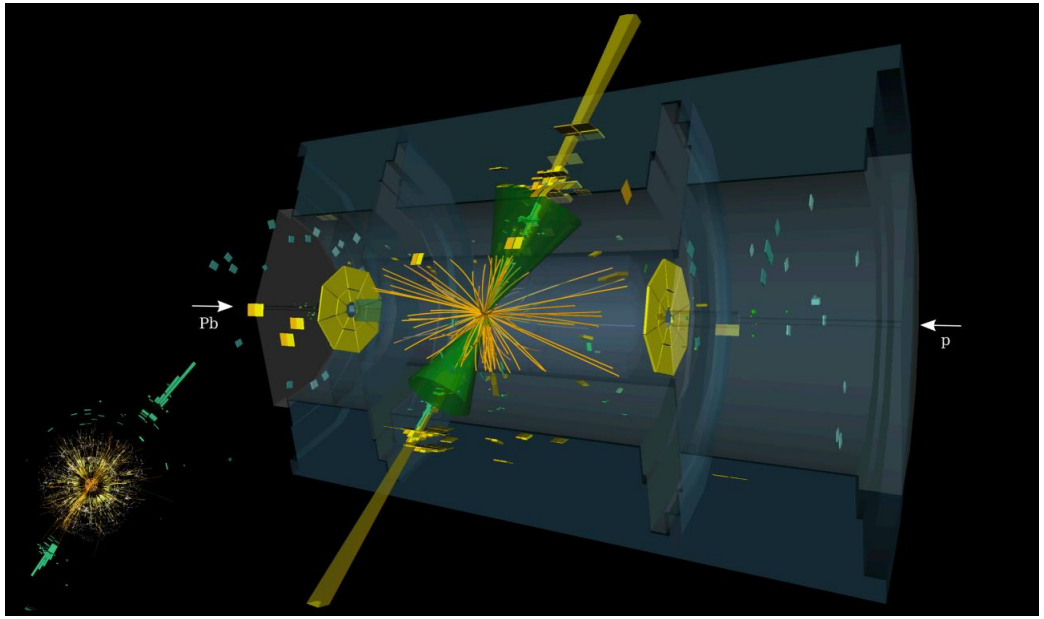

Dijet Measurements in Two Collision Systems

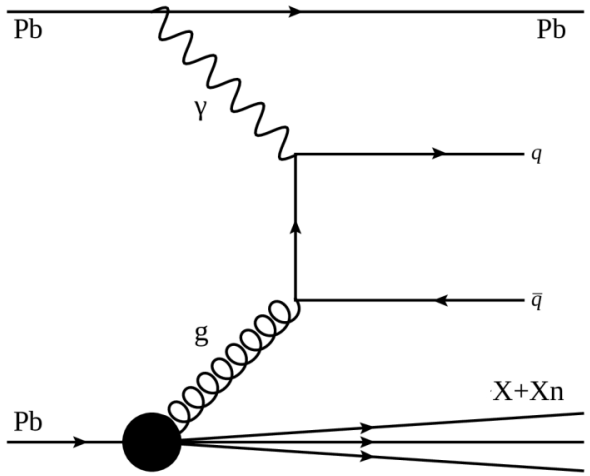

$$H_T = \sum_i p_T^i$$

$$z_\gamma = \frac{M_{jets} e^{+y_{jets}}}{\sqrt{s_{NN}}}$$

$$x_A = \frac{M_{jets} e^{-y_{jets}}}{\sqrt{s_{NN}}}$$

$$p_T^{avg} = \frac{p_T^1 + p_T^2}{2}$$

$$x_p = \frac{2p_T^{avg}\cosh(y^*)e^{+y_b}}{\sqrt{s}}$$

$$x_{Pb} = \frac{2p_T^{avg}\cosh(y^*)e^{-y_b}}{\sqrt{s}}$$

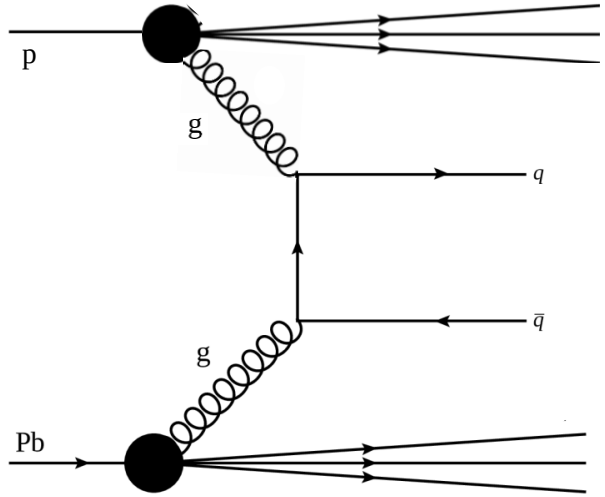

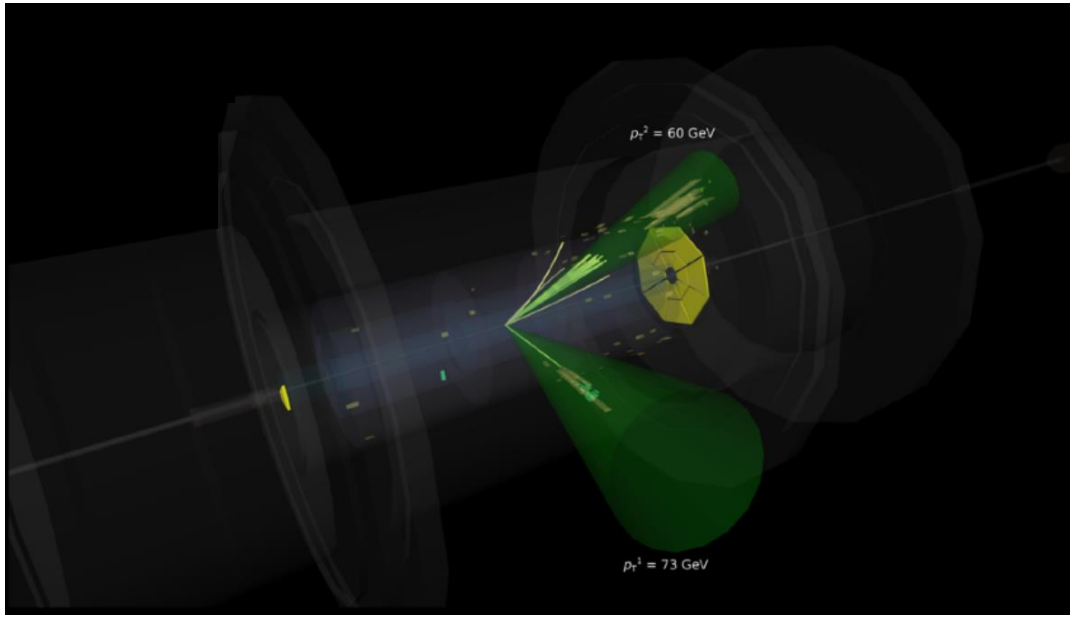

$$y_b = \frac{y_1 + y_2}{2}$$

$$y^* = \frac{|y_1 - y_2|}{2}$$

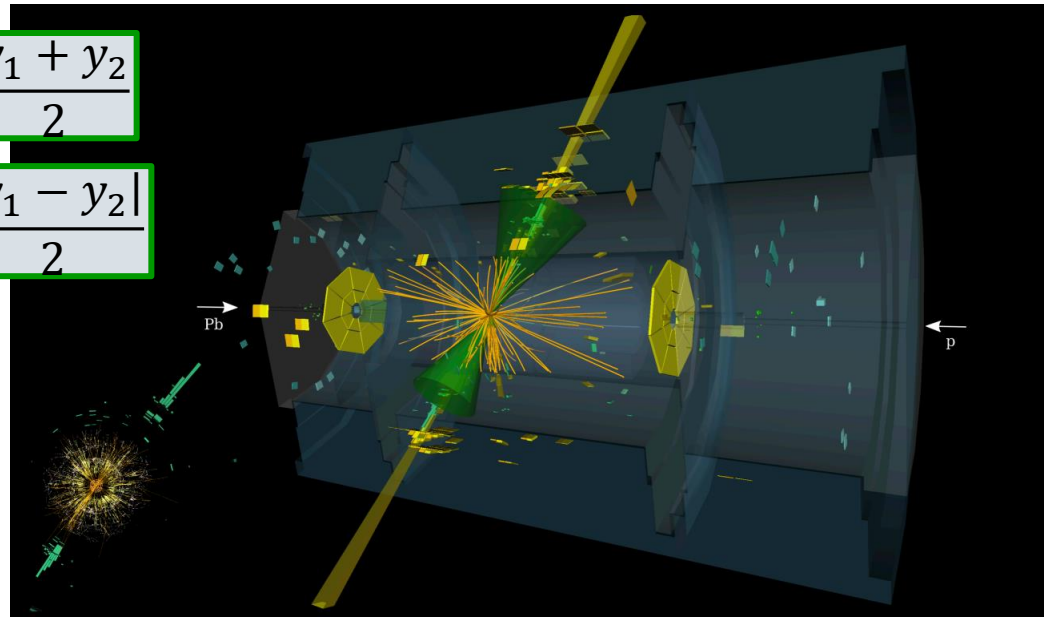

Dijet Measurements in Two Collision Systems

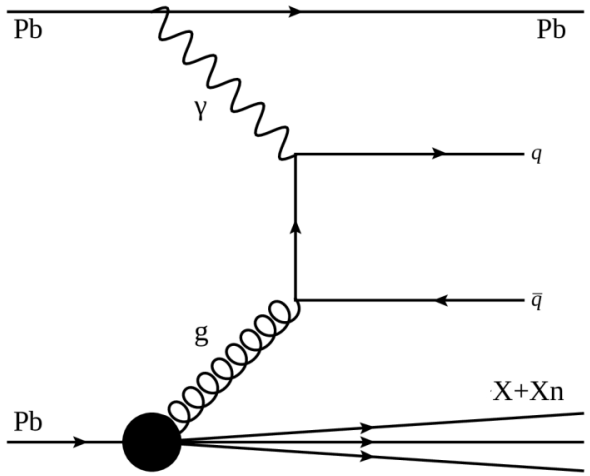

Proxy for Q^2

$$H_T = \sum_i p_T^i$$

$$z_\gamma = \frac{M_{jets} e^{+y_{jets}}}{\sqrt{s_{NN}}}$$

$$x_A = \frac{M_{jets} e^{-y_{jets}}}{\sqrt{s_{NN}}}$$

$$p_T^{avg} = \frac{p_T^1 + p_T^2}{2}$$

$$x_p = \frac{2p_T^{avg}\cosh(y^*)e^{+y_b}}{\sqrt{s}}$$

$$x_{Pb} = \frac{2p_T^{avg}\cosh(y^*)e^{-y_b}}{\sqrt{s}}$$

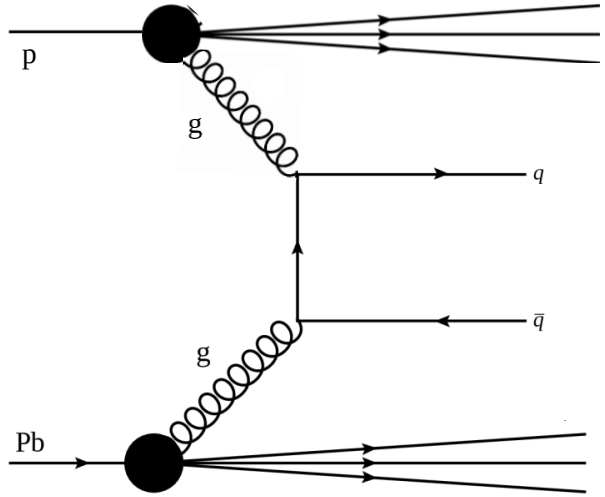

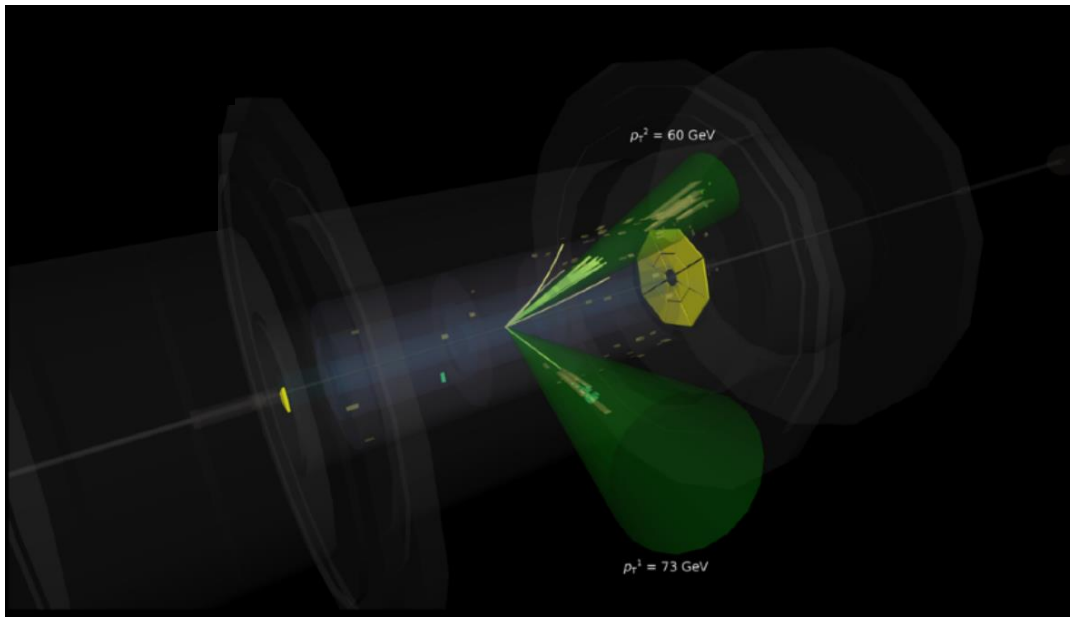

$$y_b = \frac{y_1 + y_2}{2}$$

$$y^* = \frac{|y_1 - y_2|}{2}$$

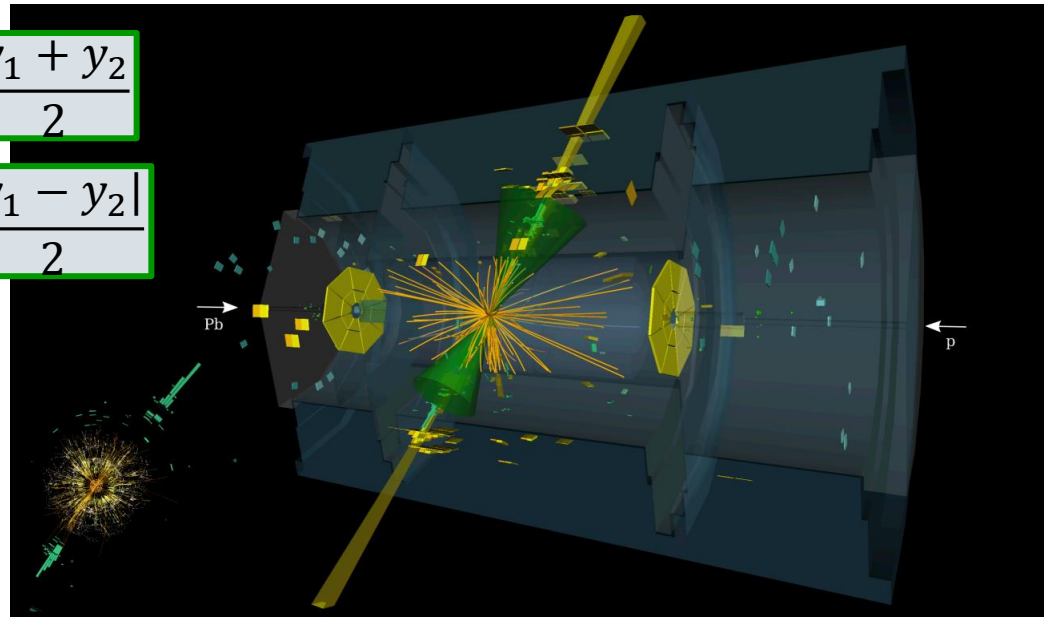

Dijet Measurements in Two Collision Systems

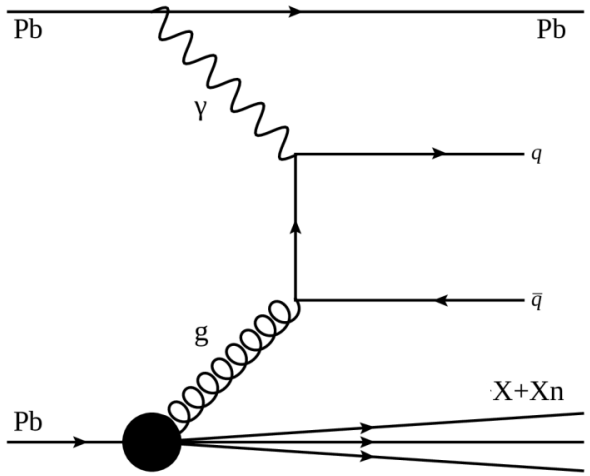

Proxy for Q^2

$$H_T = \sum_i p_T^i$$

Probe parton energy fraction

$$z_\gamma = \frac{M_{jets} e^{+y_{jets}}}{\sqrt{s_{NN}}}$$

$$x_A = \frac{M_{jets} e^{-y_{jets}}}{\sqrt{s_{NN}}}$$

$$p_T^{avg} = \frac{p_T^1 + p_T^2}{2}$$

$$x_p = \frac{2p_T^{avg}\cosh(y^*)e^{+y_b}}{\sqrt{s}}$$

$$x_{Pb} = \frac{2p_T^{avg}\cosh(y^*)e^{-y_b}}{\sqrt{s}}$$

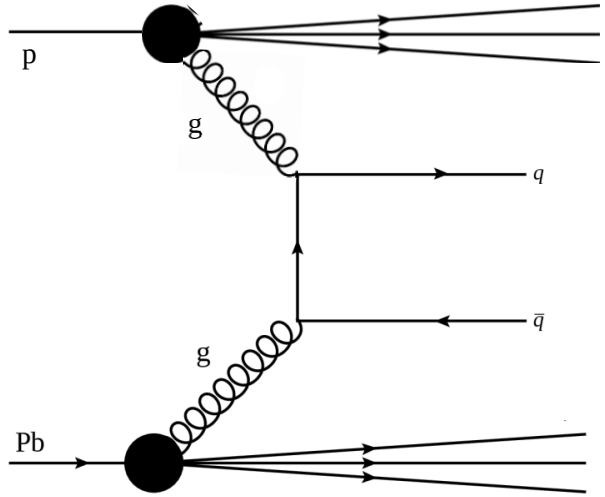

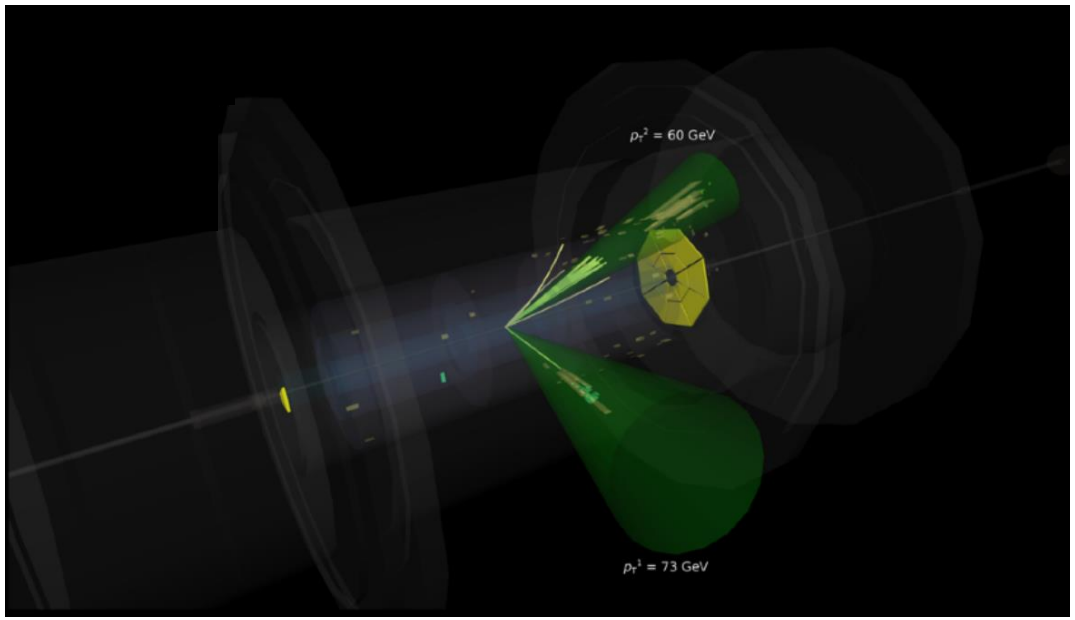

$$y_b = \frac{y_1 + y_2}{2}$$

$$y^* = \frac{|y_1 - y_2|}{2}$$

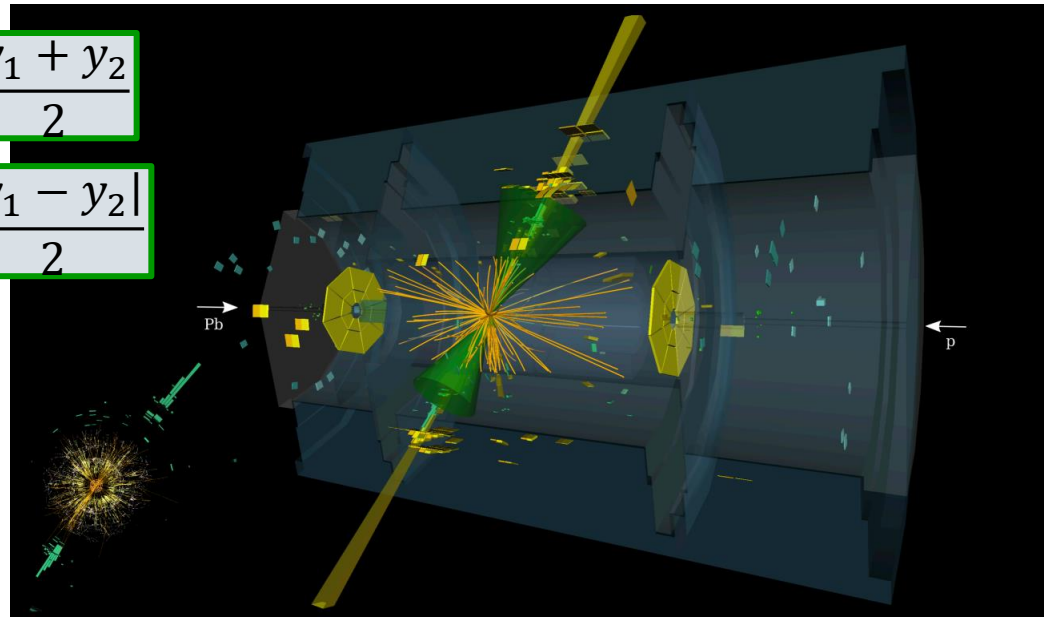

Dijet Measurements in Two Collision Systems

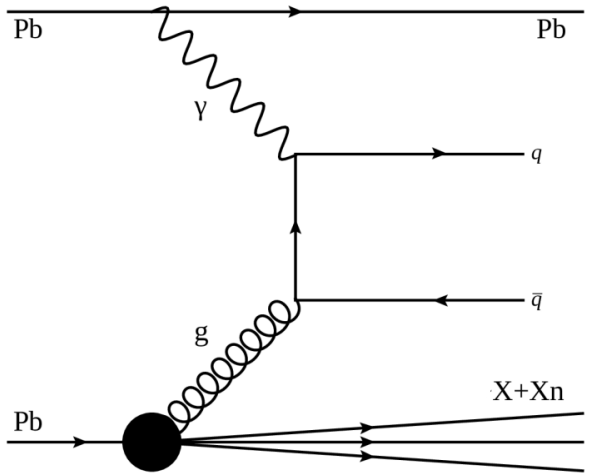

Proxy for Q^2

$$H_T = \sum_i p_T^i$$

Probe parton energy fraction

$$z_\gamma = \frac{M_{jets} e^{+y_{jets}}}{\sqrt{s_{NN}}}$$

Target parton energy fraction

$$x_A = \frac{M_{jets} e^{-y_{jets}}}{\sqrt{s_{NN}}}$$

$$p_T^{avg} = \frac{p_T^1 + p_T^2}{2}$$

$$x_p = \frac{2p_T^{avg}\cosh(y^*)e^{+y_b}}{\sqrt{s}}$$

$$x_{Pb} = \frac{2p_T^{avg}\cosh(y^*)e^{-y_b}}{\sqrt{s}}$$

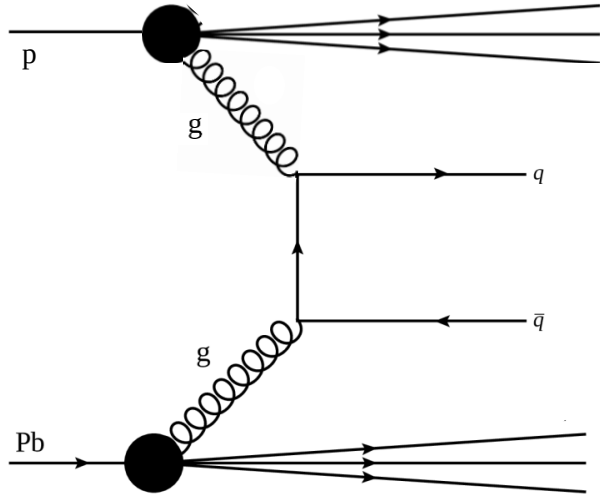

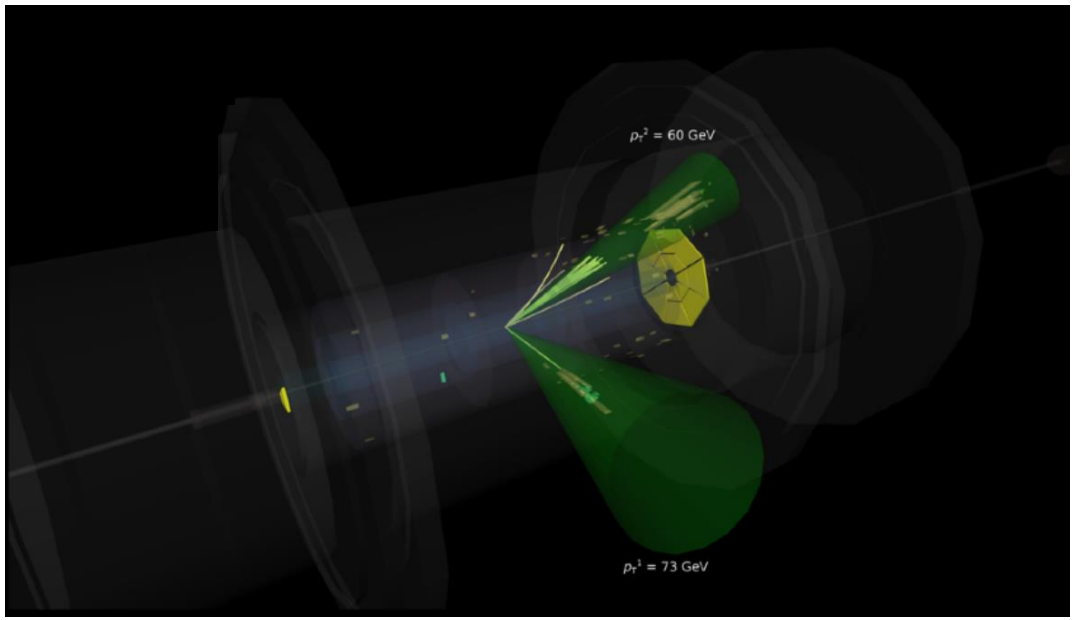

$$y_b = \frac{y_1 + y_2}{2}$$

$$y^* = \frac{|y_1 - y_2|}{2}$$

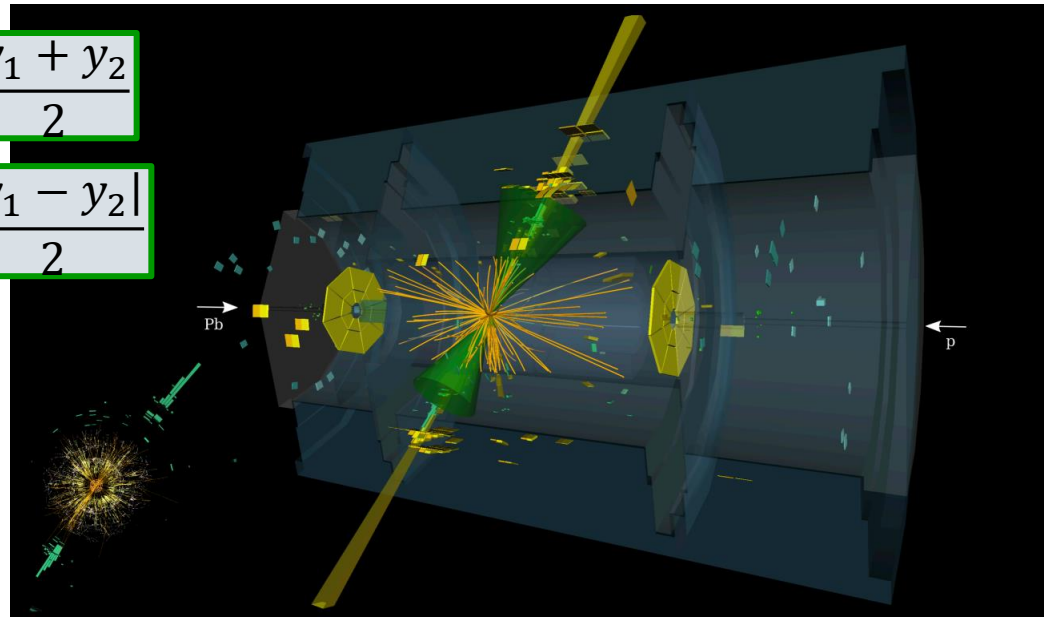

Selecting Photo-nuclear Jet Events

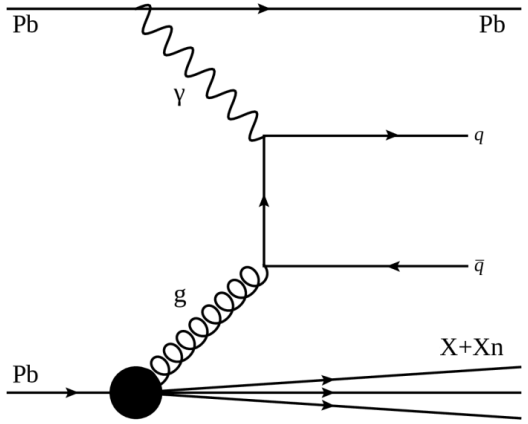

We can select photo-nuclear jet events with cuts motivated by the particular event topology.

$$H_T = \sum_i p_T^i$$

$$x_A = \frac{M_{jets} e^{-y_{jets}}}{\sqrt{s_{NN}}}$$

$$z_\gamma = \frac{M_{jets} e^{+y_{jets}}}{\sqrt{s_{NN}}}$$

Selecting Photo-nuclear Jet Events

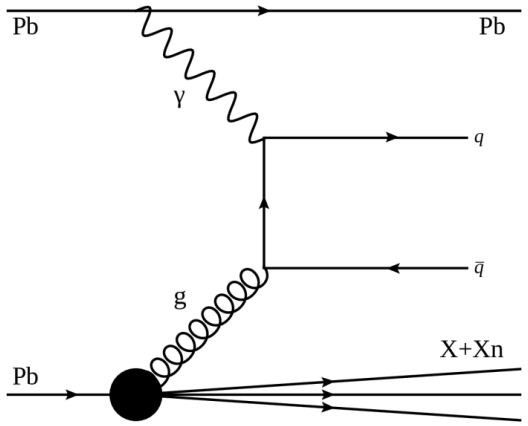

We can select photo-nuclear jet events with cuts motivated by the particular event topology.

- 0nXn requirement for nuclear breakup in exactly one ATLAS Zero-Degree Calorimeter (ZDC)

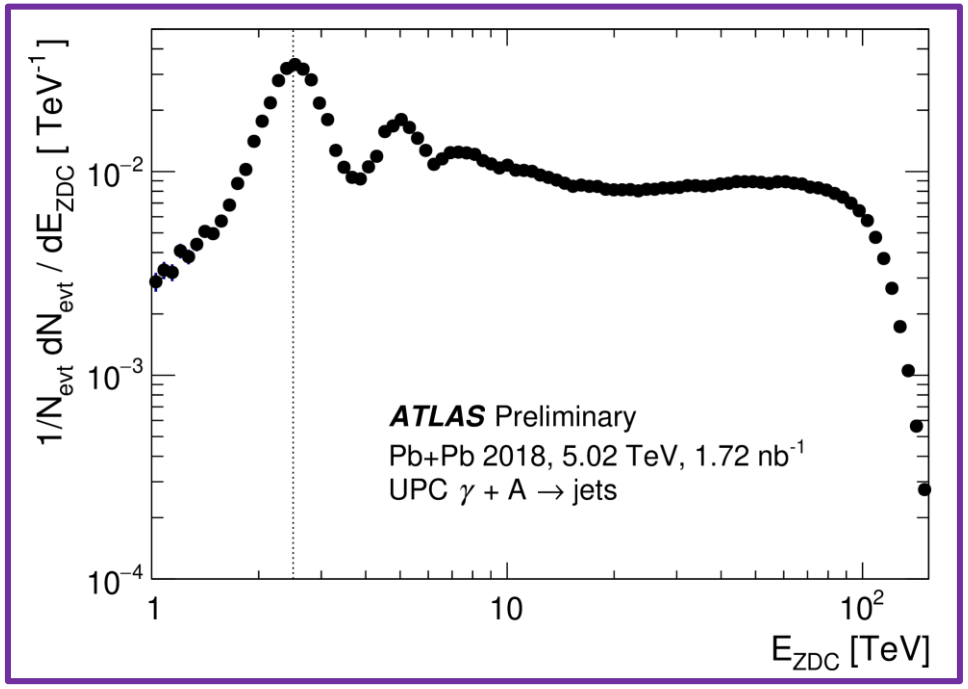

$$H_T = \sum_i p_T^i$$

$$x_A = \frac{M_{jets} e^{-y_{jets}}}{\sqrt{s_{NN}}}$$

$$z_\gamma = \frac{M_{jets} e^{+y_{jets}}}{\sqrt{s_{NN}}}$$

Selecting Photo-nuclear Jet Events

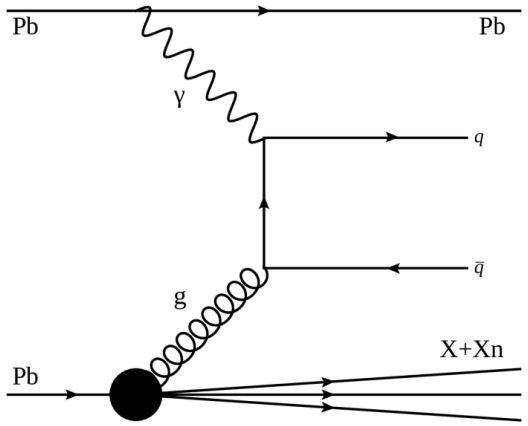

We can select photo-nuclear jet events with cuts motivated by the particular event topology.

- 0nXn requirement for nuclear breakup in exactly one ATLAS Zero-Degree Calorimeter (ZDC)
- Large rapidity gaps on one side of the detector
  - To veto $\gamma\gamma \rightarrow q\bar{q}$, also require $\Delta\eta_A^{edge} < 3$.

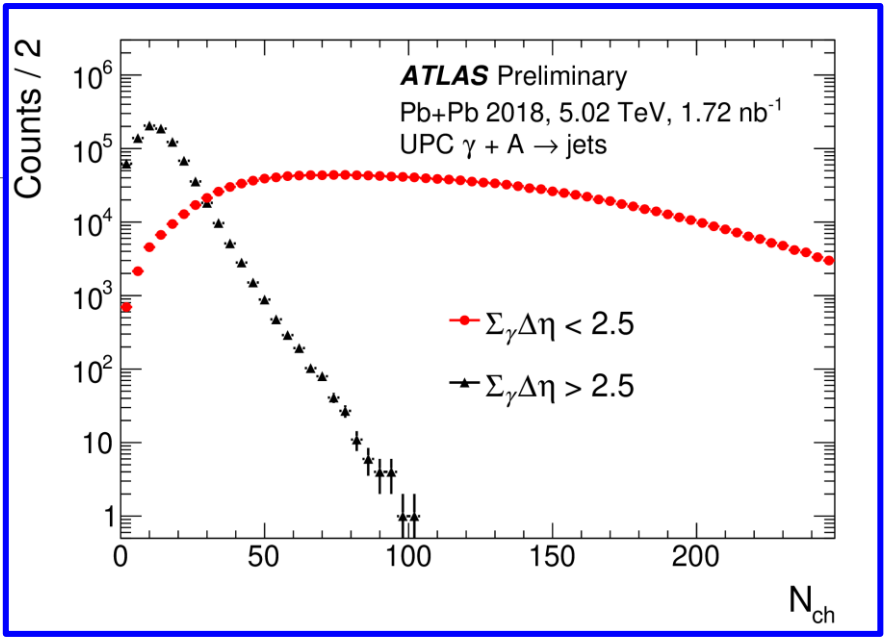

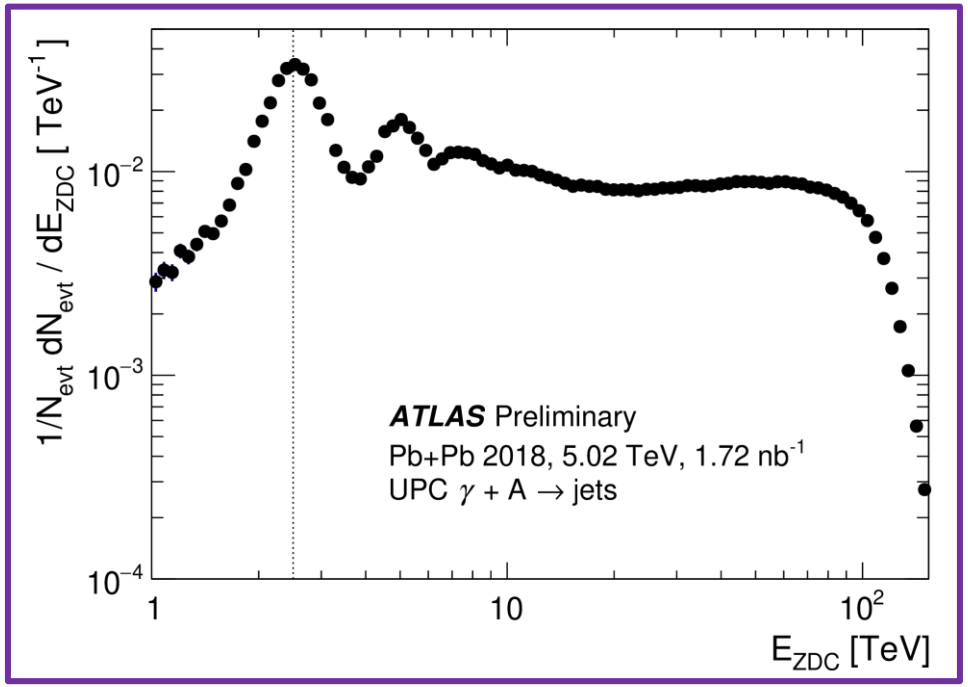

$$H_T = \sum_i p_T^i$$

$$x_A = \frac{M_{jets} e^{-y_{jets}}}{\sqrt{s_{NN}}}$$

$$z_\gamma = \frac{M_{jets} e^{+y_{jets}}}{\sqrt{s_{NN}}}$$

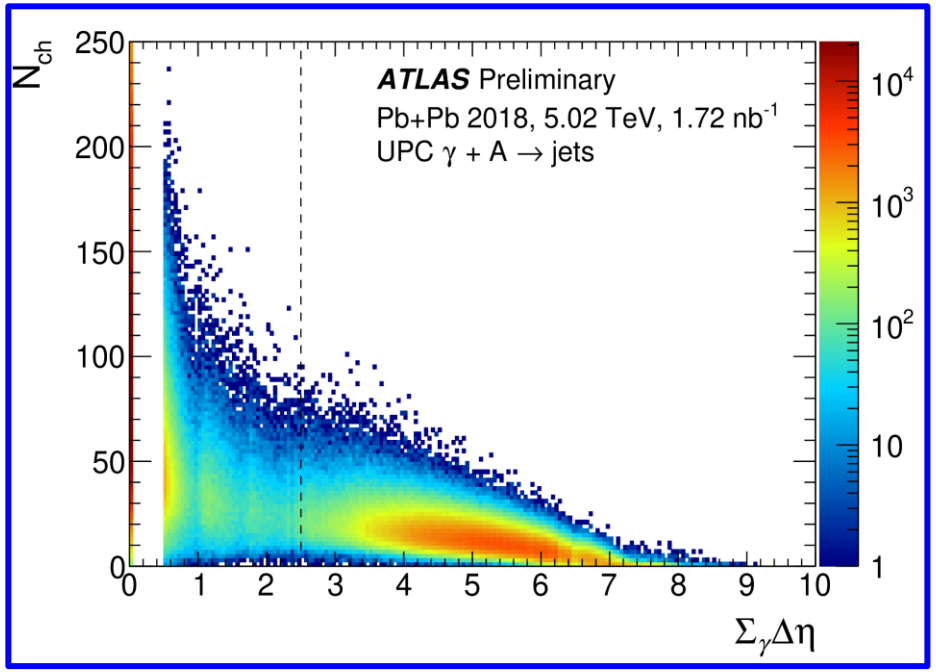

Selecting Photo-nuclear Jet Events

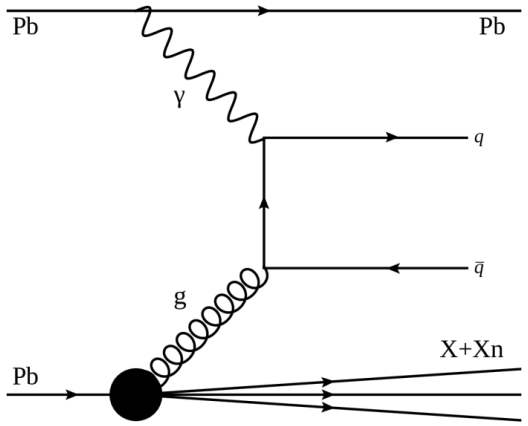

We can select photo-nuclear jet events with cuts motivated by the particular event topology.

- 0nXn requirement for nuclear breakup in exactly one ATLAS Zero-Degree Calorimeter (ZDC)
- Large rapidity gaps on one side of the detector
  - To veto $\gamma\gamma \rightarrow q\bar{q}$, also require $\Delta\eta_A^{edge} < 3$.
- At least two Particle-Flow jets with $p_T > 15$ GeV

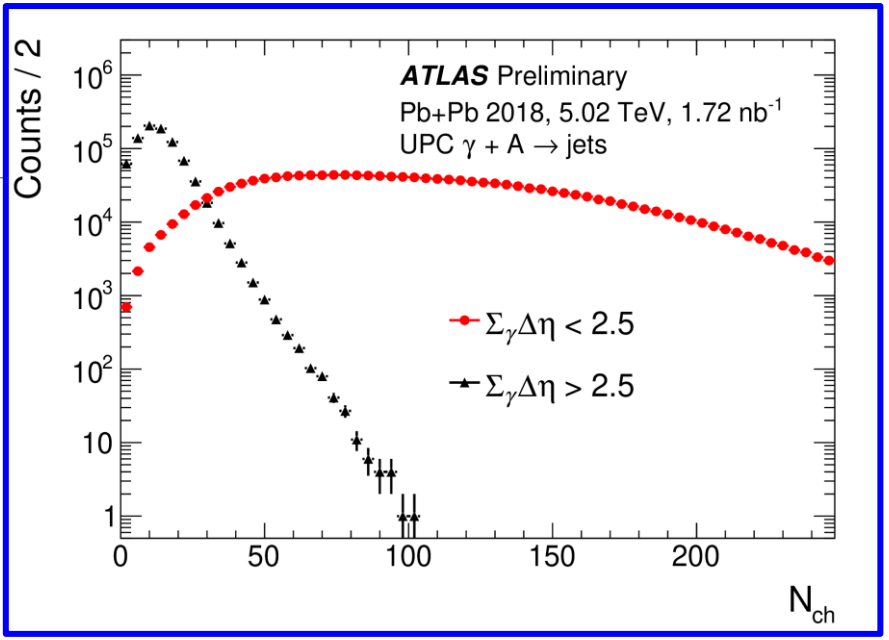

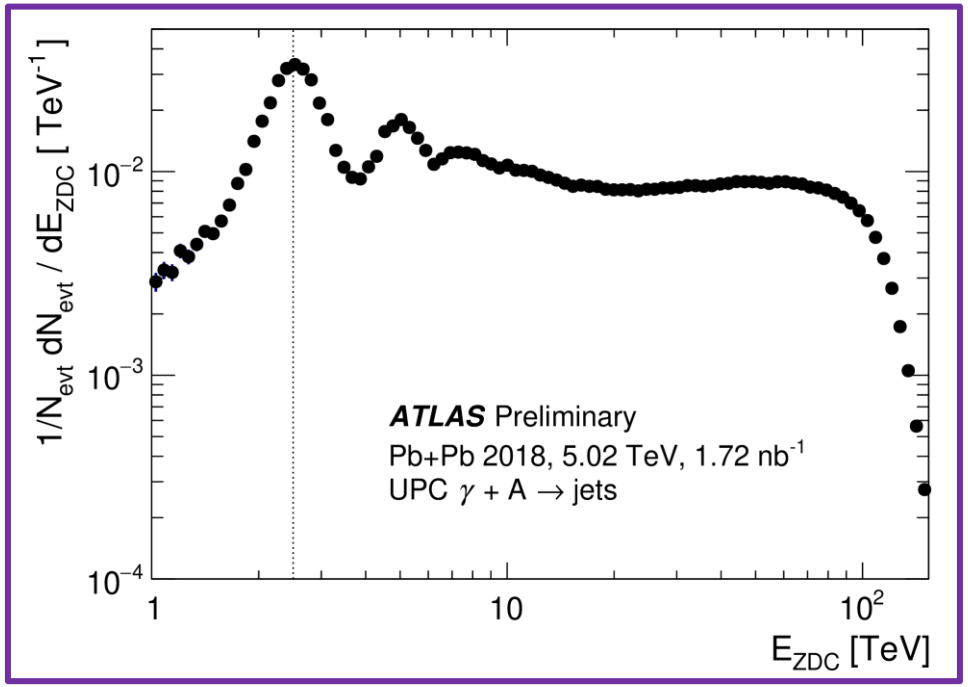

$$H_T = \sum_i p_T^i$$

$$x_A = \frac{M_{jets} e^{-y_{jets}}}{\sqrt{s_{NN}}}$$

$$z_\gamma = \frac{M_{jets} e^{+y_{jets}}}{\sqrt{s_{NN}}}$$

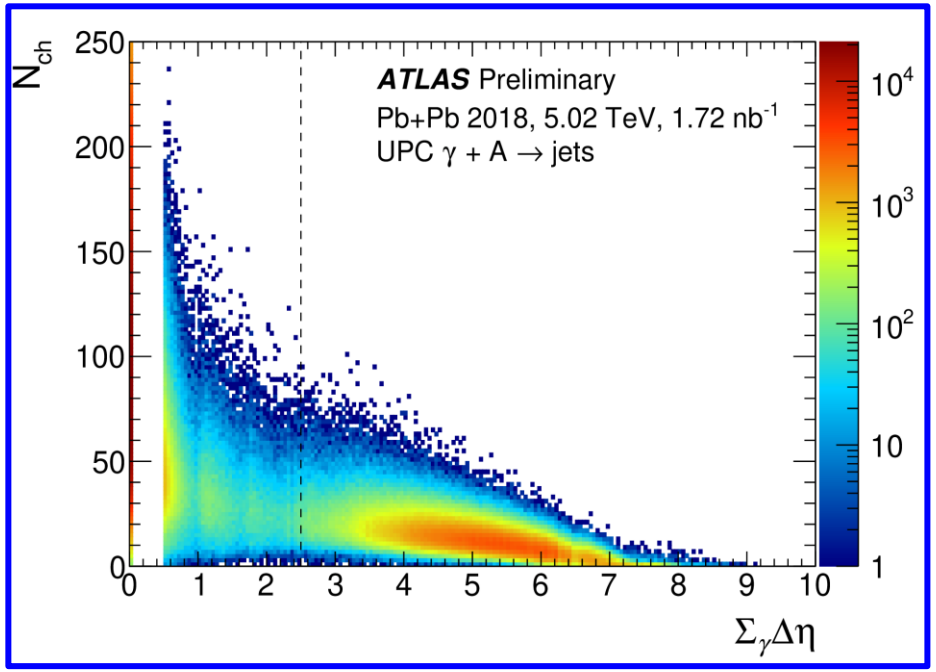

UPC Dijets: Scanning in Photon Energy

$$H_T = \sum_i p_T^i \qquad x_A = \frac{M_{jets} e^{-y_{jets}}}{\sqrt{s_{NN}}} \qquad z_\gamma = \frac{M_{jets} e^{+y_{jets}}}{\sqrt{s_{NN}}}$$

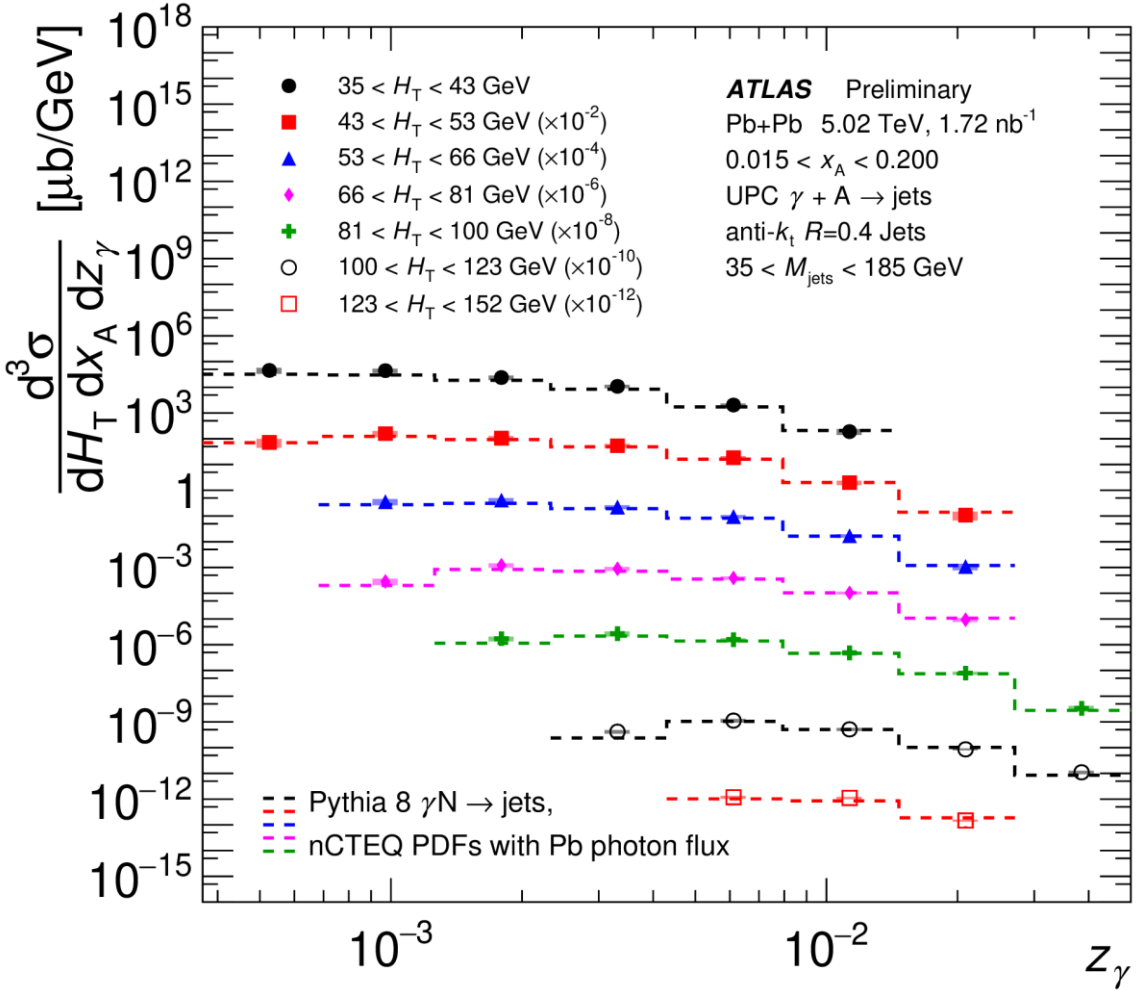

The x_A distribution has substantial acceptance effects in z_γ.

Selecting on photon energy removes this bias, allowing a more direct measurement of nPDFs.

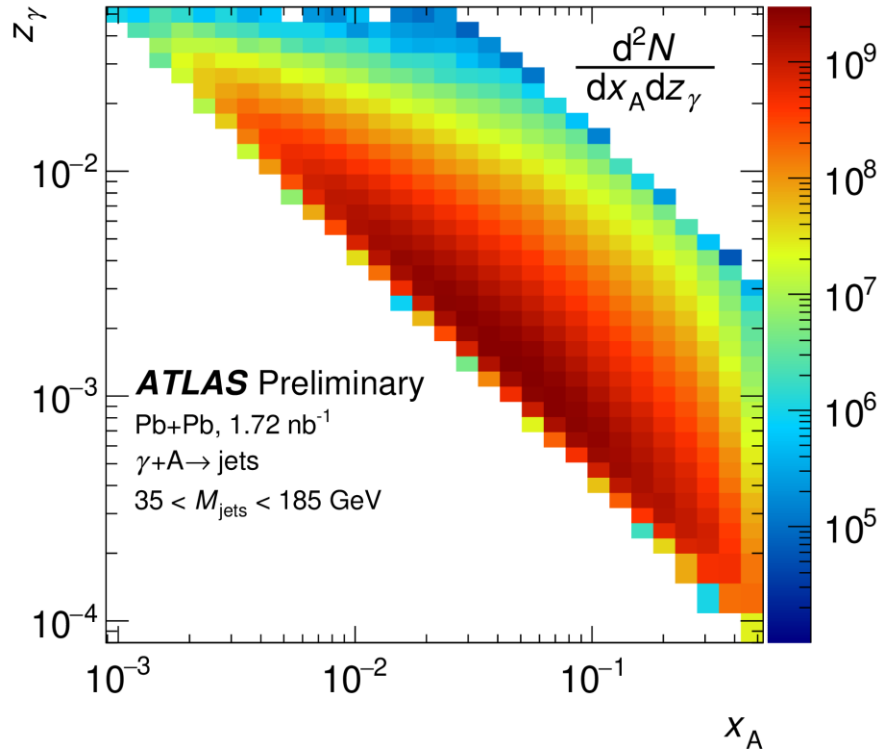

UPC Dijets: Scanning in Photon Energy

$$H_T = \sum_i p_T^i \qquad x_A = \frac{M_{jets} e^{-y_{jets}}}{\sqrt{s_{NN}}} \qquad z_\gamma = \frac{M_{jets} e^{+y_{jets}}}{\sqrt{s_{NN}}}$$

The x_A distribution has substantial acceptance effects in z_γ.

Selecting on photon energy removes this bias, allowing a more direct measurement of nPDFs.

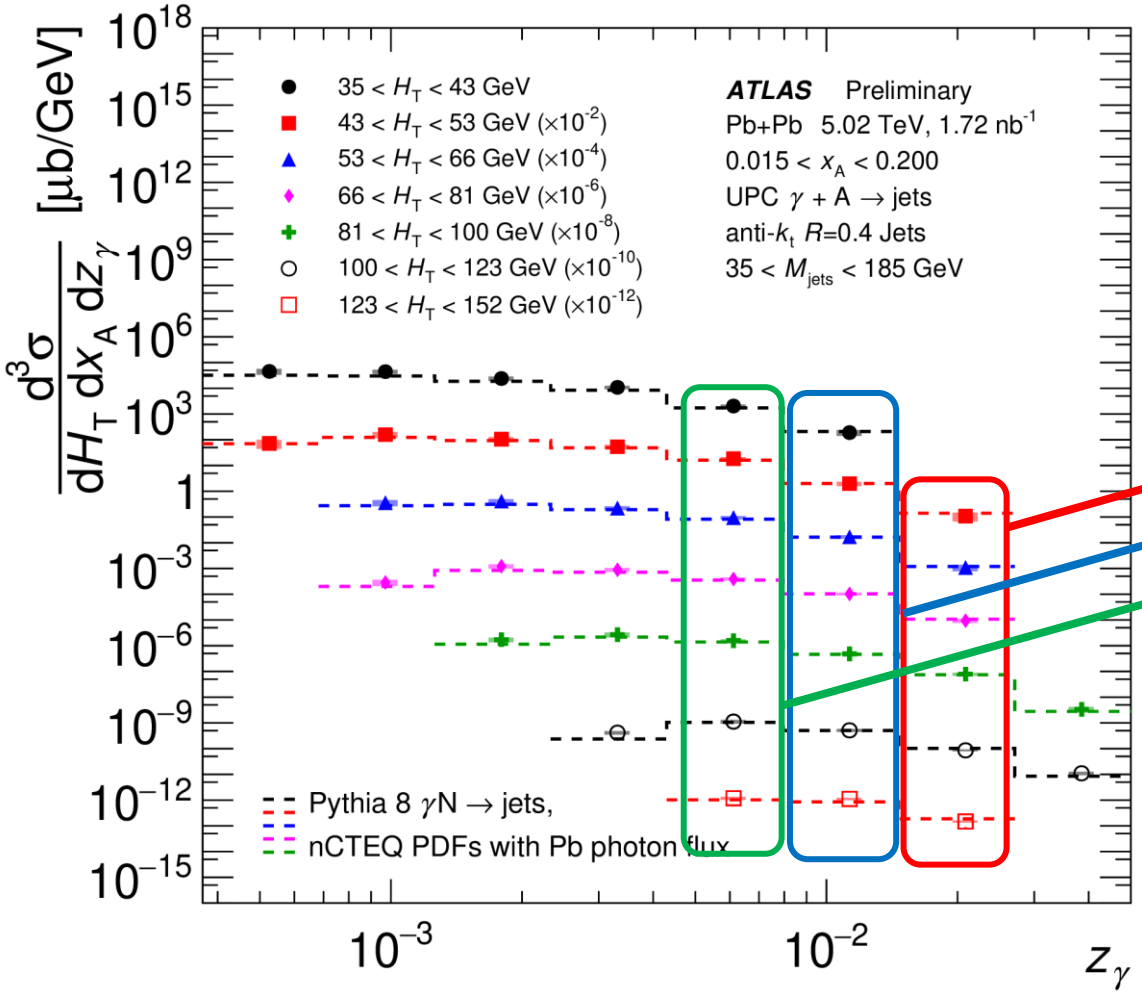

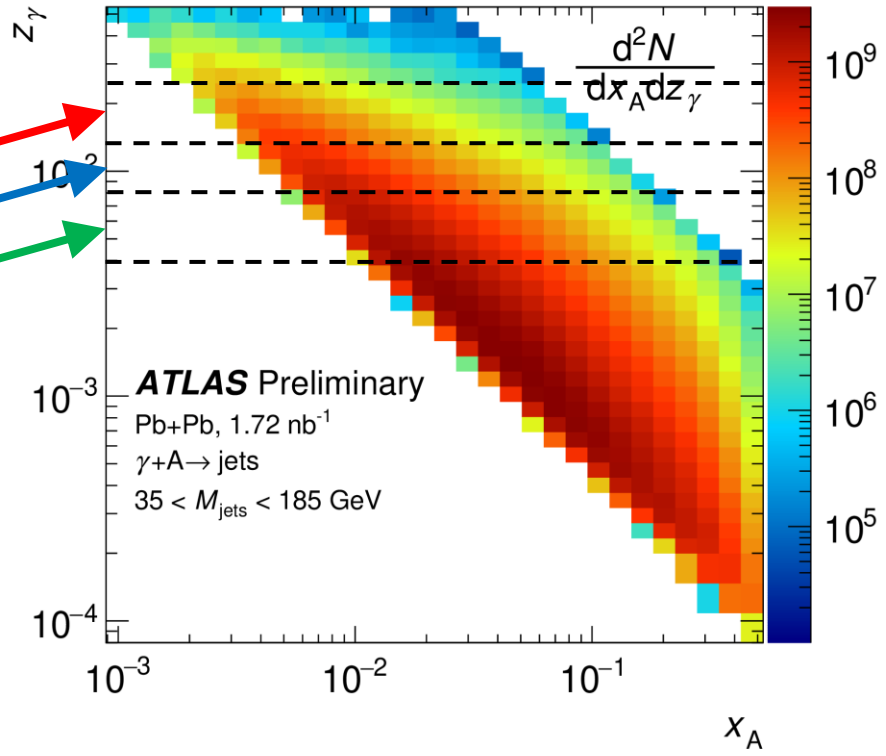

UPC Dijet Cross-Sections

- At intermediate photon energies, we can access higher-x partons.
- Systematic uncertainties grow near the acceptance edge at high-x.

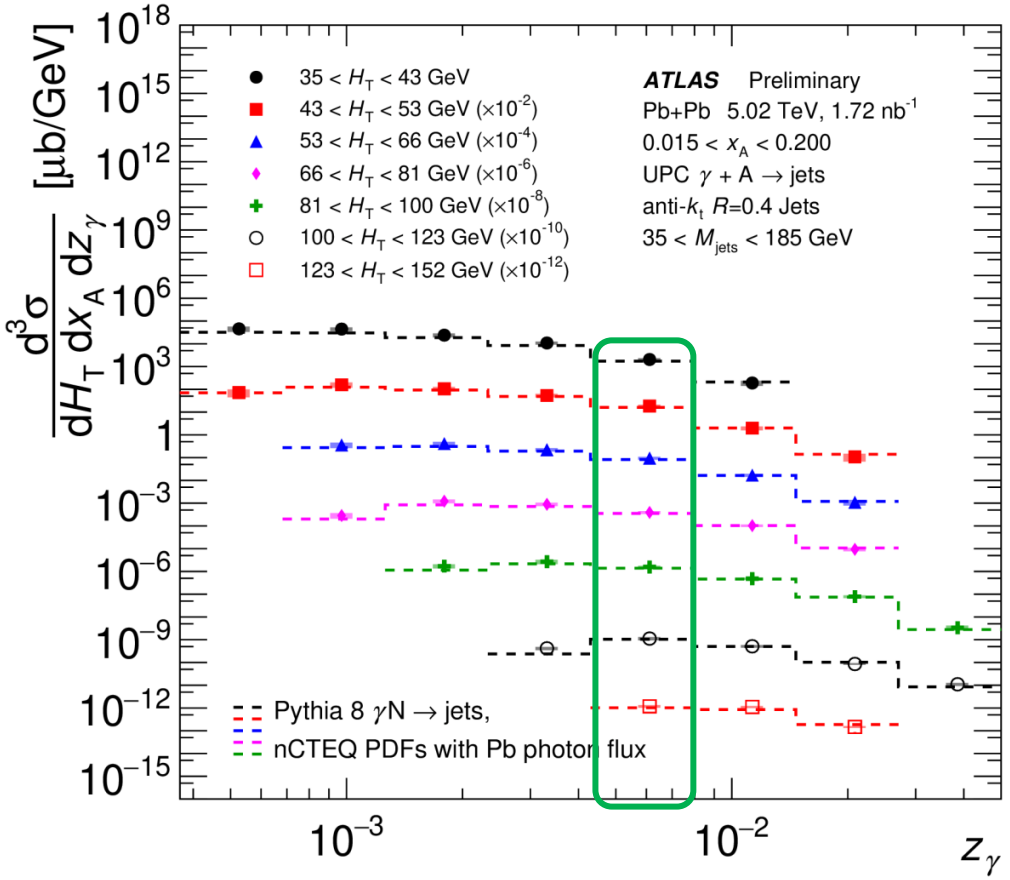

Photon Energy

$0.004 < z_\gamma < 0.008$

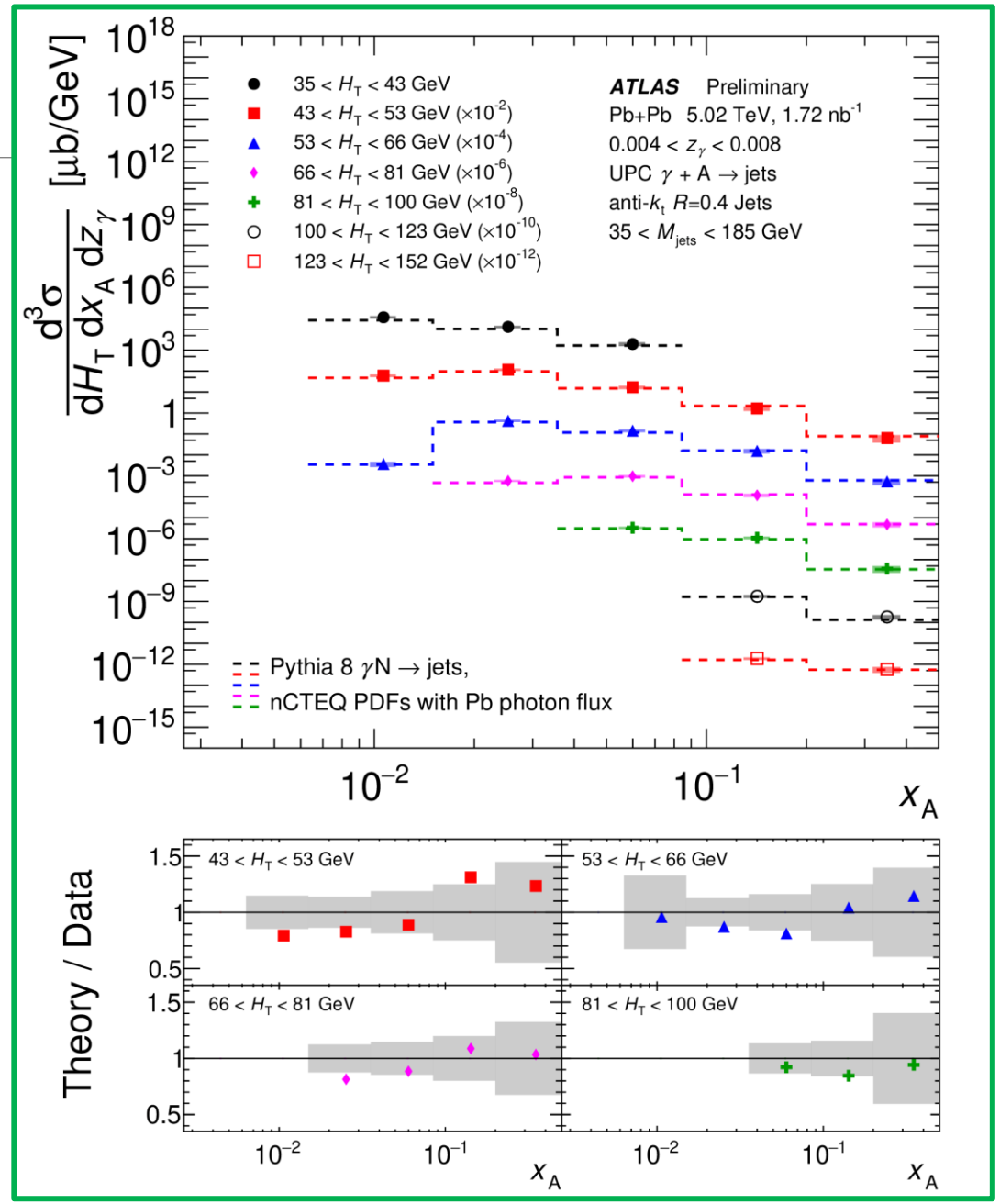

UPC Dijet Cross-Sections

- Higher photon energy opens up the low-x shadowing region.
- Results are quite consistent with the theoretical model.

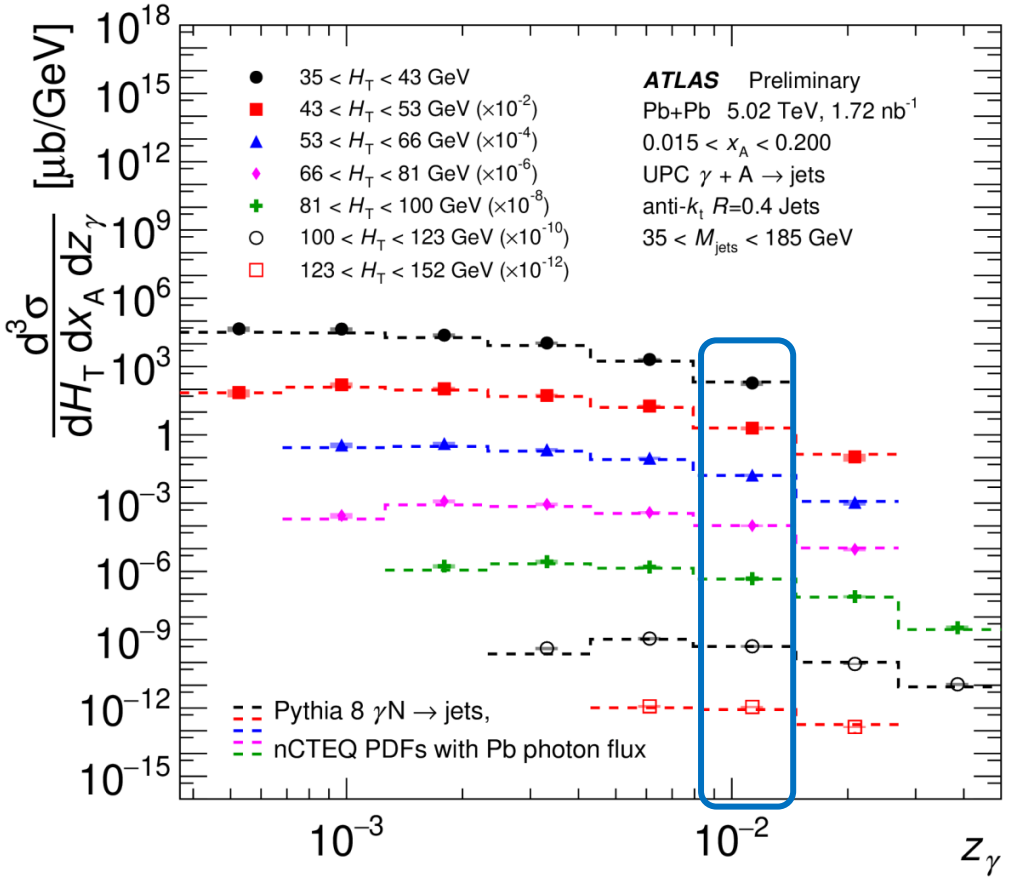

Photon Energy

$0.008 < z_\gamma < 0.015$

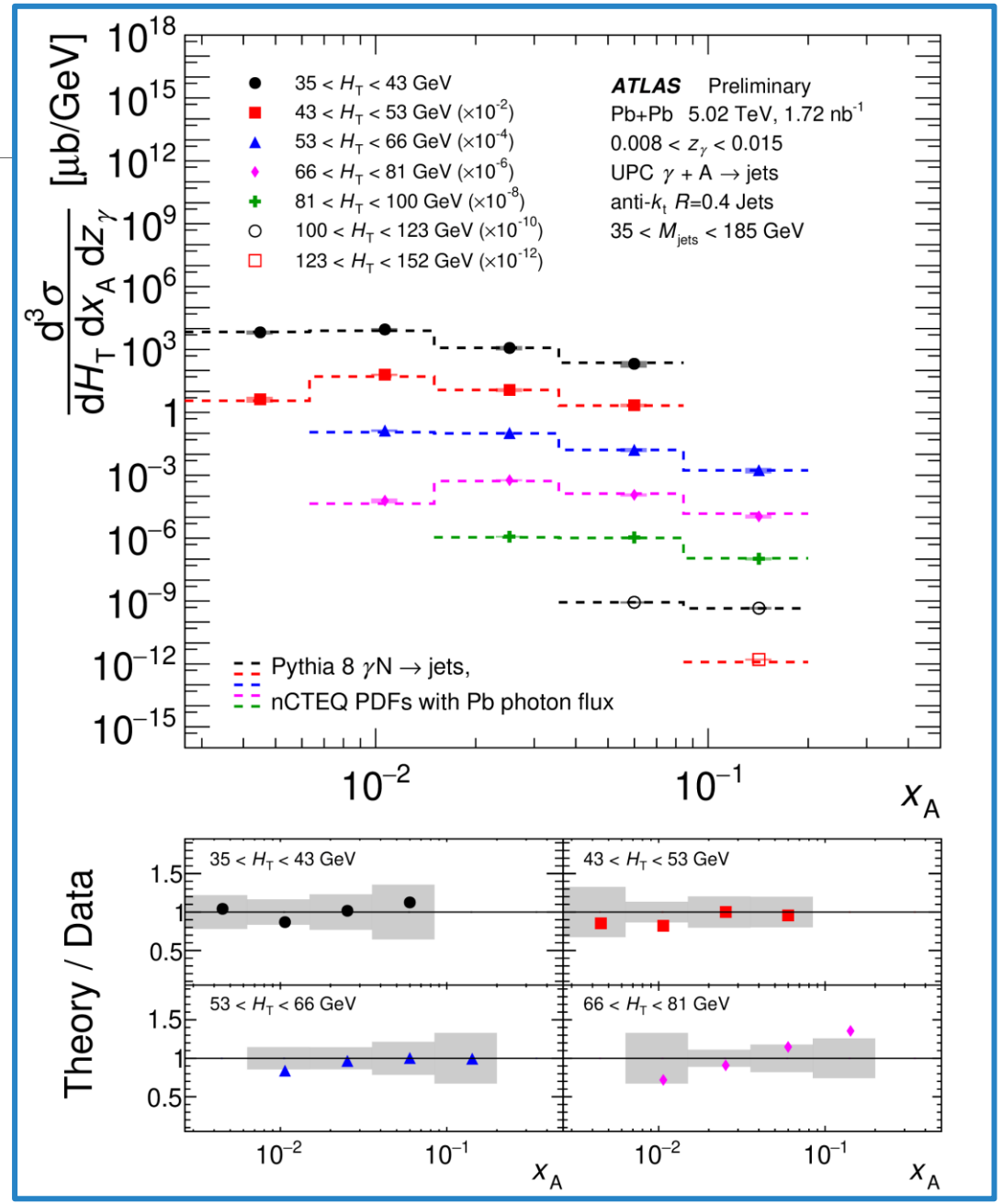

UPC Dijet Cross-Sections

- The highest photon energy allows the most access to low x.
- Systematic control is more challenging near acceptance edges.

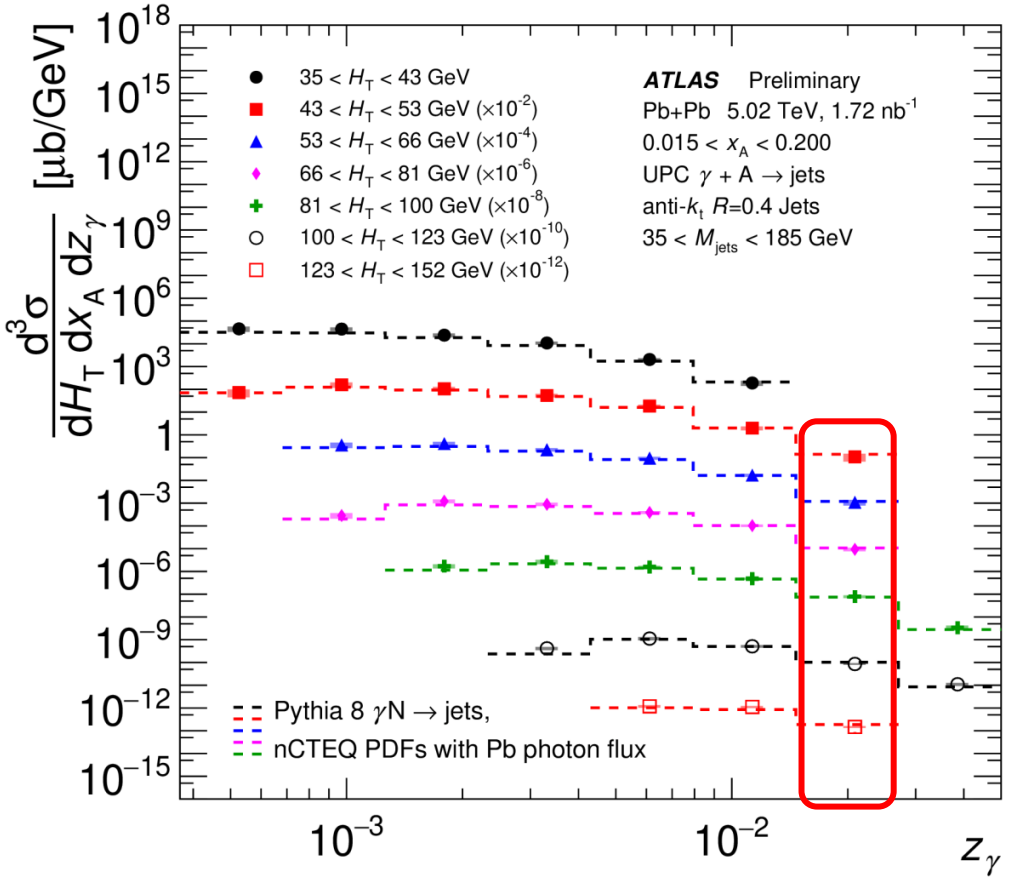

Photon Energy

$0.015 < z_\gamma < 0.027$

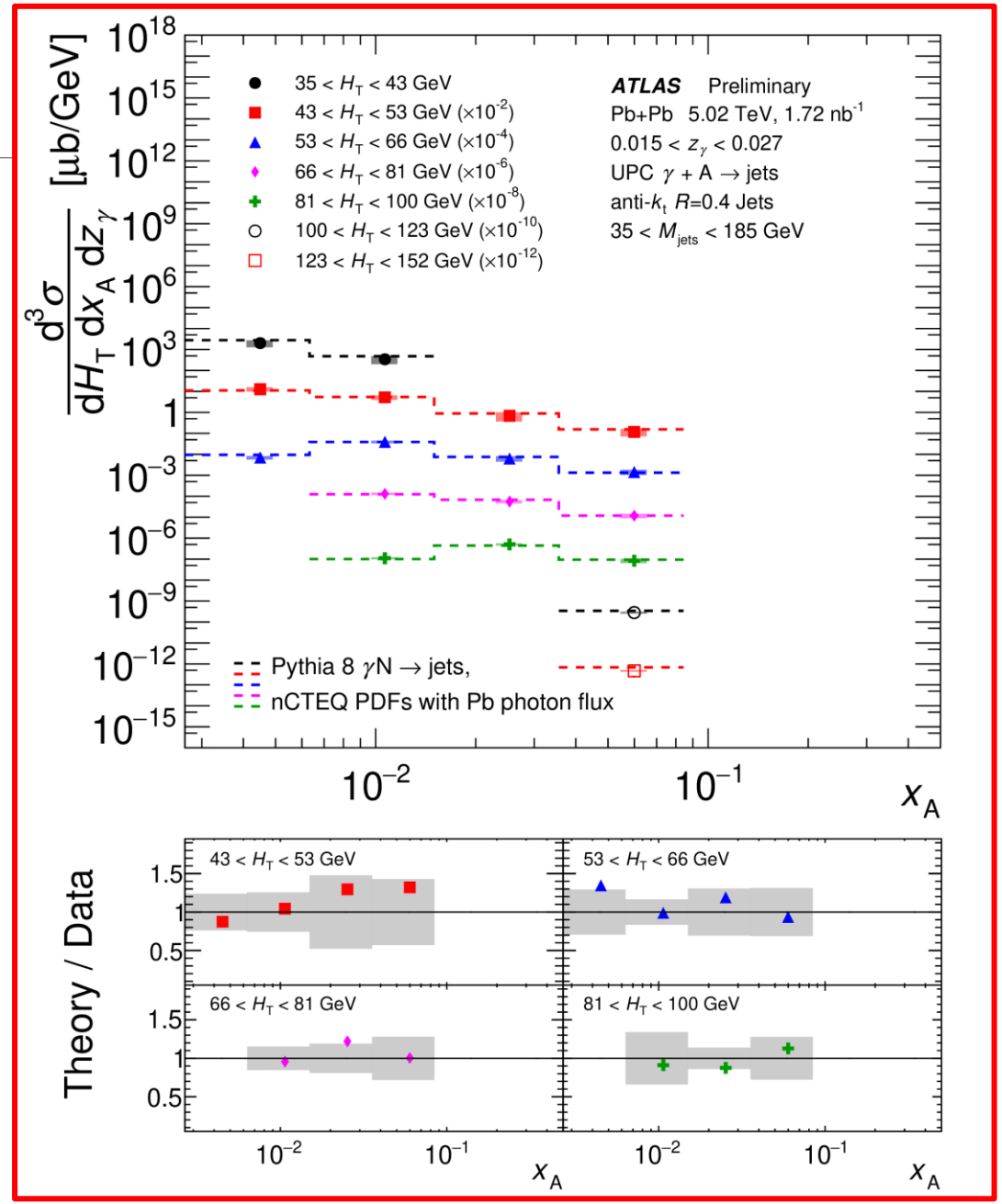

Acceptance and Observables: p+Pb Dijets

$$p_{T,avg} = \frac{p_T^1 + p_T^2}{2} \qquad y^* = \frac{|y_1 - y_2|}{2} \qquad y_b = \frac{y_1 + y_2}{2}$$

$$x_p = \frac{2p_T^{avg}\cosh(y^*)e^{+y_b}}{\sqrt{s}} \qquad x_{Pb} = \frac{2p_T^{avg}\cosh(y^*)e^{-y_b}}{\sqrt{s}}$$

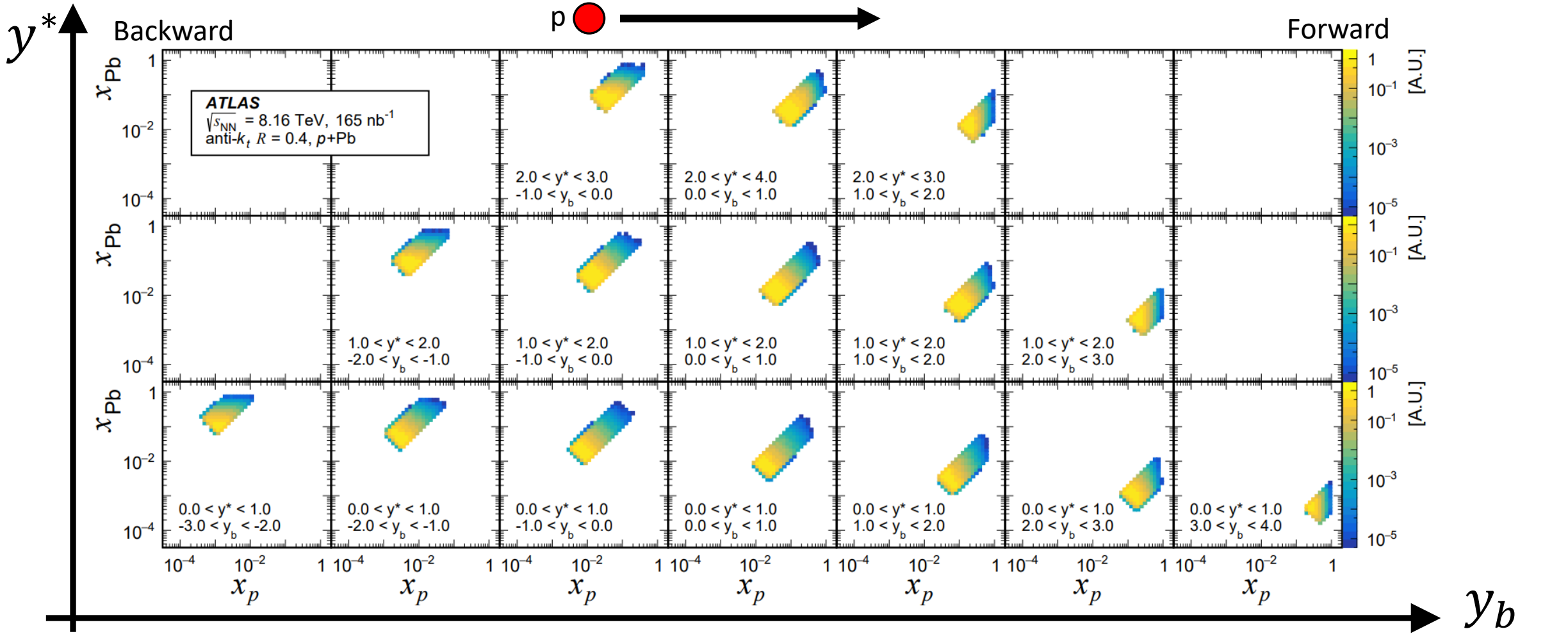

P+Pb Dijet Results in p_T^{avg}, y_b, y^*

$$p_{T,avg} = \frac{p_T^1 + p_T^2}{2}$$

$$y^* = \frac{|y_1 - y_2|}{2}$$

$$y_b = \frac{y_1 + y_2}{2}$$

$$x_p = \frac{2 p_T^{avg} \cosh(y^*) e^{+y_b}}{\sqrt{s}}$$

$$x_{Pb} = \frac{2 p_T^{avg} \cosh(y^*) e^{-y_b}}{\sqrt{s}}$$

$$R_{CP}^{\frac{0-10\%}{60-90\%}}(p_T^{avg}, y_b, y^*) = \frac{\frac{1}{< T_{AB}^{0-10\%} >} \frac{1}{N_{evt}^{0-10\%}} \frac{dN_{dijet}^{0-10\%}}{dp_T^{avg} dy_b dy^*}}{\frac{1}{< T_{AB}^{60-90\%} >} \frac{1}{N_{evt}^{60-90\%}} \frac{dN_{dijet}^{60-90\%}}{dp_T^{avg} dy_b dy^*}}$$

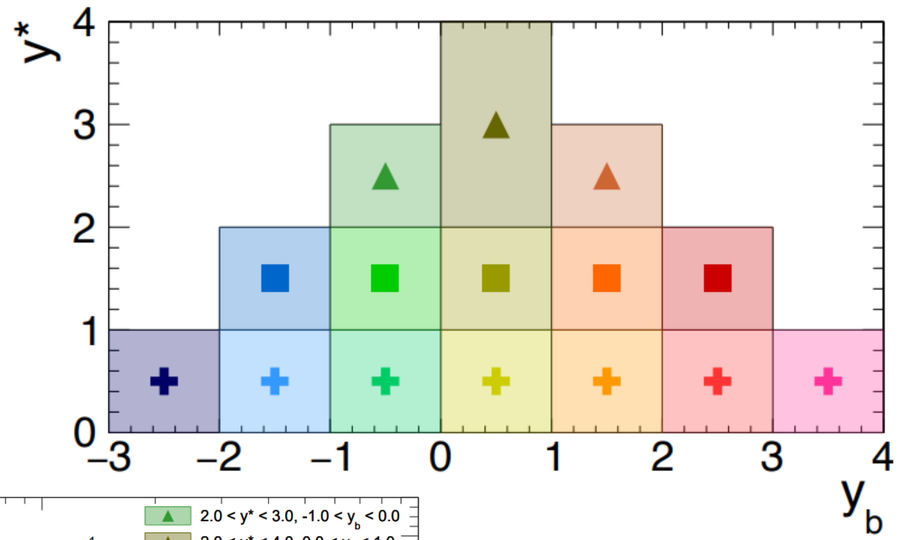

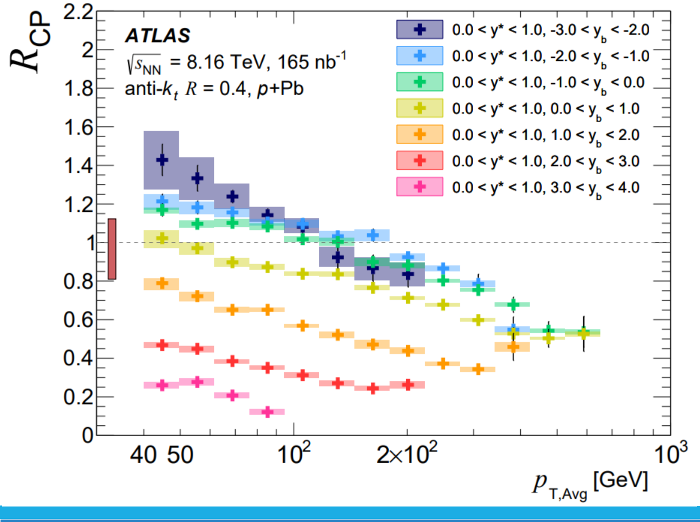

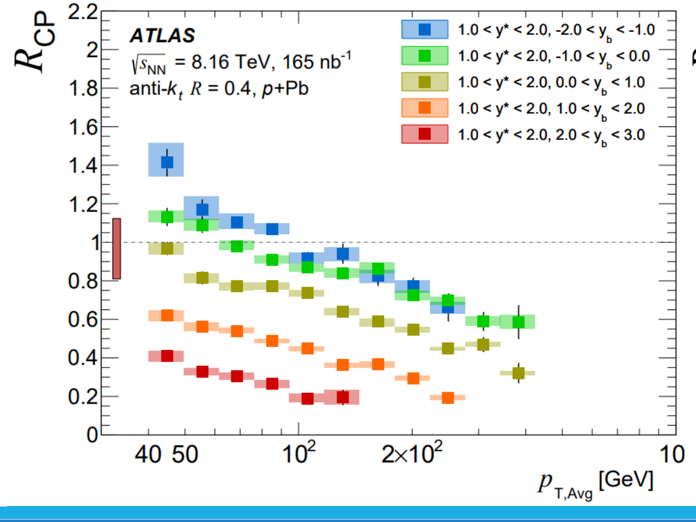

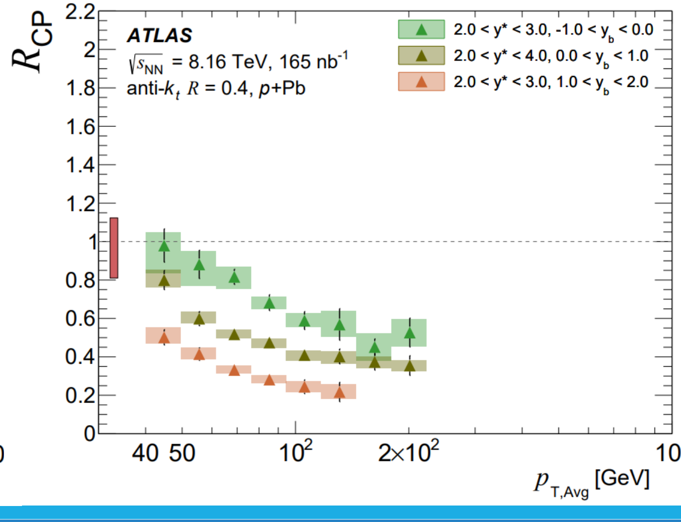

Different panels represent different y^* ranges.

General trend is more suppression with higher p_T^{avg} and y_b.

P+Pb Dijet Results in p_T^{avg}, y_b, y^*

$$p_{T,avg} = \frac{p_T^1 + p_T^2}{2} \qquad y^* = \frac{|y_1 - y_2|}{2} \qquad y_b = \frac{y_1 + y_2}{2} \quad \Rightarrow \quad x_p = \frac{2p_T^{avg}\cosh(y^*)e^{+y_b}}{\sqrt{s}} \qquad x_{Pb} = \frac{2p_T^{avg}\cosh(y^*)e^{-y_b}}{\sqrt{s}}$$

$$R_{CP}^{\frac{0-10\%}{60-90\%}}(p_T^{avg}, y_b, y^*) = \frac{\frac{1}{< T_{AB}^{0-10\%} >}\frac{1}{N_{evt}^{0-10\%}}\frac{dN_{dijet}^{0-10\%}}{dp_T^{avg}dy_b dy^*}}{\frac{1}{< T_{AB}^{60-90\%} >}\frac{1}{N_{evt}^{60-90\%}}\frac{dN_{dijet}^{60-90\%}}{dp_T^{avg}dy_b dy^*}}$$

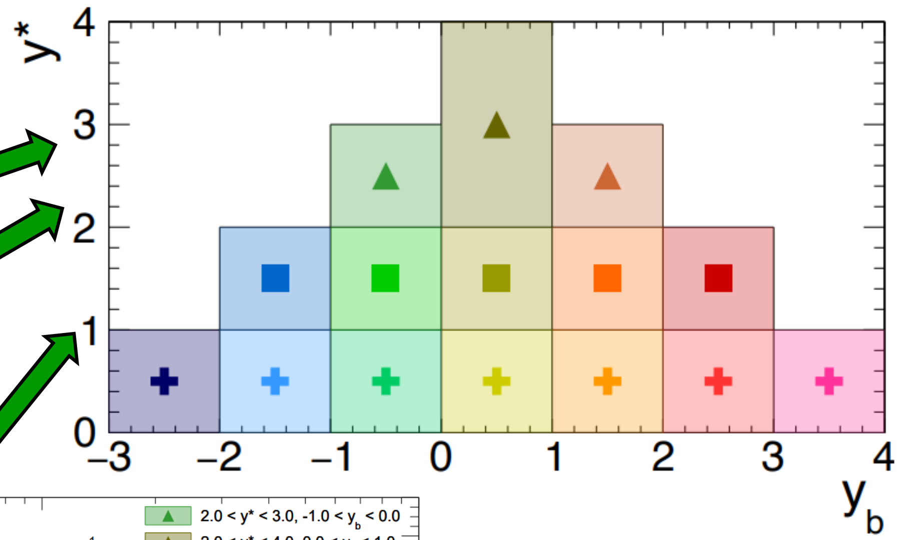

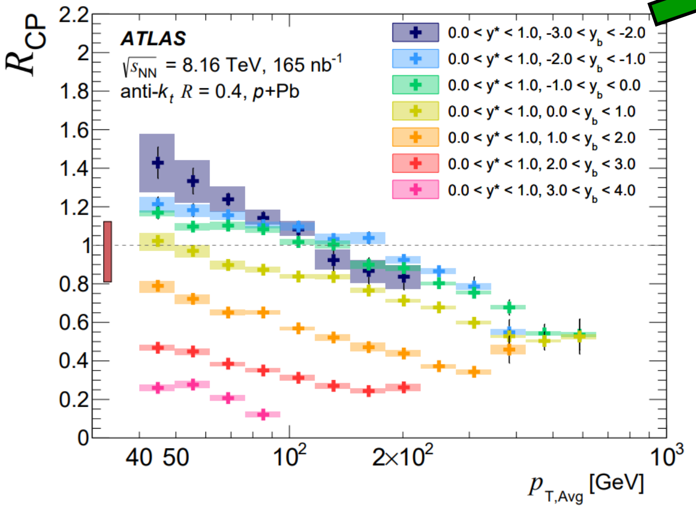

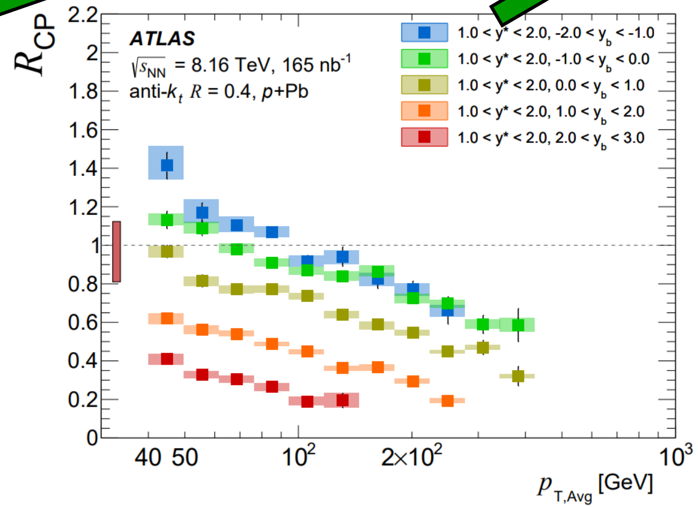

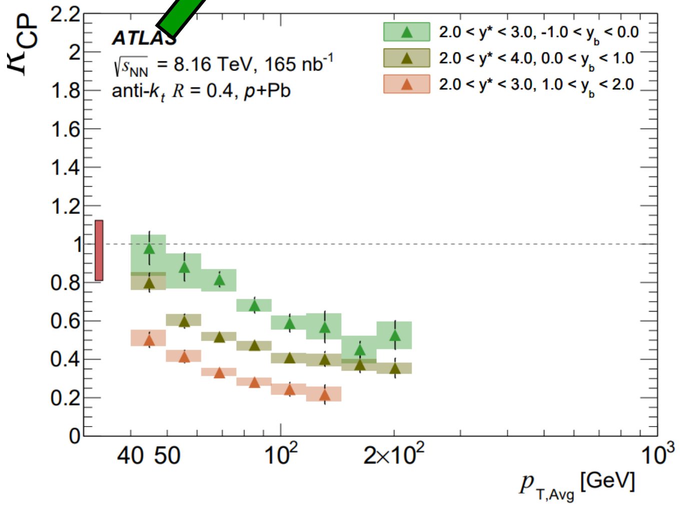

Different panels represent different y^* ranges.

General trend is more suppression with higher p_T^{avg} and y_b.

Mapping Results to Parton Kinematics

$$p_{T,avg} = \frac{p_T^1 + p_T^2}{2} \qquad y^* = \frac{|y_1 - y_2|}{2} \qquad y_b = \frac{y_1 + y_2}{2}$$

$$x_p = \frac{2p_T^{avg}\cosh(y^*)e^{+y_b}}{\sqrt{s}} \qquad x_{Pb} = \frac{2p_T^{avg}\cosh(y^*)e^{-y_b}}{\sqrt{s}}$$

For mapping the results, bin centers are used in p_T^{avg}.

The y^* and y_b mapping uses each bin's mean value.

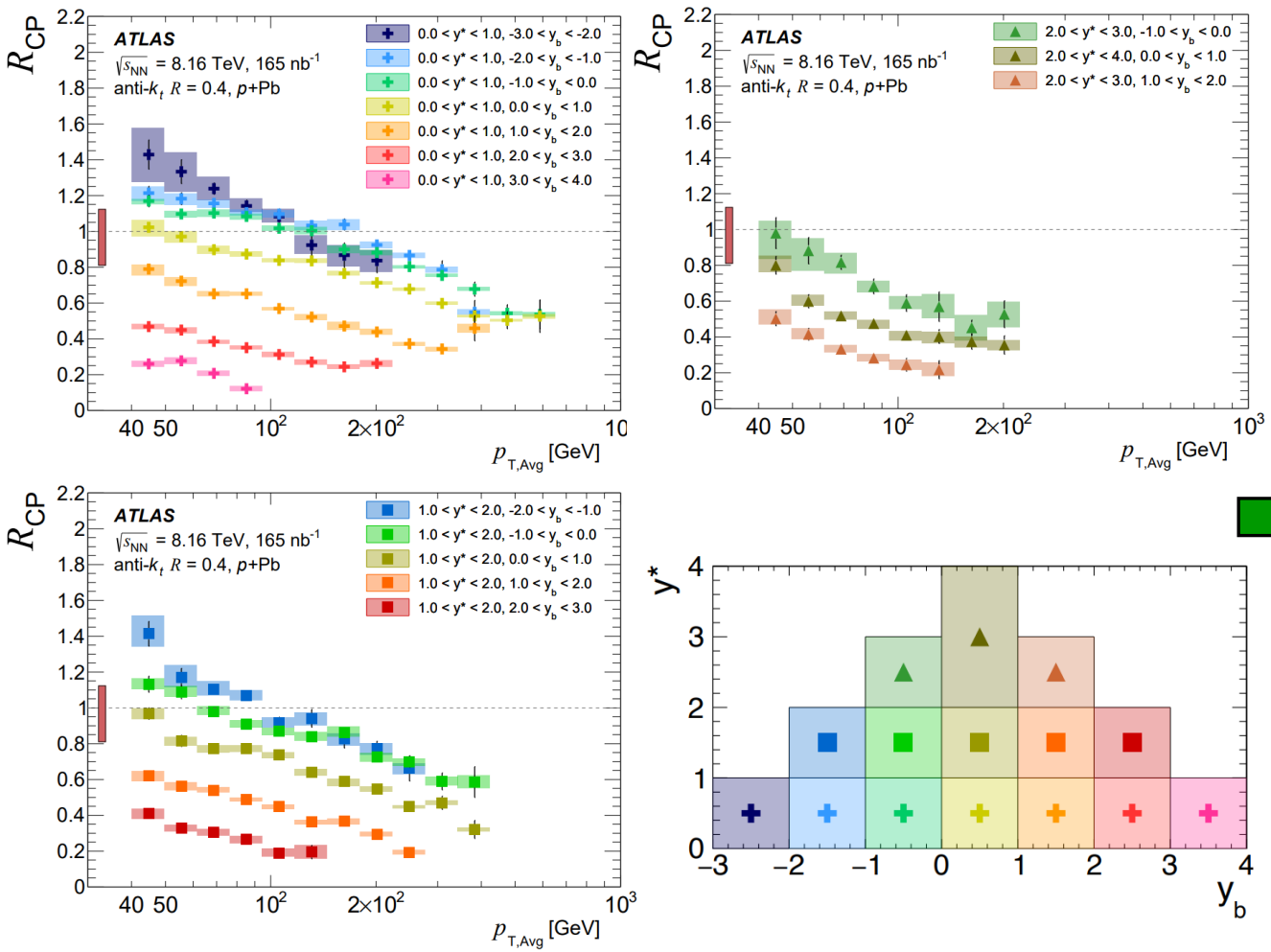

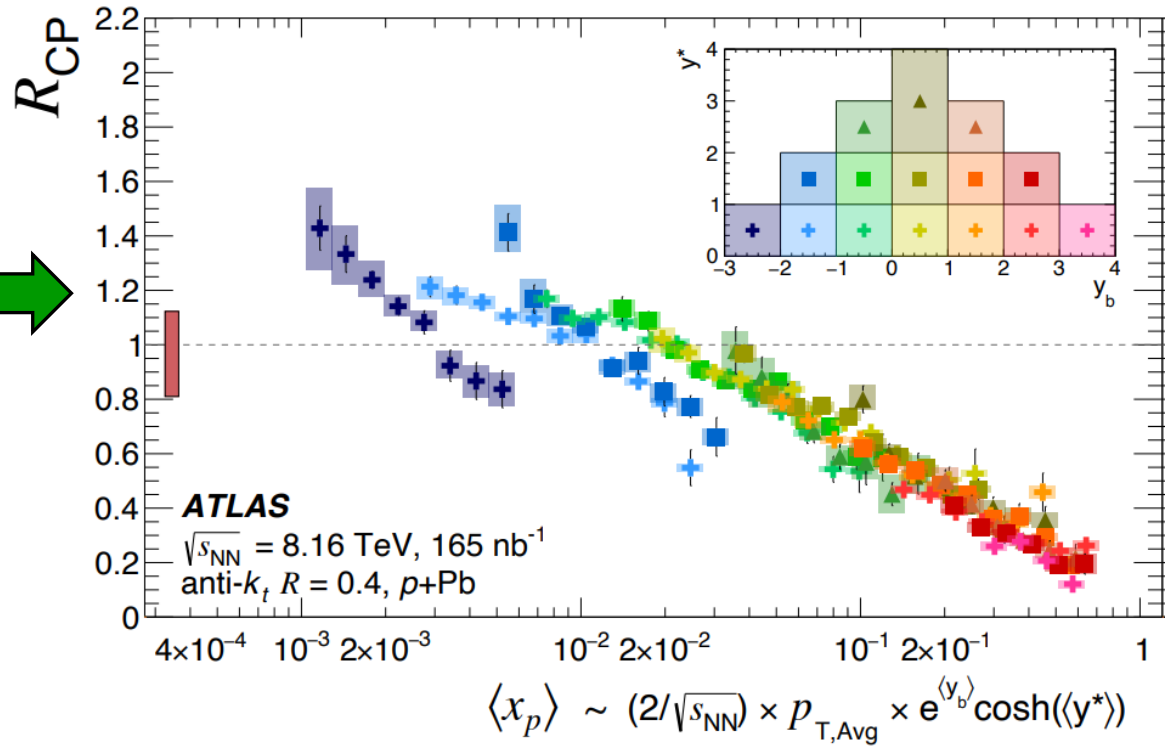

P+Pb Dijet Results: Trends in R_{CP}

More details available in poster by R. Longo

Credit: R. Longo

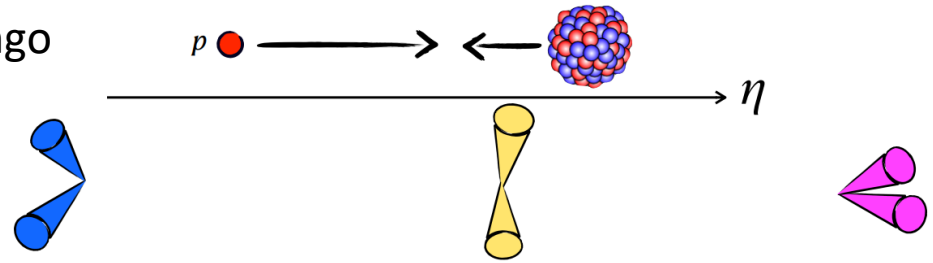

$$x_p = \frac{2p_T^{avg}\cosh(y^*)e^{+y_b}}{\sqrt{s}}$$

$$x_{Pb} = \frac{2p_T^{avg}\cosh(y^*)e^{-y_b}}{\sqrt{s}}$$

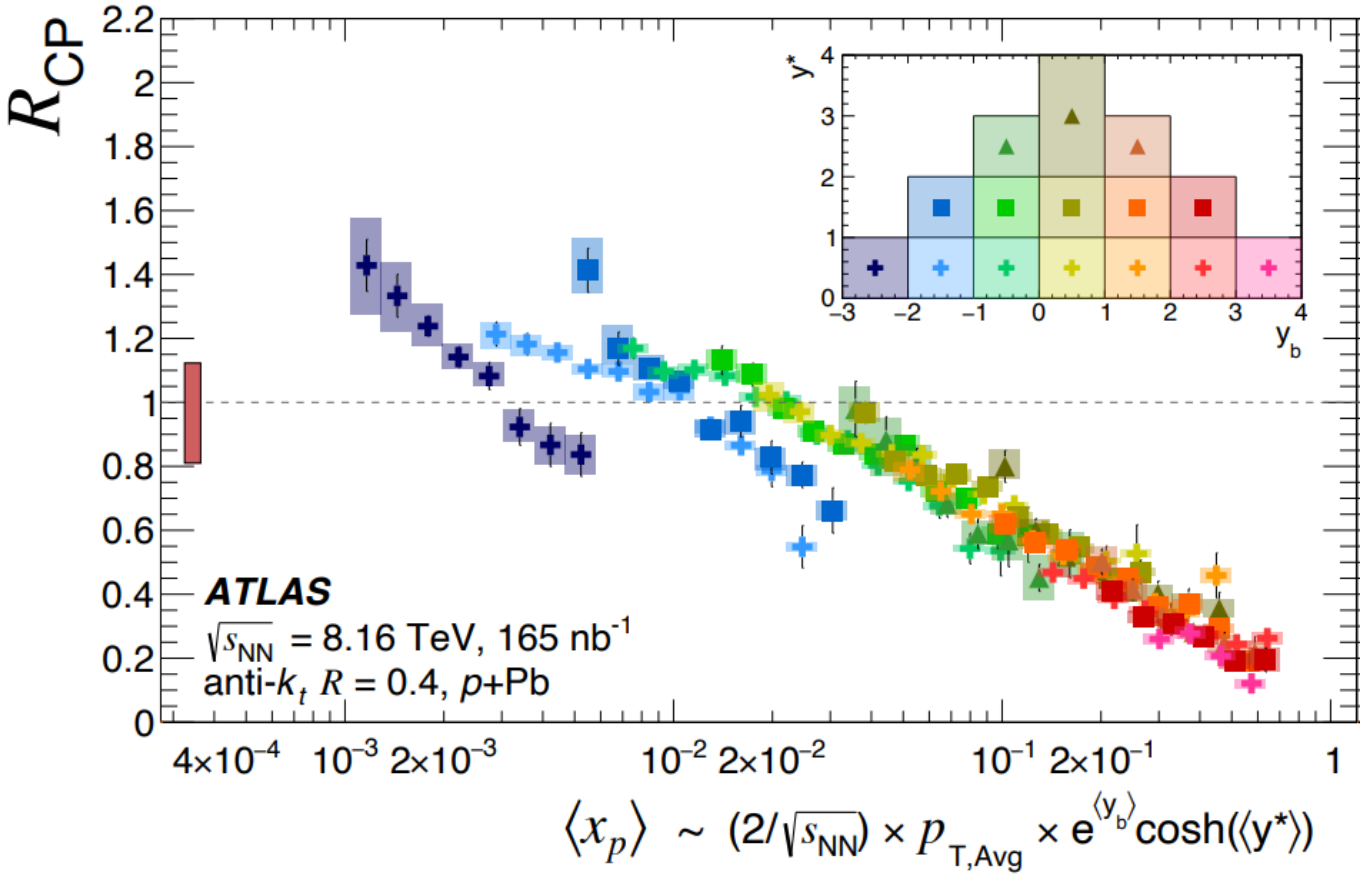

P+Pb Dijet Results: Trends in R_{CP}

More details available in poster by R. Longo

Credit: R. Longo

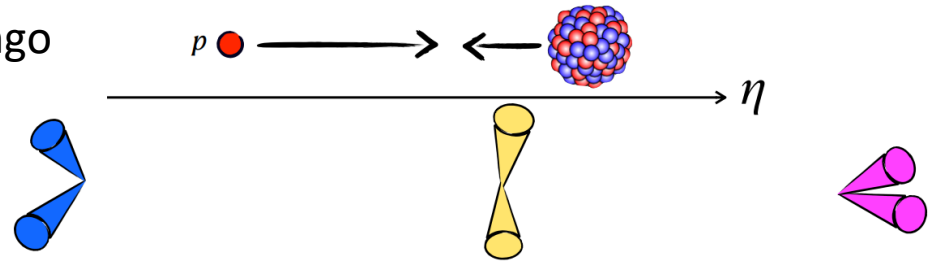

$$x_p = \frac{2p_T^{avg}\cosh(y^*)e^{+y_b}}{\sqrt{s}}$$

$$x_{Pb} = \frac{2p_T^{avg}\cosh(y^*)e^{-y_b}}{\sqrt{s}}$$

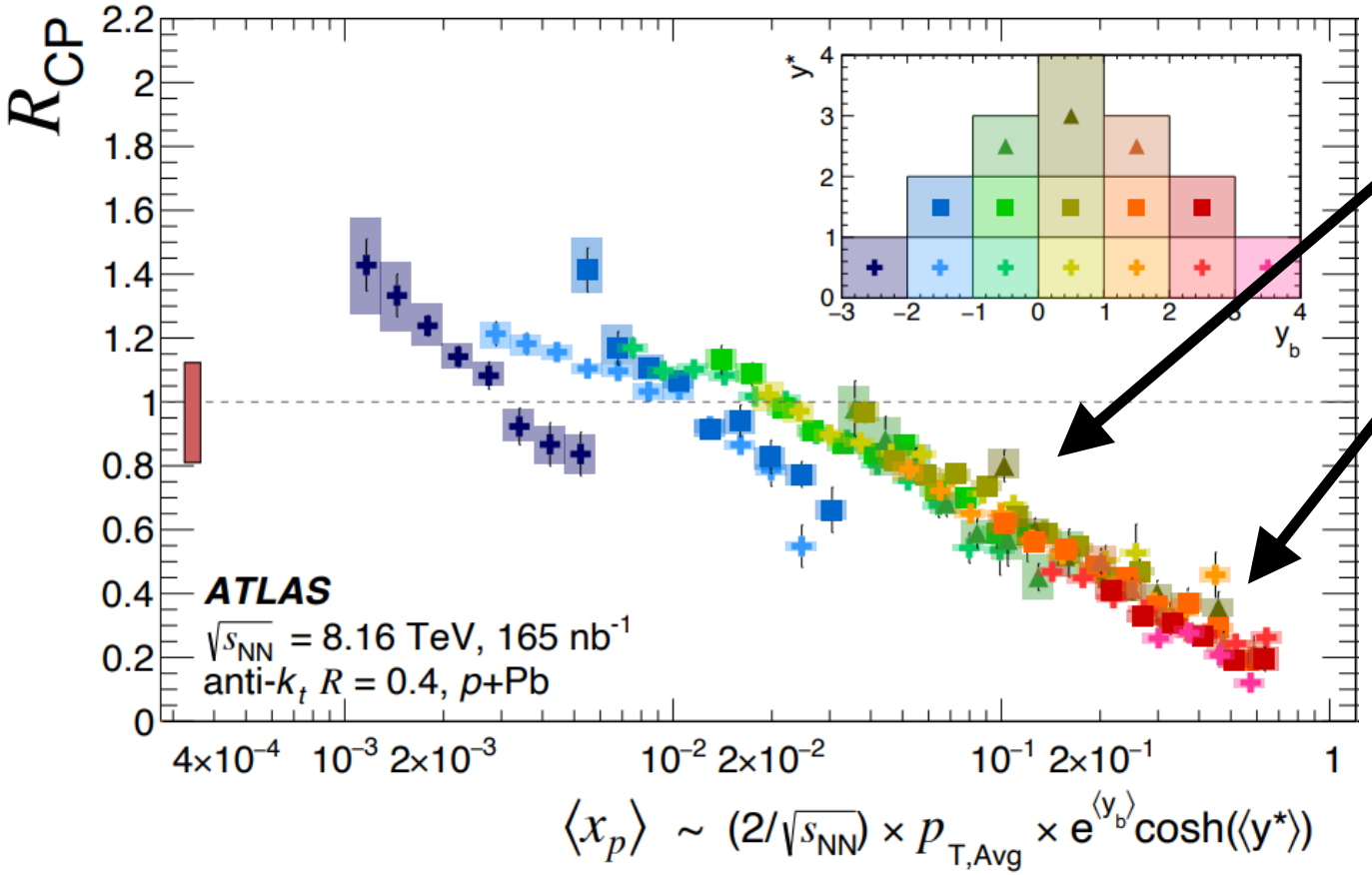

The expected log-linear decrease with x_p from **color transparency** is observed in the valence region.

The very strong suppression at the highest values of x_p is also consistent with this expectation.

P+Pb Dijet Results: Trends in R_{CP}

More details available in poster by R. Longo

Credit: R. Longo

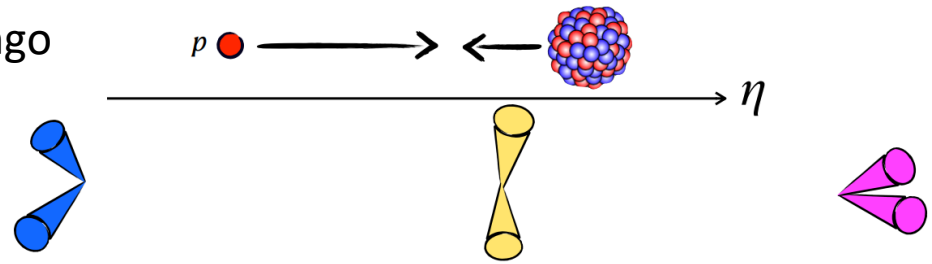

$$x_p = \frac{2p_T^{avg}\cosh(y^*)e^{+y_b}}{\sqrt{s}}$$

$$x_{Pb} = \frac{2p_T^{avg}\cosh(y^*)e^{-y_b}}{\sqrt{s}}$$

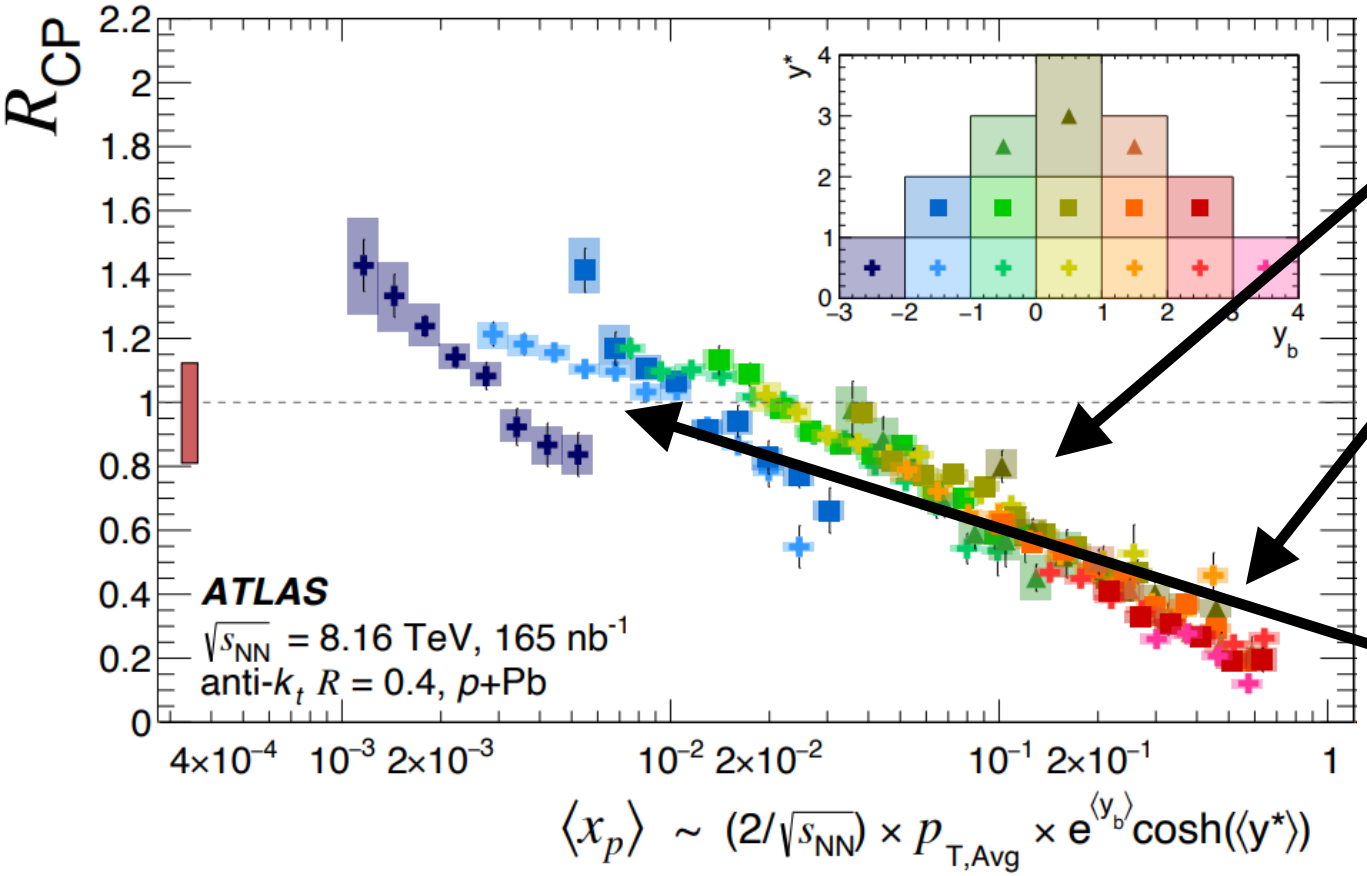

The expected <u>log-linear decrease with x_p</u> from **color transparency** is observed in the valence region.

The very strong suppression at the <u>highest values of x_p</u> is also consistent with this expectation.

The log-linear trend appears to break down in the low-x_p region

P+Pb Dijet Results: Trends in R_{CP}

More details available in poster by R. Longo

Credit: R. Longo

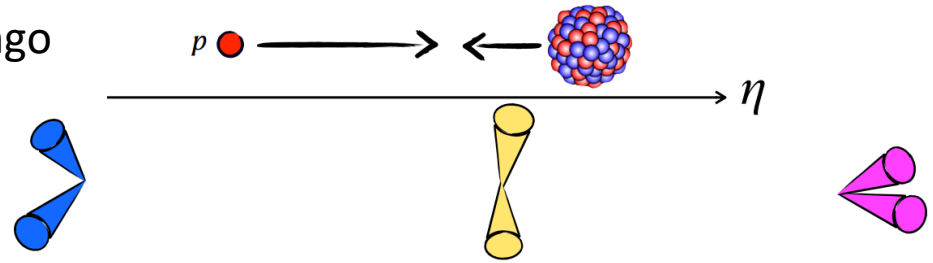

$$x_p = \frac{2p_T^{avg}\cosh(y^*)e^{+y_b}}{\sqrt{s}}$$

$$x_{Pb} = \frac{2p_T^{avg}\cosh(y^*)e^{-y_b}}{\sqrt{s}}$$

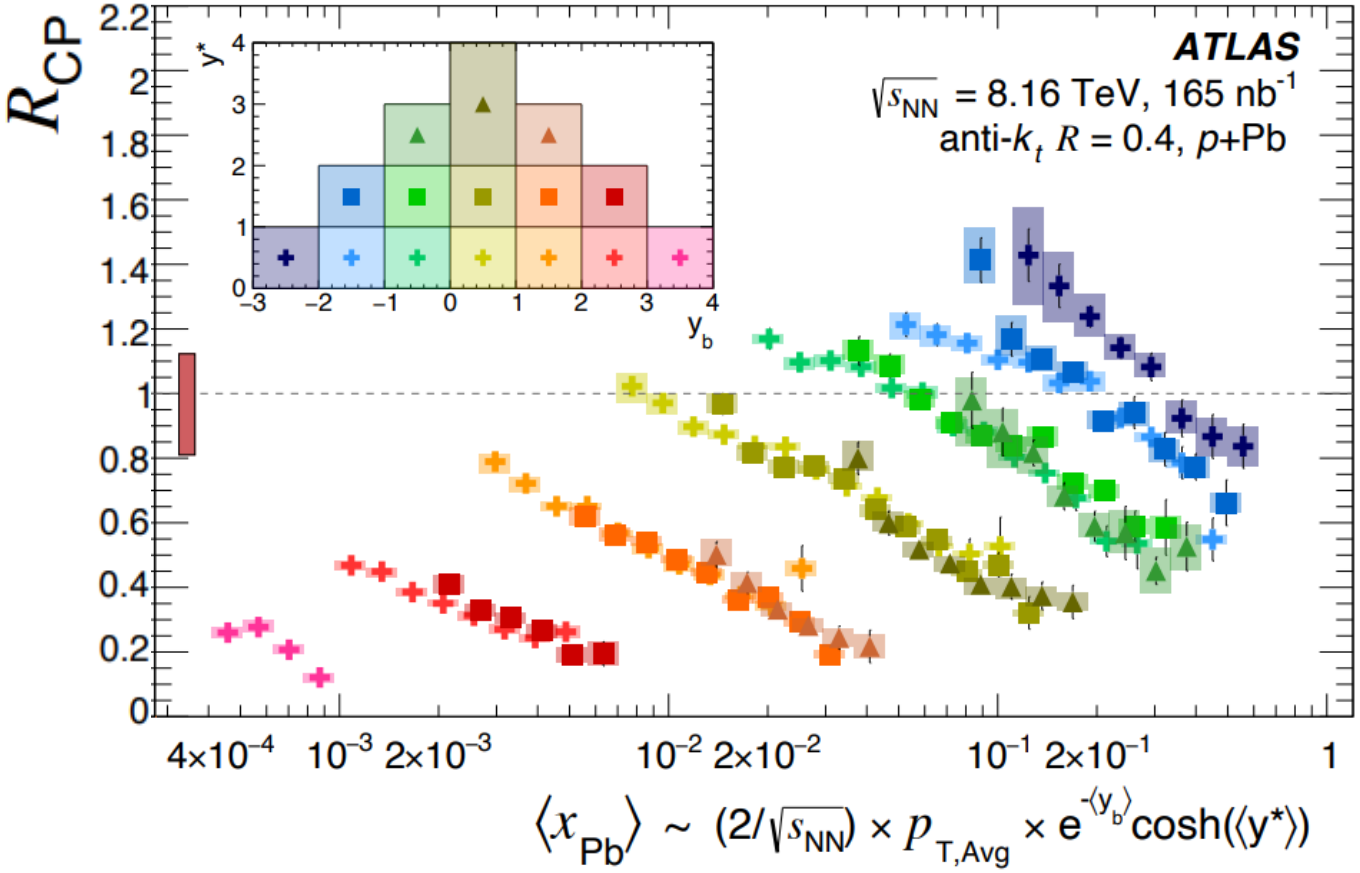

P+Pb Dijet Results: Trends in R_{CP}

More details available in poster by R. Longo

Credit: R. Longo

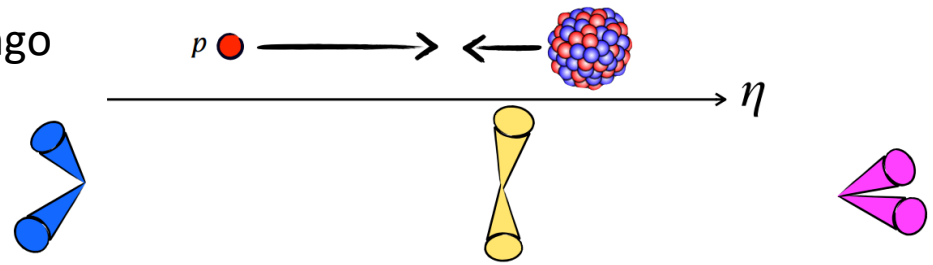

$$x_p = \frac{2p_T^{avg}\cosh(y^*)e^{+y_b}}{\sqrt{s}}$$

$$x_{Pb} = \frac{2p_T^{avg}\cosh(y^*)e^{-y_b}}{\sqrt{s}}$$

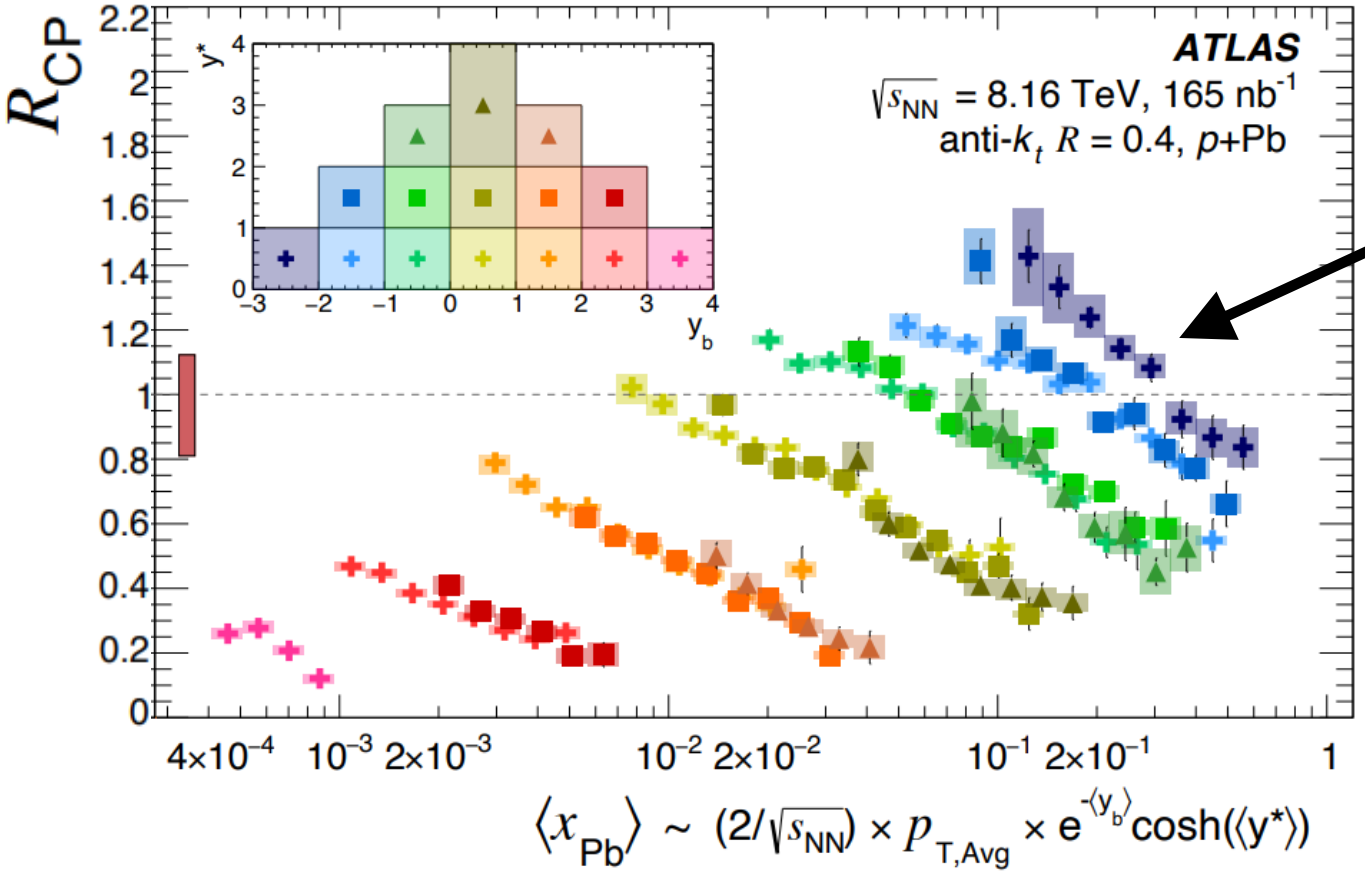

The trend with R_{CP} is much less consistent in x_{Pb} than in x_p .

Suppression depends on y_b and $p_{T,Avg}$ without a clear trend in x_{Pb}.

Conclusions and Next Steps

- Photo-nuclear jet production was measured by ATLAS in 5.02 TeV Pb+Pb collisions with 2018 data.
  - Particle-Flow jets allow for the measurement to be extended even lower in jet p_T while maintaining systematic control.
  - This data can add a wide range of kinematic coverage to existing nPDF constraints.

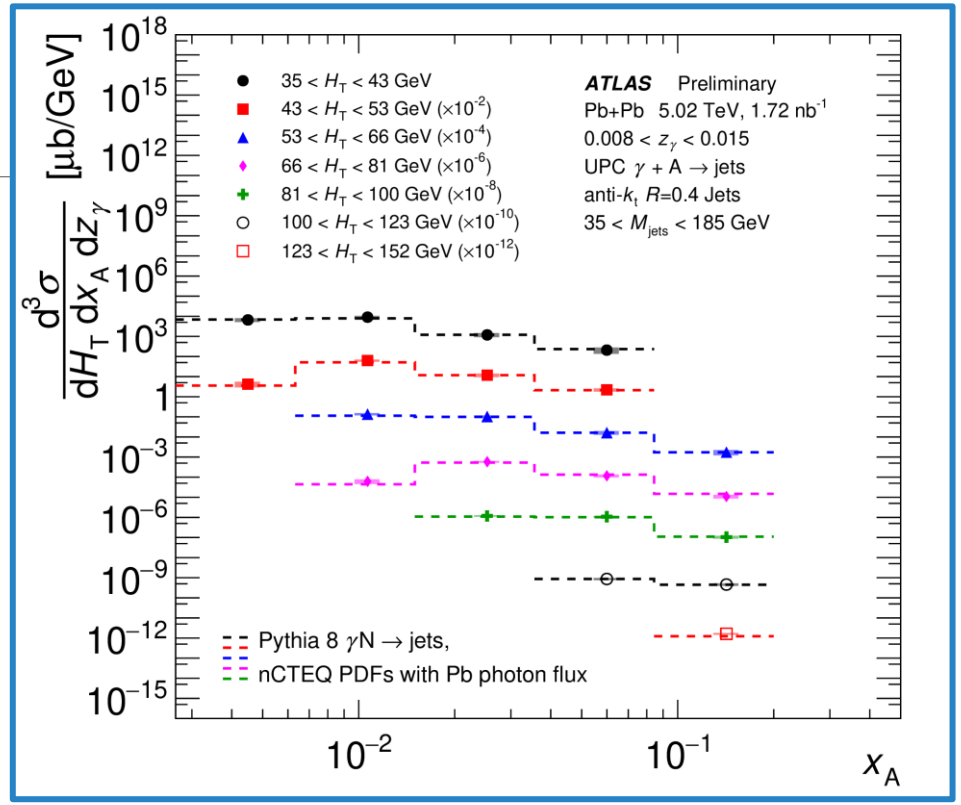

Conclusions and Next Steps

- Photo-nuclear jet production was measured by ATLAS in 5.02 TeV Pb+Pb collisions with 2018 data.
  - Particle-Flow jets allow for the measurement to be extended even lower in jet p_T while maintaining systematic control.
  - This data can add a wide range of kinematic coverage to existing nPDF constraints.
- The centrality dependence of dijet yields in 8.16 TeV p+Pb collisions was measured by ATLAS.
  - Triple-differential dijet yields allow for detailed studies of the approximate partonic system.
  - The resulting trend in R_{CP} suggests that these results are consistent with color transparency.

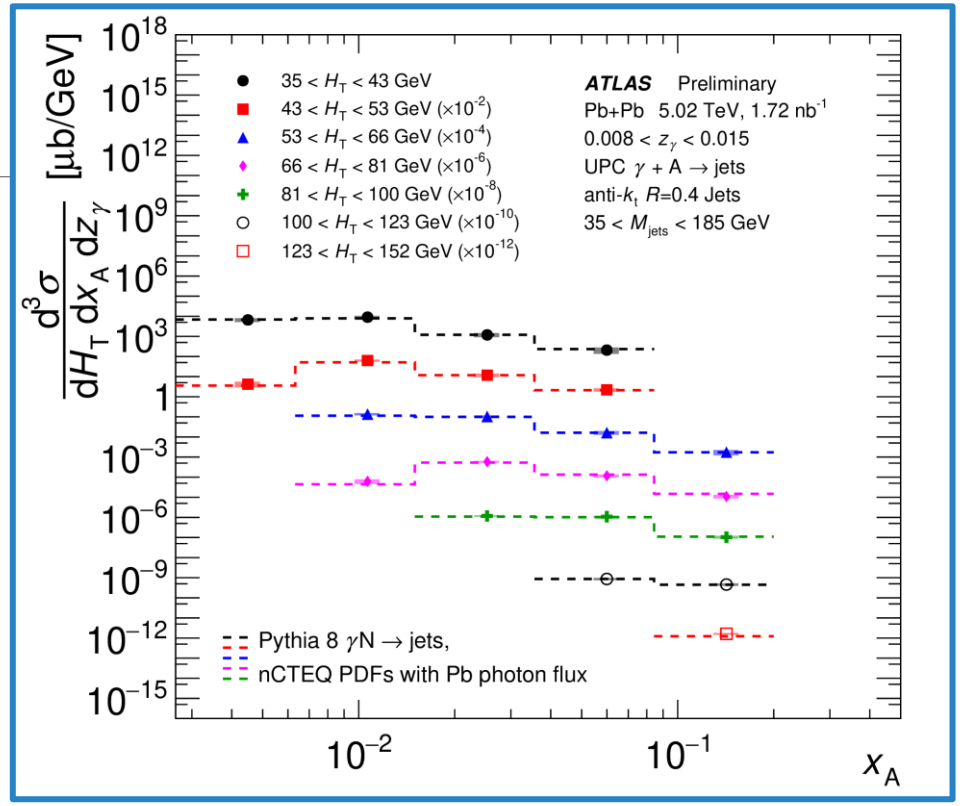

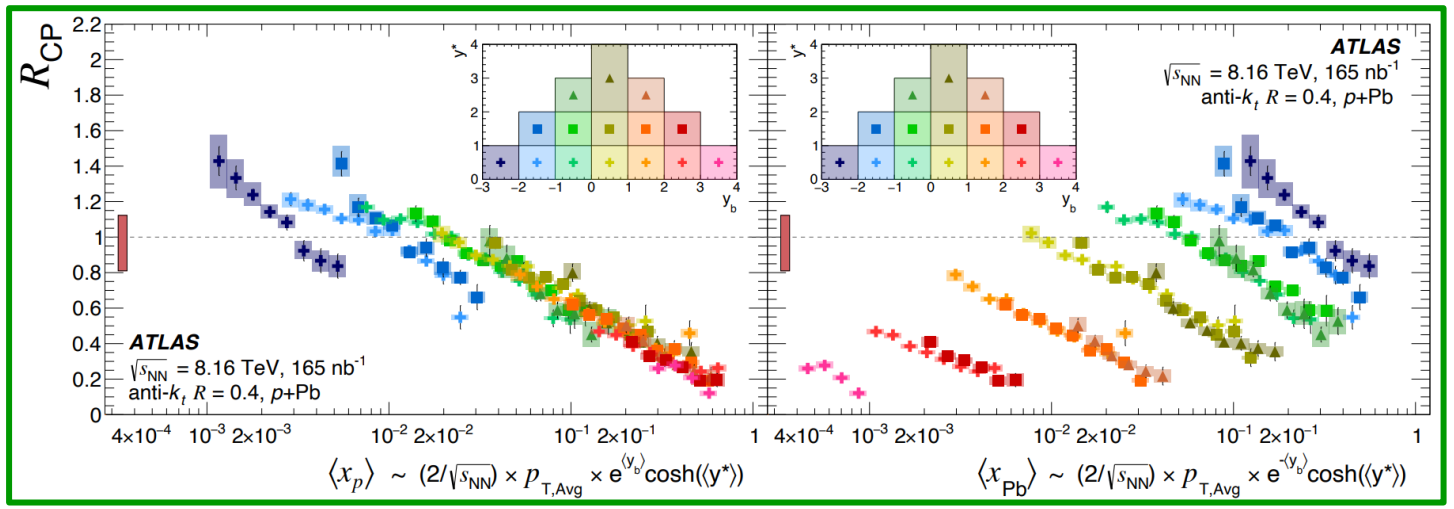

Conclusions and Next Steps

- Photo-nuclear jet production was measured by ATLAS in 5.02 TeV Pb+Pb collisions with 2018 data.
  - Particle-Flow jets allow for the measurement to be extended even lower in jet p_T while maintaining systematic control.
  - This data can add a wide range of kinematic coverage to existing nPDF constraints.
- The centrality dependence of dijet yields in 8.16 TeV p+Pb collisions was measured by ATLAS.
  - Triple-differential dijet yields allow for detailed studies of the approximate partonic system.
  - The resulting trend in R_{CP} suggests that these results are consistent with color transparency.

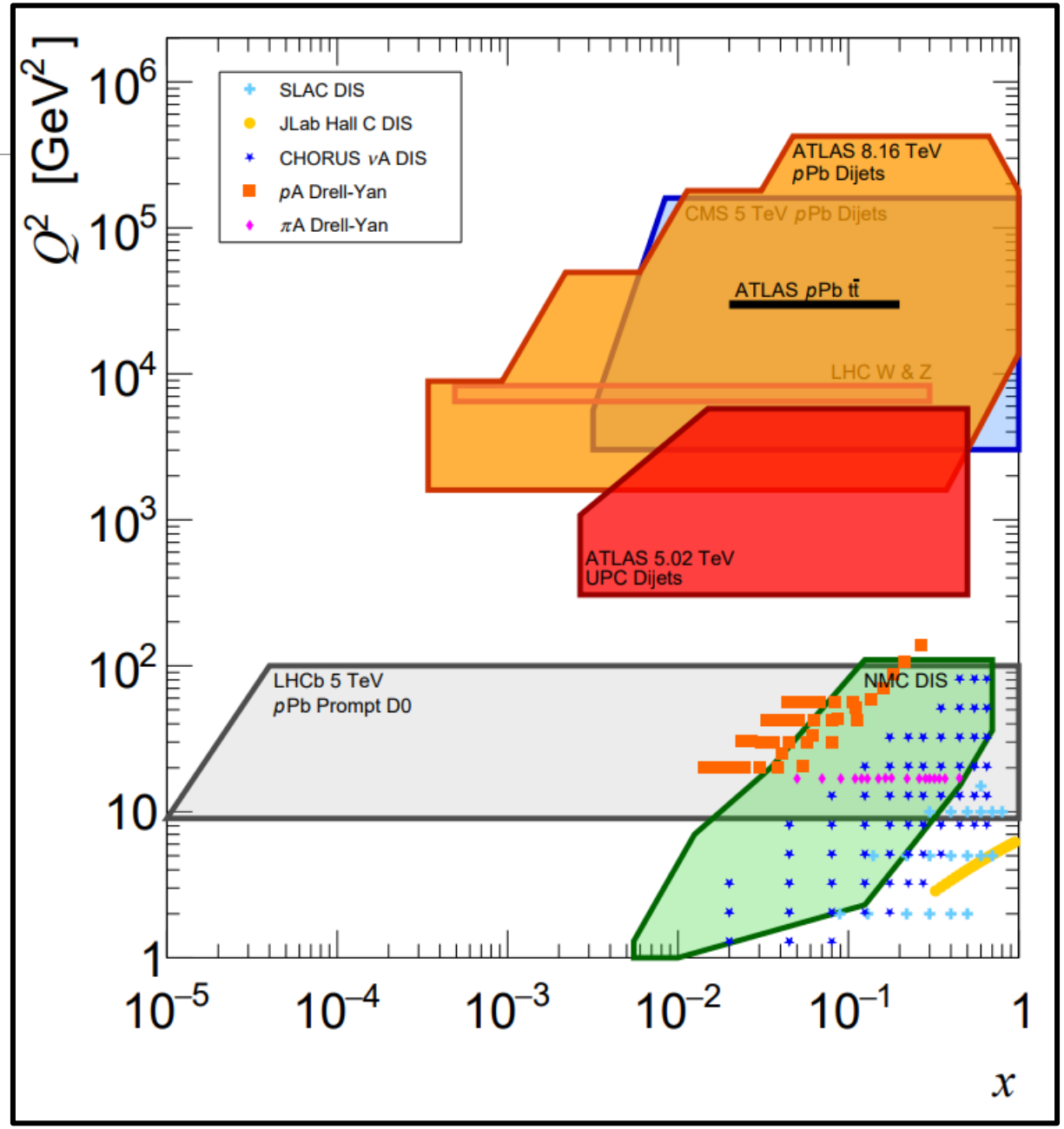

Conclusions and Next Steps

- Photo-nuclear jet production was measured by ATLAS in 5.02 TeV Pb+Pb collisions with 2018 data.
  - Particle-Flow jets allow for the measurement to be extended even lower in jet p_T while maintaining systematic control.
  - This data can add a wide range of kinematic coverage to existing nPDF constraints.
- The centrality dependence of dijet yields in 8.16 TeV p+Pb collisions was measured by ATLAS.
  - Triple-differential dijet yields allow for detailed studies of the approximate partonic system.
  - The resulting trend in R_{CP} suggests that these results are consistent with color transparency.

These results are closely related to the early physics goals of the EIC!

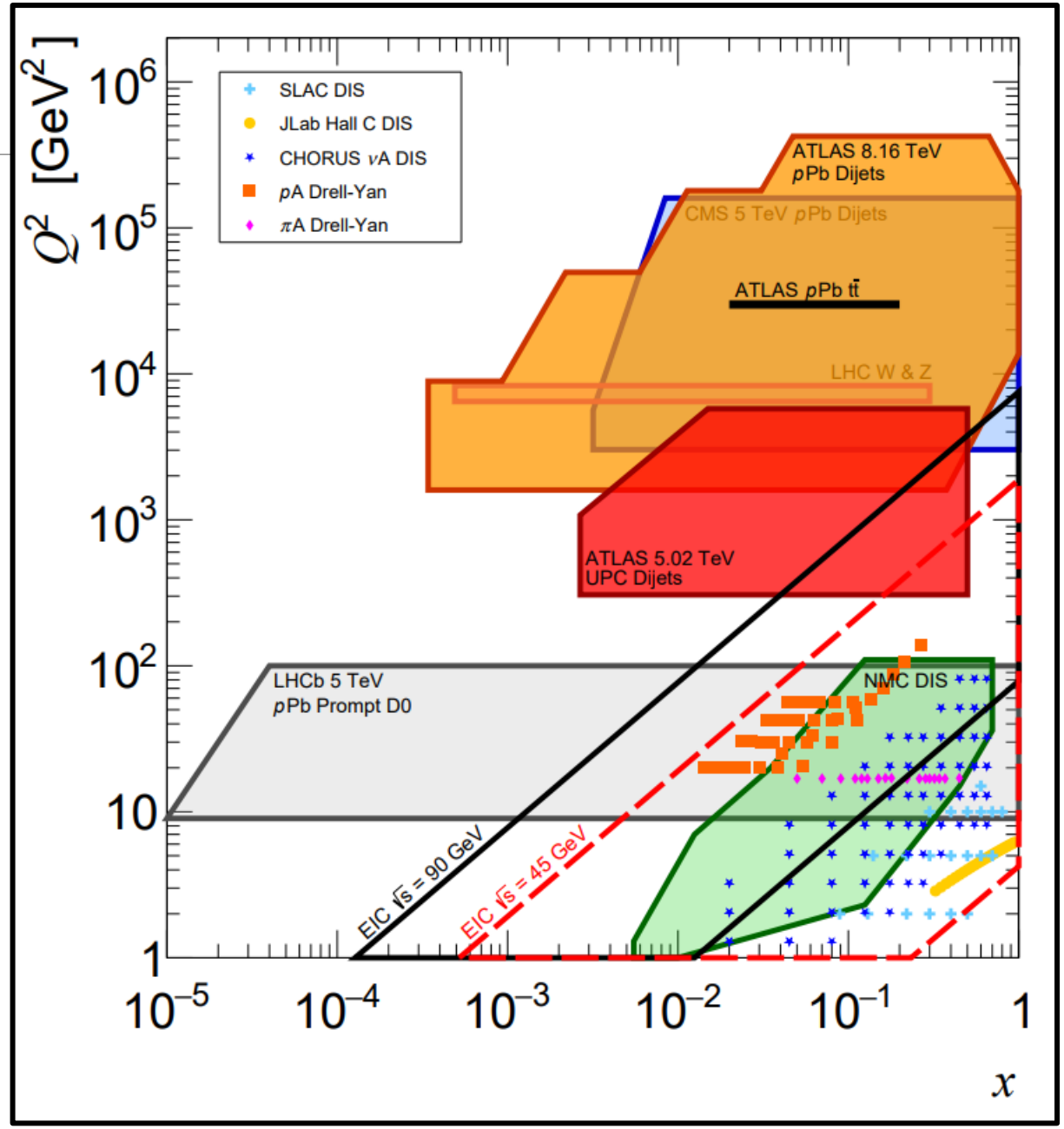

Backup

Selecting Photo-nuclear Jet Events

Event Selections

- 0nXn requirement for nuclear breakup in exactly one ATLAS Zero-Degree Calorimeter (ZDC)
- Large rapidity gaps on one side of the detector
  - To veto $\gamma\gamma \rightarrow q\bar{q}$, also require $\Delta\eta_A^{edge} < 3$.
- At least two Particle-Flow jets with $p_T > 15$ GeV.

Selecting at least two jets allows access to the hard-scattering kinematics.

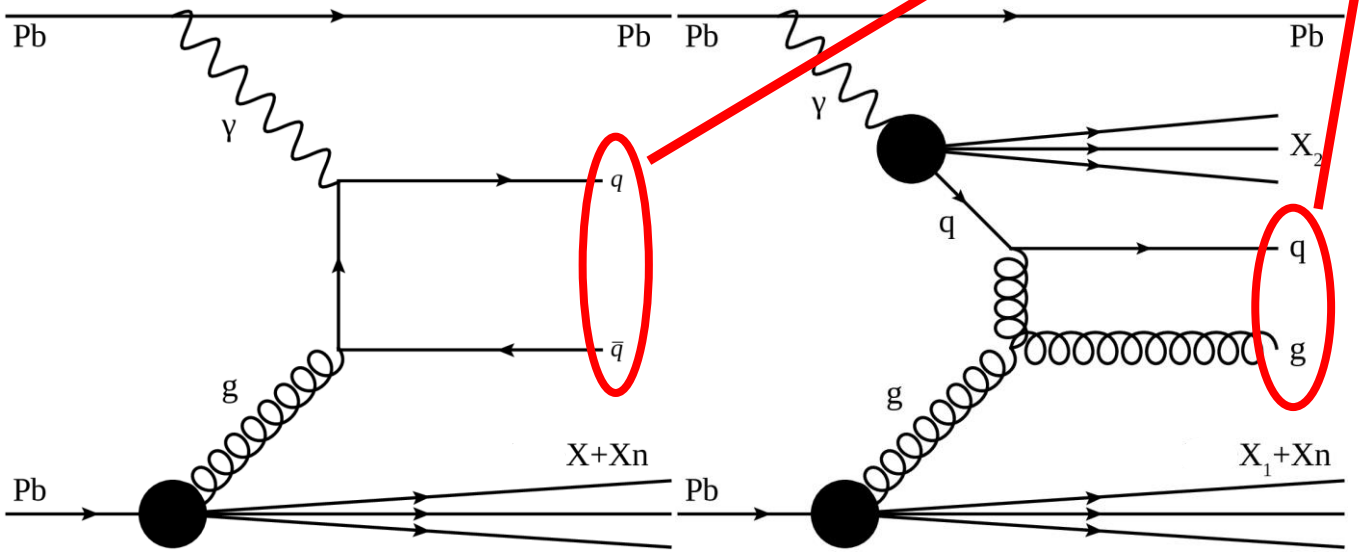

$$H_T = \sum_i p_T^i$$

$$x_A = \frac{M_{jets} e^{-y_{jets}}}{\sqrt{s_{NN}}}$$

$$z_\gamma = \frac{M_{jets} e^{+y_{jets}}}{\sqrt{s_{NN}}}$$

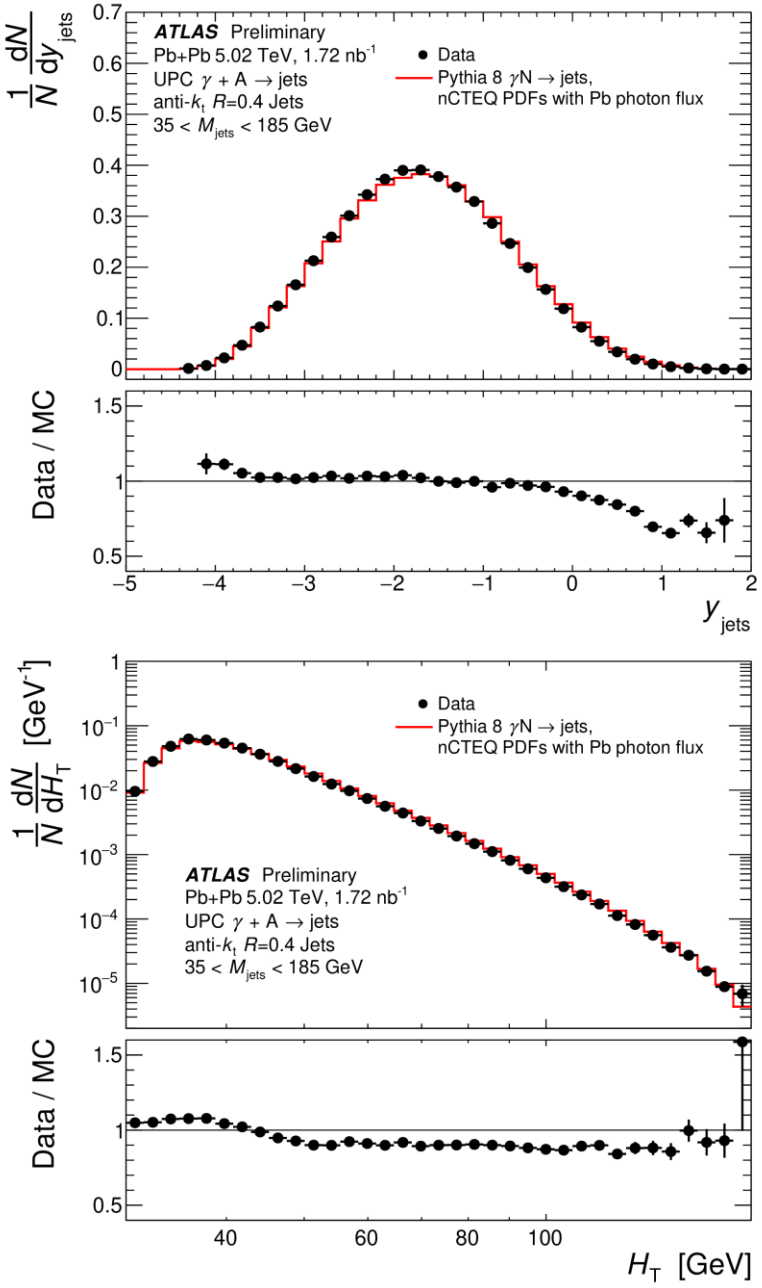

Theoretical Modeling of Nuclear Breakup

- The photon flux available through Pythia makes certain overly-simplified assumptions which we correct via modeling with STARlight.

We integrate over A-A impact parameter (b) and the impact parameter relative to the photon-emitting nucleus (s_A).

Correction for the probability of breakup due to additional EM interactions

Nuclear thickness function

$$F^{\text{eff}}_{\gamma/A}(E_\gamma) \equiv \int \mathrm{d}^2b\mathrm{d}^2s_A P_{\text{no had}}(b) P_{\text{no EM}}(b) f_{\gamma/A}(E_\gamma, s) T_B(\vec{s}_A - \vec{b})$$

Correction for the probability of breakup due to hadronic interactions (overlap veto)

The photon flux from Pythia uses a point source, so this term corrects for coherent nuclear emission.

Importance of Forward Neutrons: *XnXn* Events

The photo-nuclear jet requirements select events with very high-energy photons.

- $E_\gamma \propto 1/b \rightarrow$ Biases towards lower impact parameter collisions
- Much higher probability of breakup due to additional EM interactions

This theoretical model for breakup is used to compare theory to data.

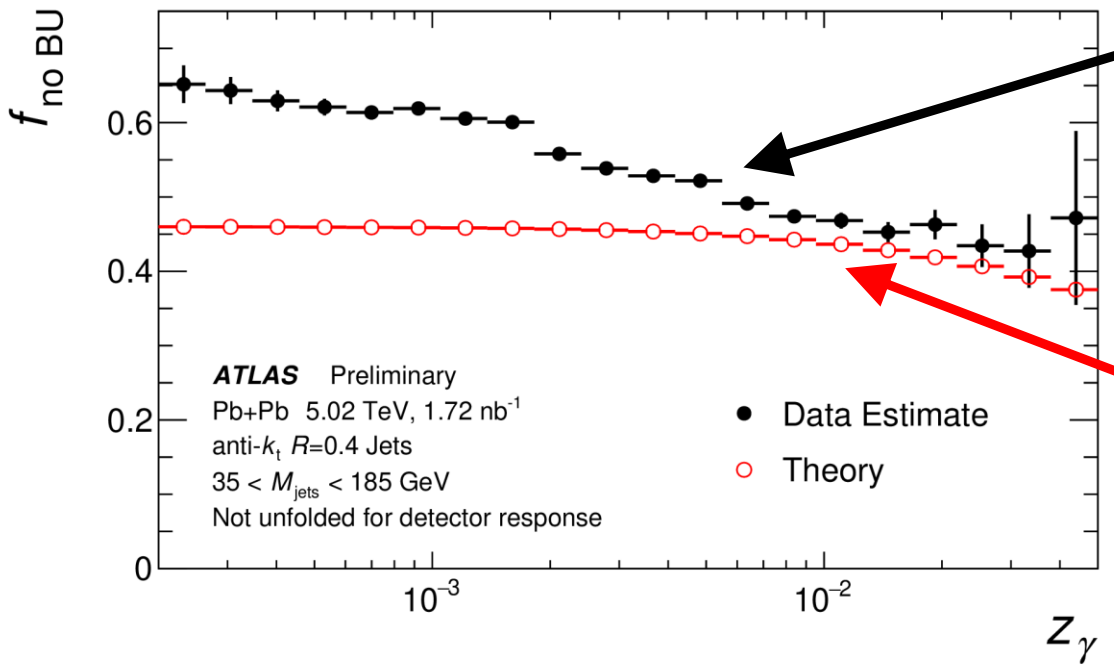

Studies of dijet events with large gaps on one side estimate about 50% of photo-nuclear jet production breaks up!

Basic theoretical modeling predicts an even higher rate.

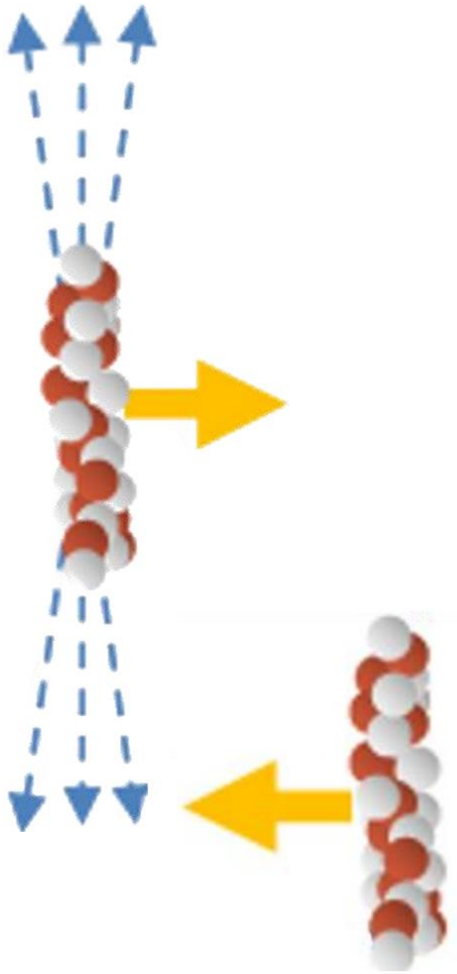

Acceptance and Observables: UPC Dijets

$$H_T = \sum_i p_T^i \qquad x_A = \frac{M_{jets} e^{-y_{jets}}}{\sqrt{s_{NN}}} \qquad z_\gamma = \frac{M_{jets} e^{+y_{jets}}}{\sqrt{s_{NN}}} \qquad \frac{d^3\sigma}{dH_T dx_A dz_\gamma} = \frac{1}{\mathcal{L}} \frac{\Delta Y}{\Delta H_T \Delta x_A \Delta z_\gamma}$$

Cross-sections are measured and unfolded in H_T, x_A, and z_γ

Results are corrected using a theoretical model for the EM dissociation probability.

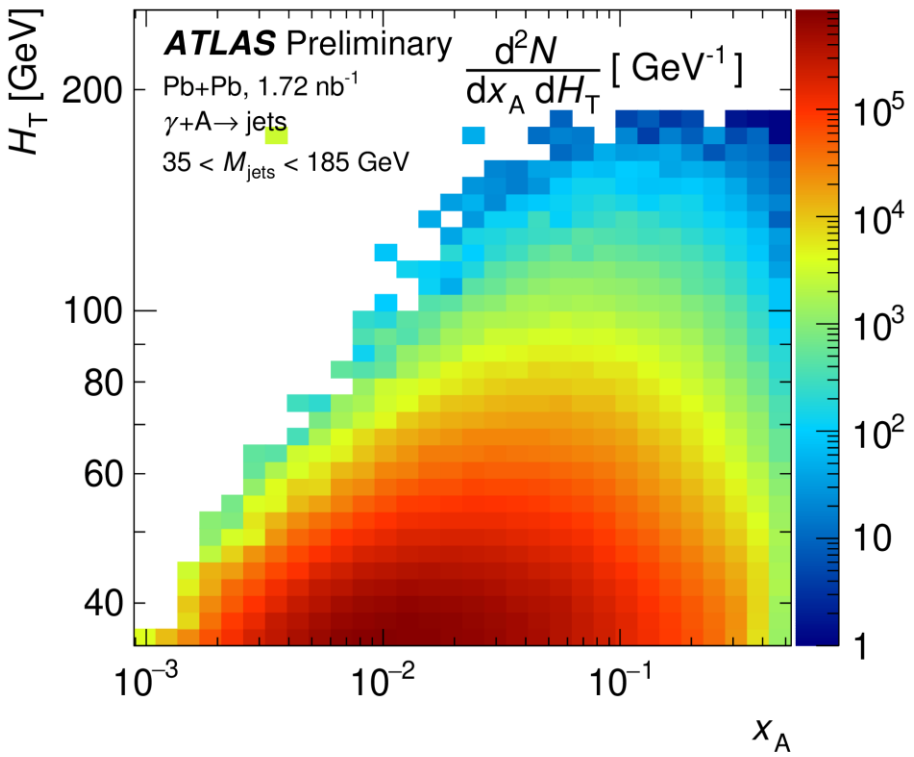

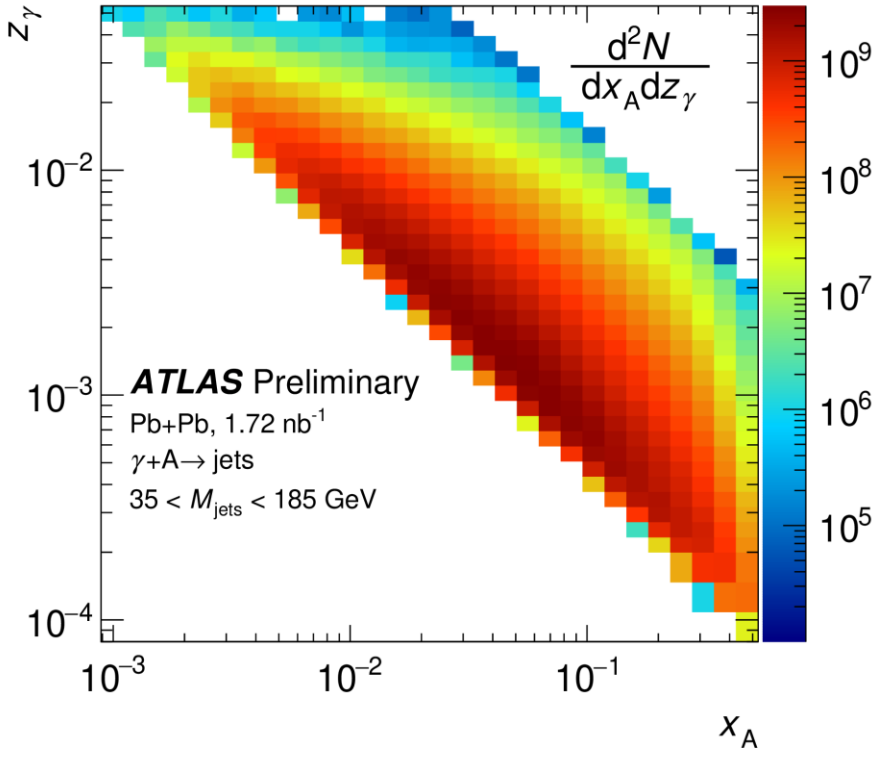

Acceptance and Observables: UPC Dijets

$$H_T = \sum_i p_T^i \qquad x_A = \frac{M_{jets} e^{-y_{jets}}}{\sqrt{s_{NN}}} \qquad z_\gamma = \frac{M_{jets} e^{+y_{jets}}}{\sqrt{s_{NN}}} \qquad \frac{d^3\sigma}{dH_T dx_A dz_\gamma} = \frac{1}{\mathcal{L}} \frac{\Delta Y}{\Delta H_T \Delta x_A \Delta z_\gamma}$$

H_T does not depend strongly on x_A or z_γ.

Acceptance in x_A is strongly dependent on the photon energy, z_γ.

Cross-sections are measured and unfolded in H_T, x_A, and z_γ.

Results are corrected using a theoretical model for the EM dissociation probability.

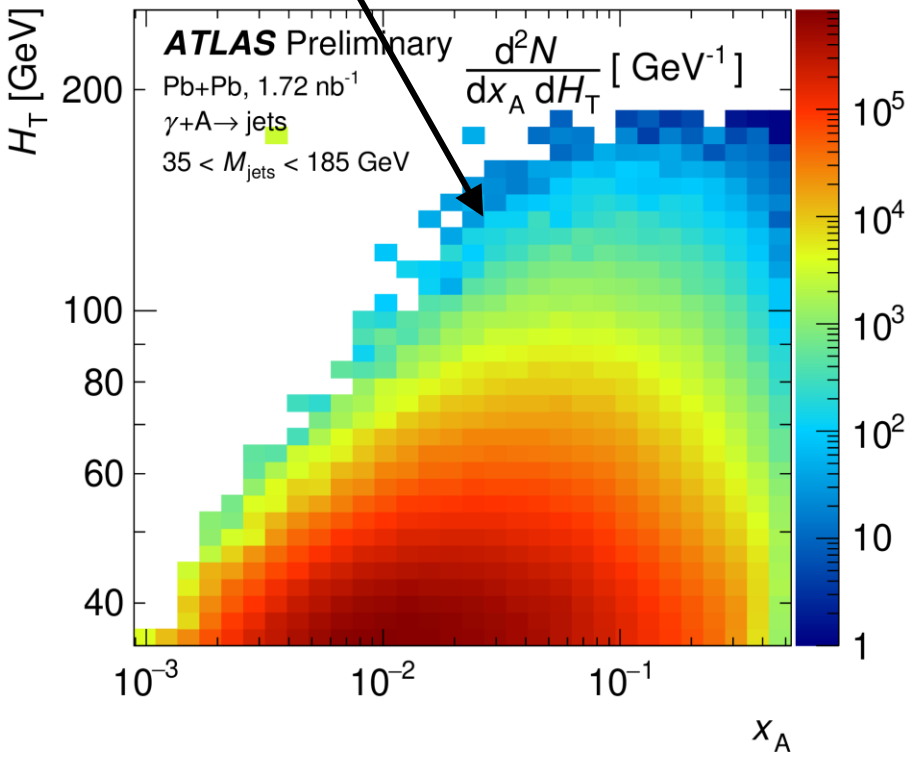

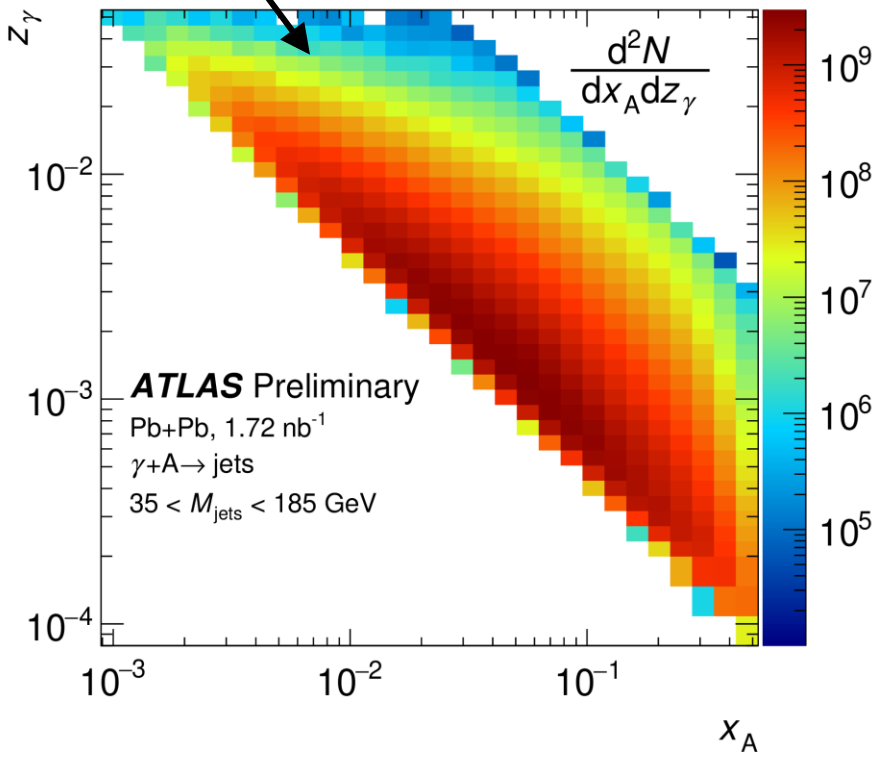

The Measured Photon Flux

- The distribution of z_γ values for large x_A in bins of H_T (right) demonstrates the measured photon flux.
  - The breakup model performs well within systematic uncertainties.
  - Disagreements appear to arise at low z_γ, where the breakup model tends to over-correct.

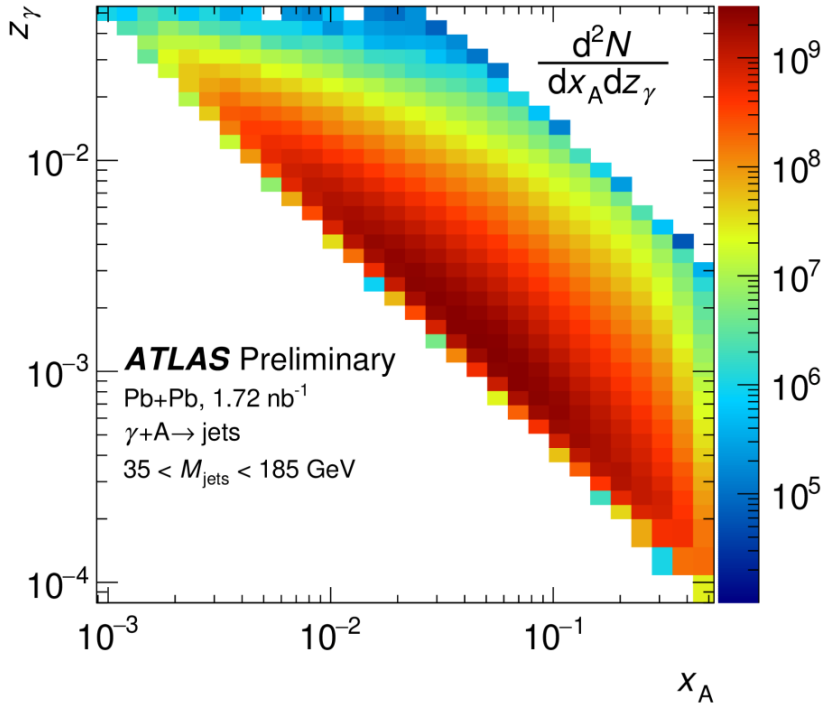

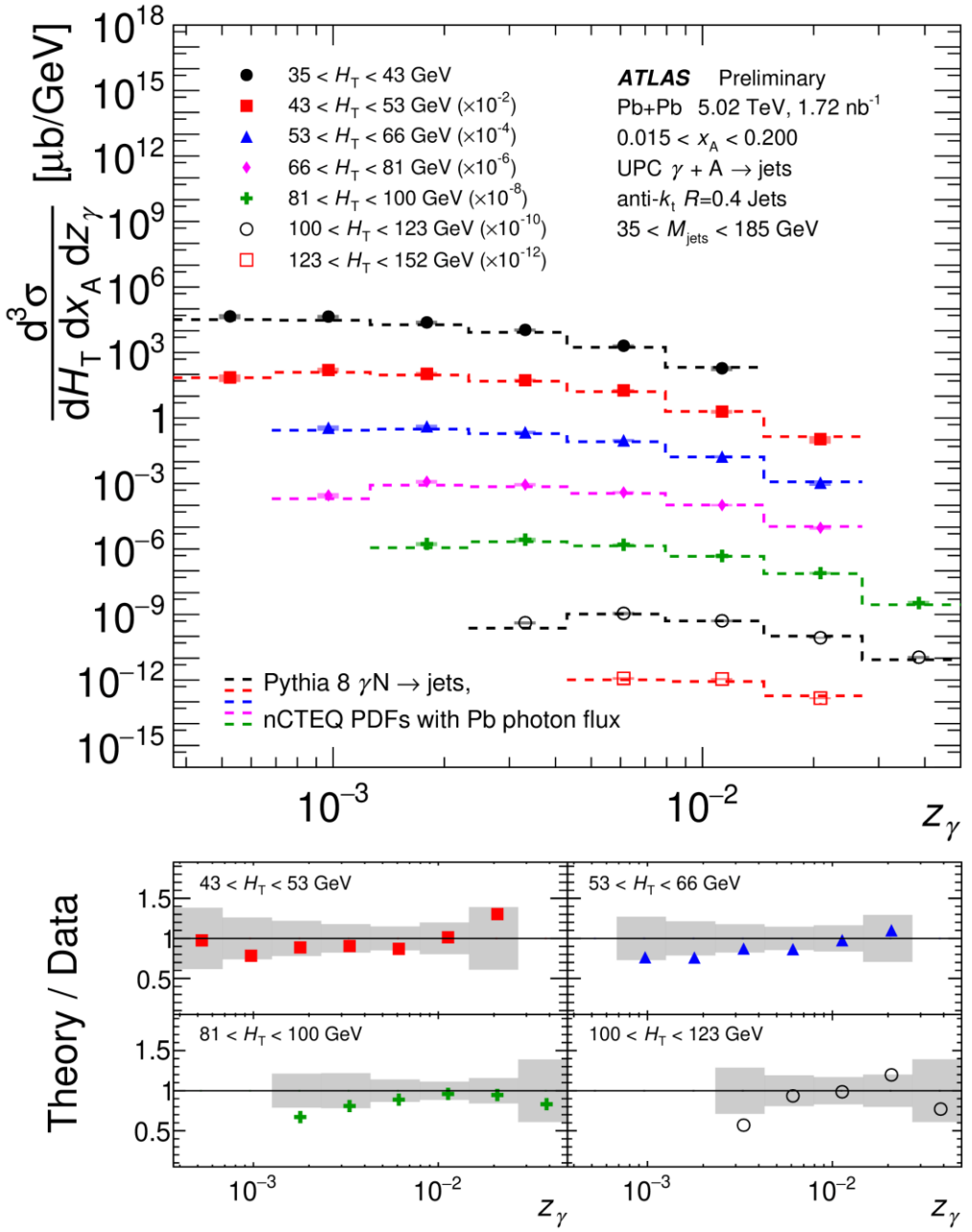

Importance of Forward Neutrons: *0n0n* Events

For the first time, ATLAS has observed dijet production in UPCs without nuclear breakup (0n0n).

Gaps are required on both sides of the detector: $\sum \Delta\eta > 2.0$

A factor of 10 more events are observed in data than are predicted from $\gamma\gamma \rightarrow$ jets, estimated by Pythia or comparison to $\gamma\gamma \rightarrow \mu^+\mu^-$ studies.

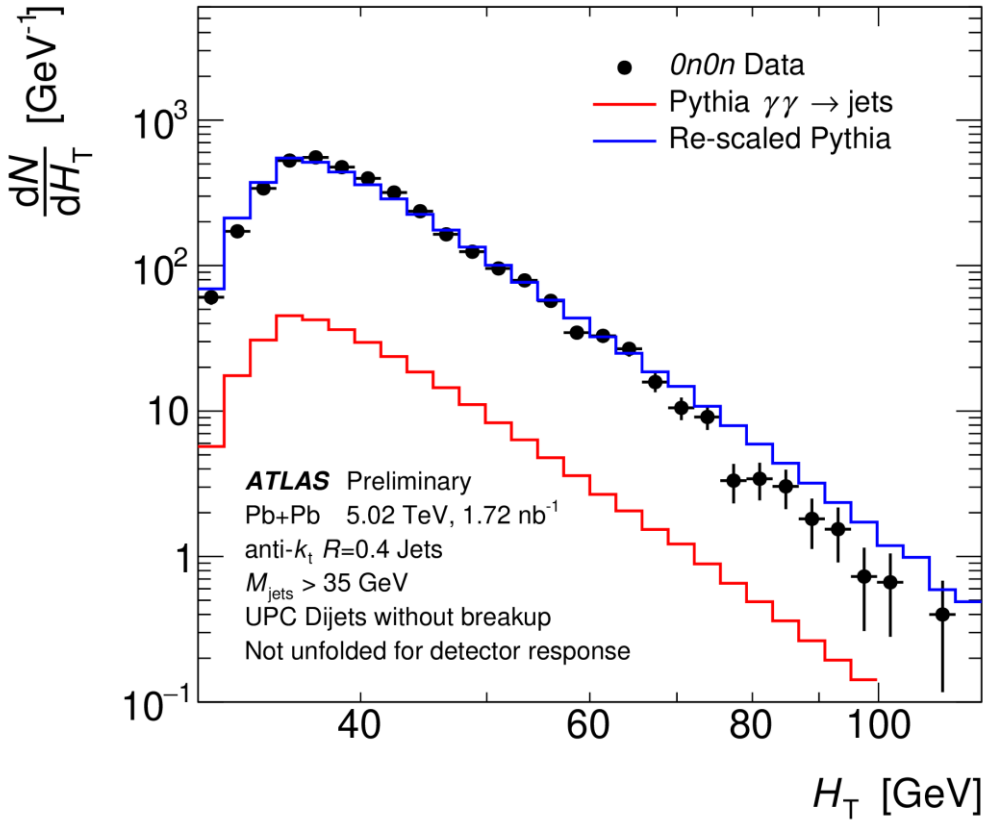

Importance of Forward Neutrons: *0n0n* Events

For the first time, ATLAS has observed dijet production in UPCs without nuclear breakup (0n0n).

Gaps are required on both sides of the detector: $\sum \Delta\eta > 2.0$

A factor of 10 more events are observed in data than are predicted from $\gamma\gamma \rightarrow$ jets, estimated by Pythia or comparison to $\gamma\gamma \rightarrow \mu^+\mu^-$ studies.

The distribution shapes are clearly different from pure $\gamma\gamma \rightarrow$ jets.

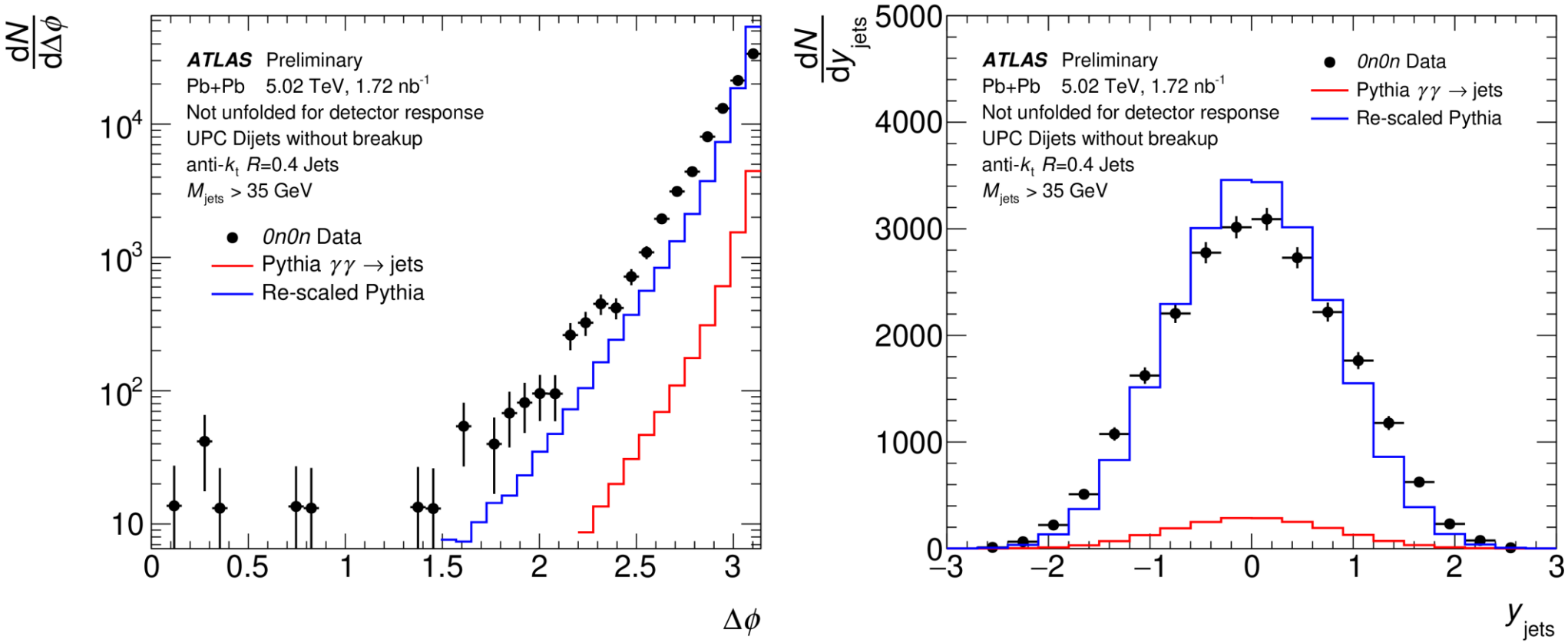

Importance of Forward Neutrons: *0n0n* Events

For the first time, ATLAS has observed dijet production in UPCs without nuclear breakup (0n0n).

Gaps are required on both sides of the detector: $\sum \Delta\eta > 2.0$

A factor of 10 more events are observed in data than are predicted from $\gamma\gamma \rightarrow$ jets, estimated by Pythia or comparison to $\gamma\gamma \rightarrow \mu^+\mu^-$ studies.

The distribution shapes are clearly different from pure $\gamma\gamma \rightarrow$ jets.

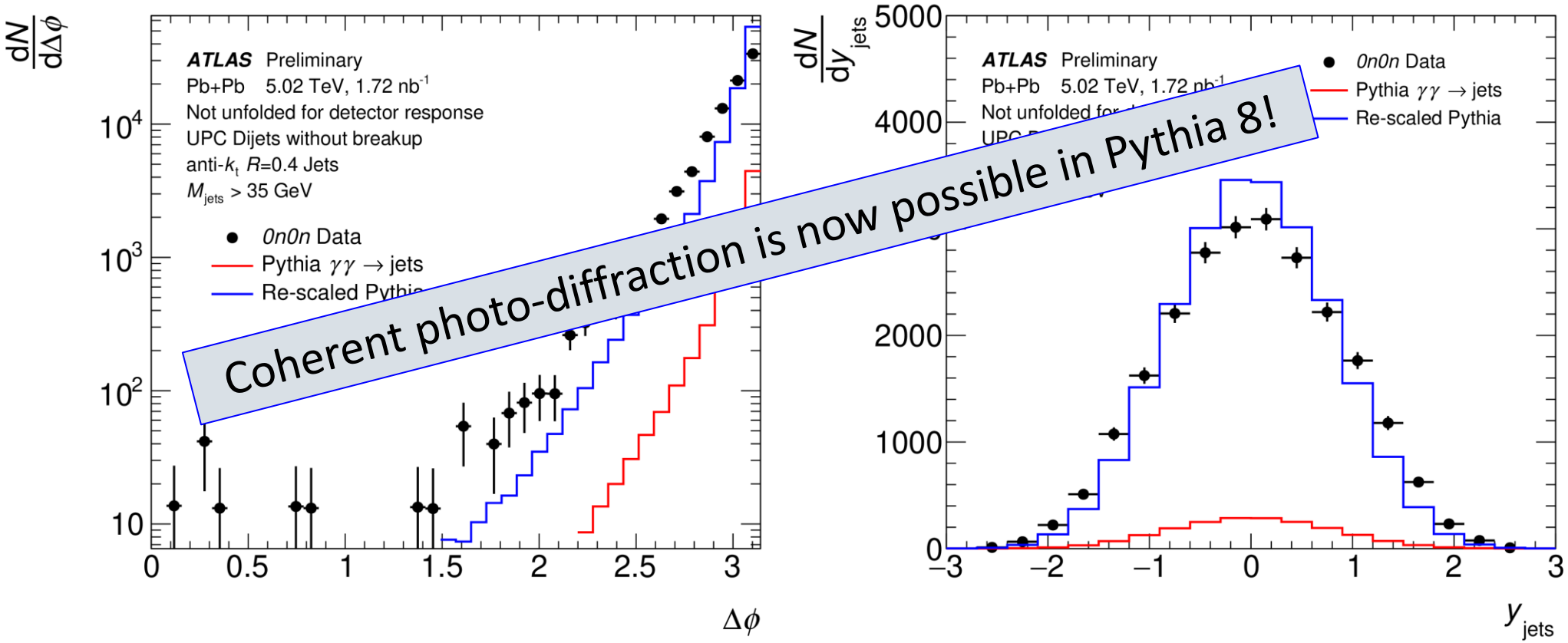

Unfolding Measured Cross-Sections

The measured cross-sections are then unfolded in 3 dimensions to correct for detector effects.

- Low-p_T flavor effects are the largest correction.

$$H_T = \sum_i p_T^i$$

$$x_A = \frac{M_{jets} e^{-y_{jets}}}{\sqrt{s_{NN}}}$$

$$z_\gamma = \frac{M_{jets} e^{+y_{jets}}}{\sqrt{s_{NN}}}$$

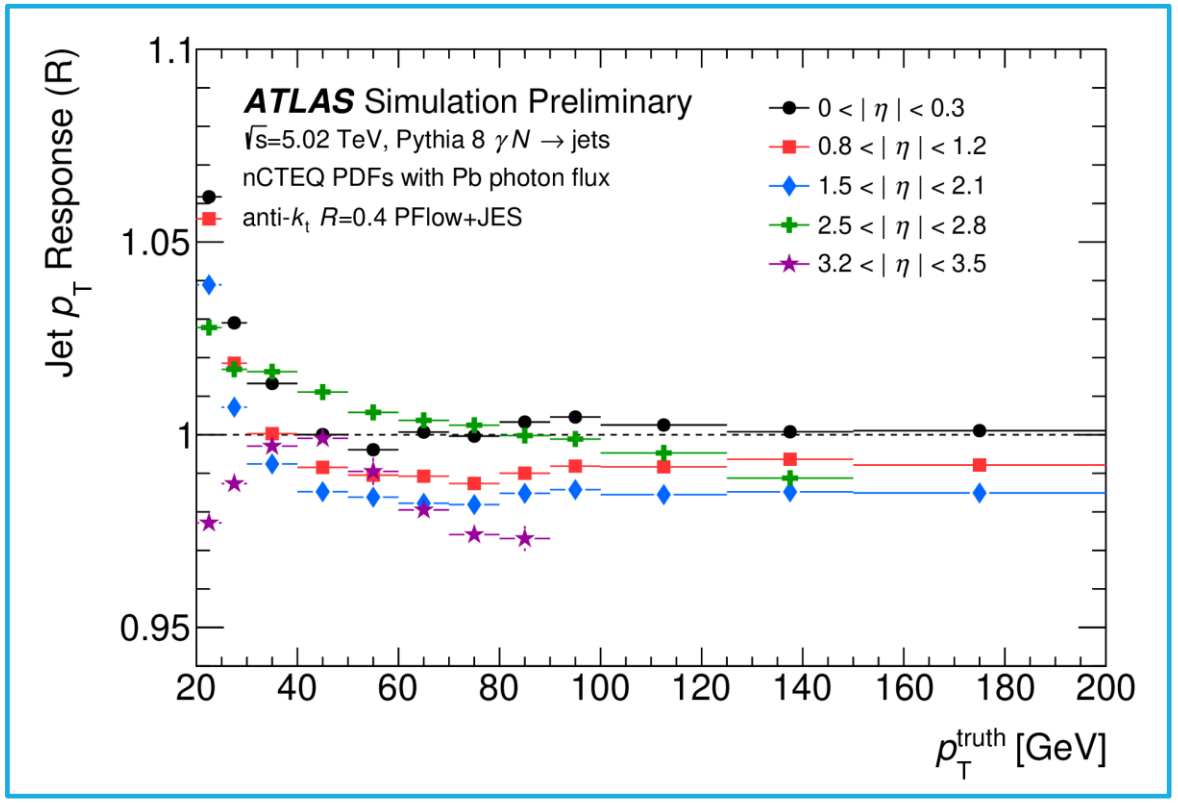

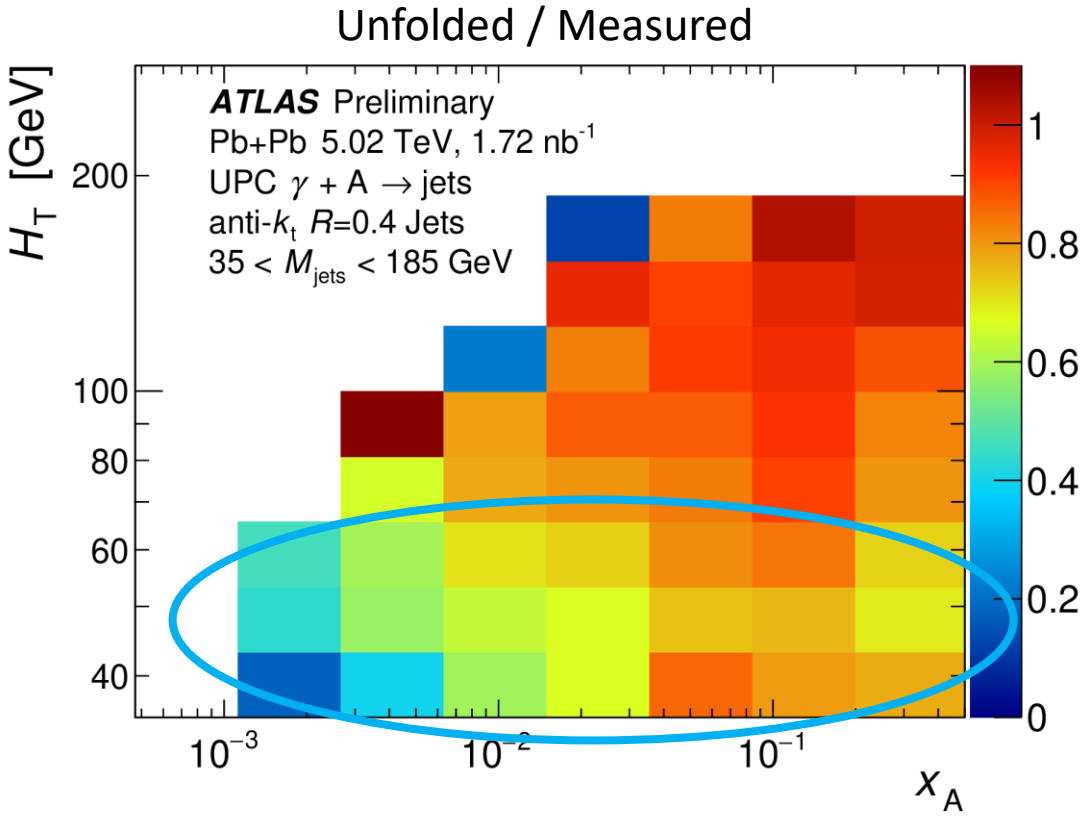

Systematic Uncertainties

Systematic uncertainties are the key limiting factor in our sensitivity to nuclear PDFs.

The jet energy scale and resolution uncertainties are typically 5-10%.

Control over the preliminary low-μ calibration currently provides the dominant source of uncertainty.

Systematic uncertainties are also evaluated on the unfolding and event selections.

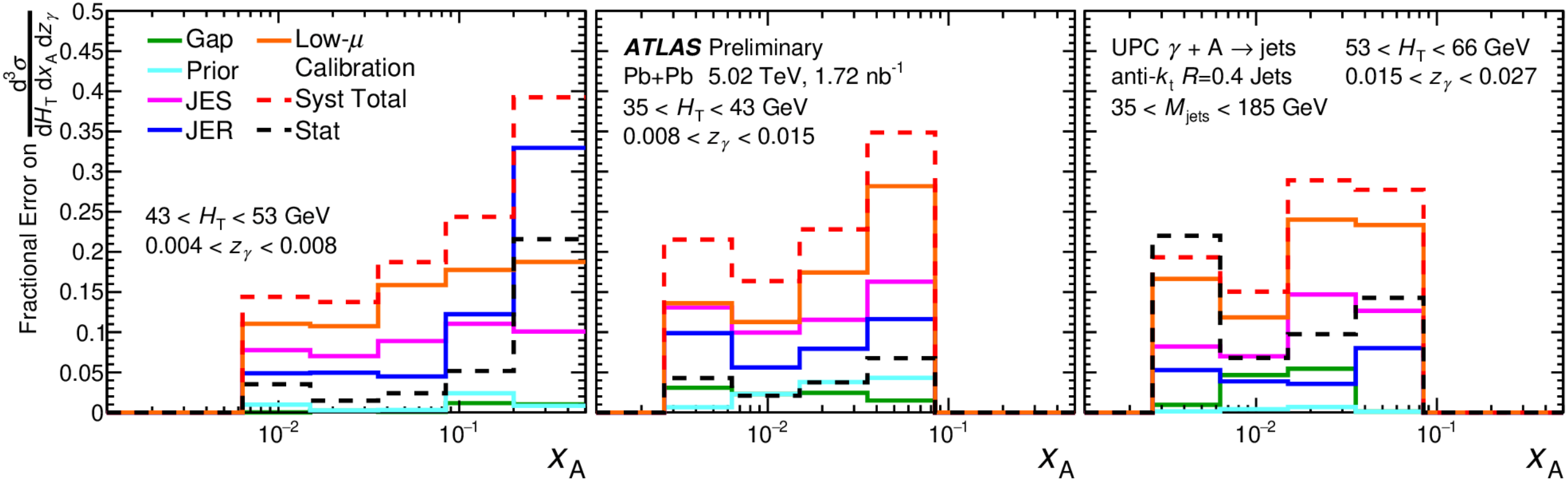

Measured Cross-Sections

- At intermediate photon energies, we can access higher-x partons.

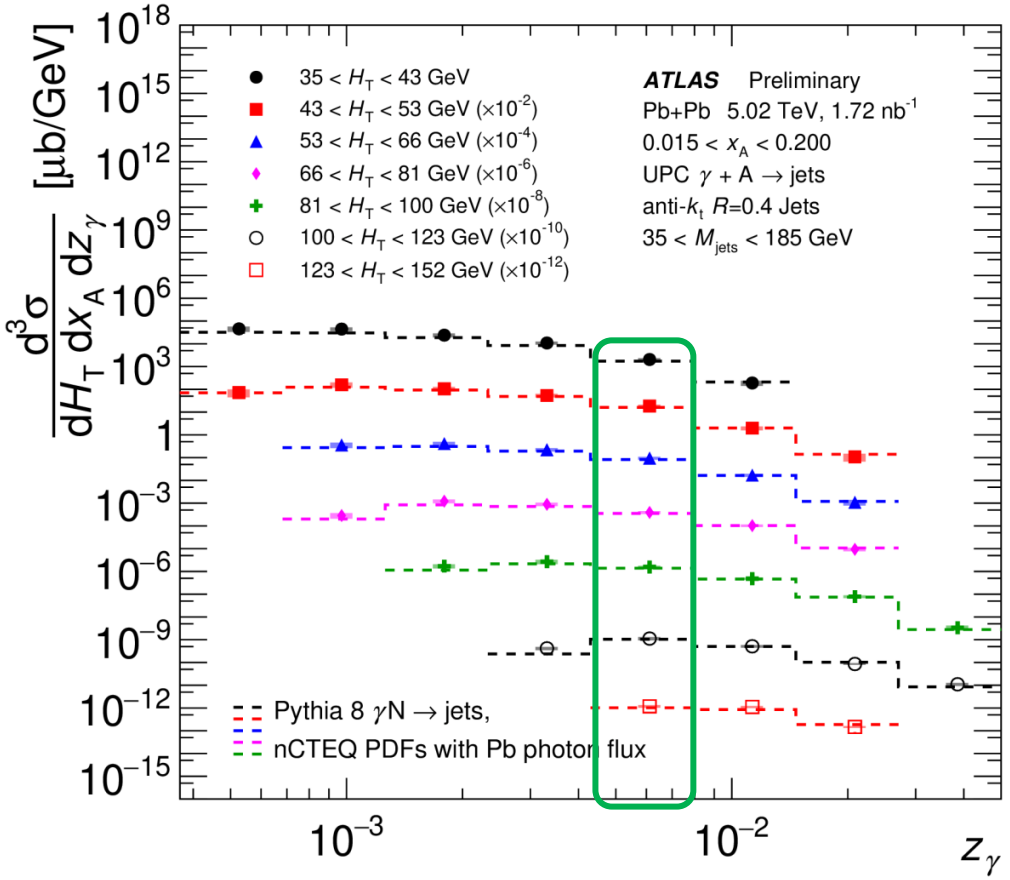

Photon Energy

$0.004 < z_\gamma < 0.008$

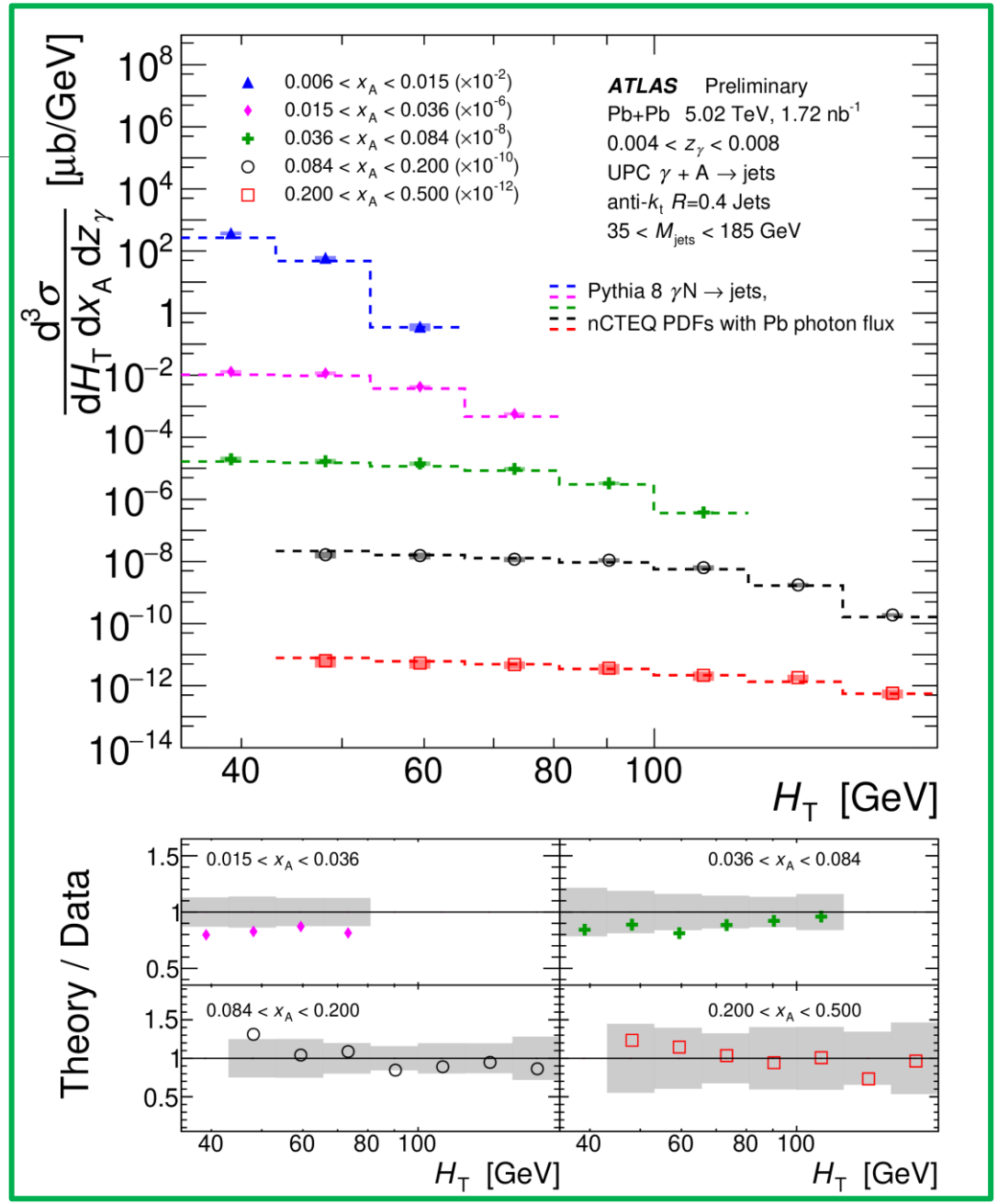

Measured Cross-Sections

- Higher photon energy opens up the low-x shadowing region.
- Results are quite consistent with the theoretical model.

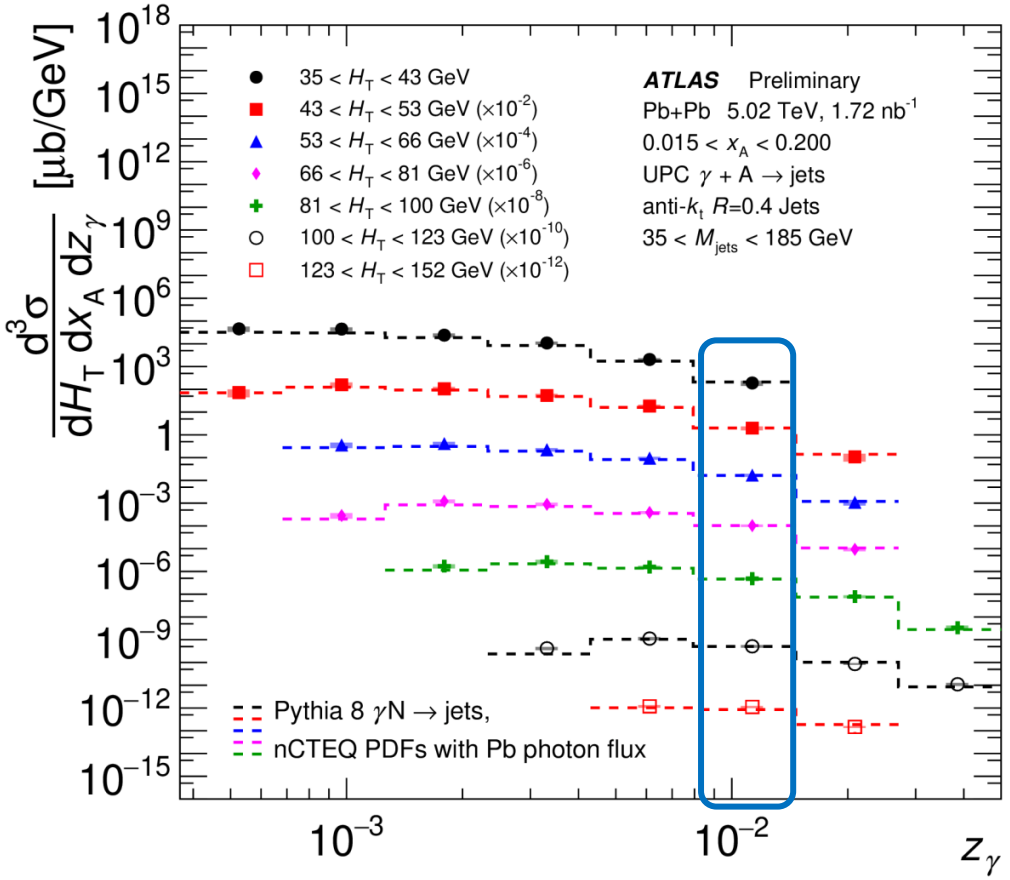

Photon Energy

$0.008 < z_\gamma < 0.015$

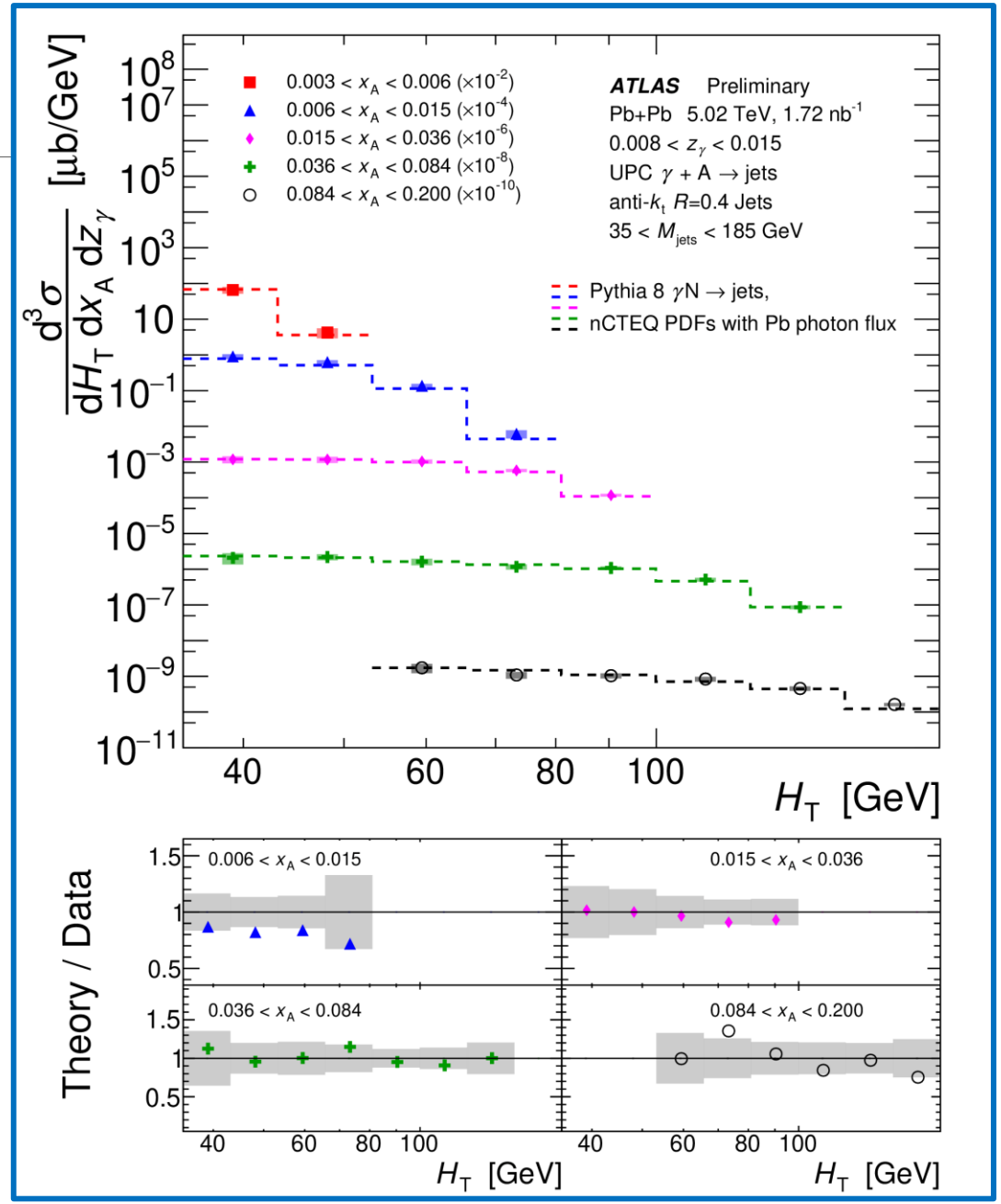

Measured Cross-Sections

- The highest photon energy allows the most access to low x.
- Systematic control is more challenging near acceptance edges.

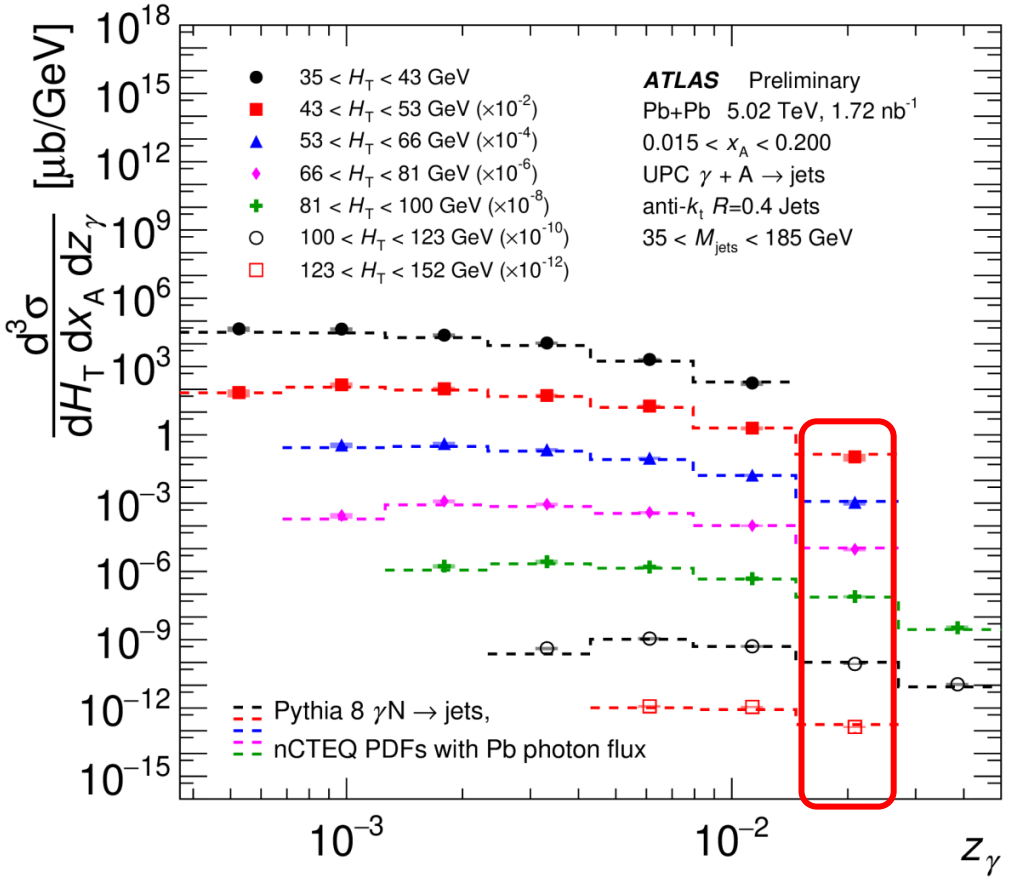

Photon Energy

$0.015 < z_\gamma < 0.027$

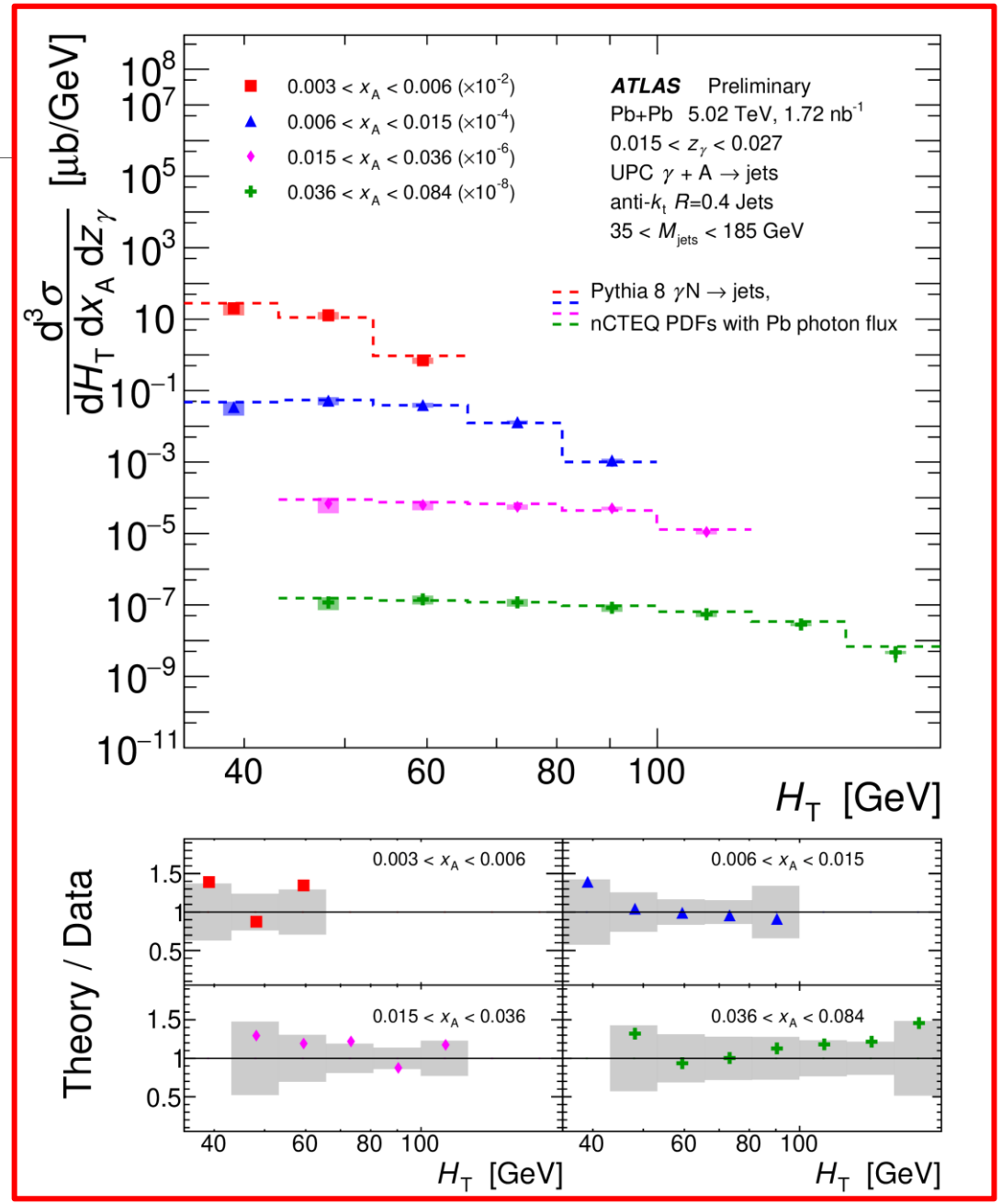

Acceptance and Observables: p+Pb Dijets

$$p_T^{avg} = \frac{p_T^1 + p_T^2}{2} \qquad y^* = \frac{|y_1 - y_2|}{2} \qquad y_b = \frac{y_1 + y_2}{2}$$

$$\Rightarrow \quad x_p = \frac{2p_T^{avg}\cosh(y^*)e^{+y_b}}{\sqrt{s}} \qquad x_{Pb} = \frac{2p_T^{avg}\cosh(y^*)e^{-y_b}}{\sqrt{s}}$$

$$R_{CP}^{\frac{0-10\%}{60-90\%}}(p_T^{avg}, y_b, y^*) = \frac{\frac{1}{< T_{AB}^{0-10\%} >}\frac{1}{N_{evt}^{0-10\%}}\frac{dN_{dijet}^{0-10\%}}{dp_T^{avg}dy_b dy^*}}{\frac{1}{< T_{AB}^{60-90\%} >}\frac{1}{N_{evt}^{60-90\%}}\frac{dN_{dijet}^{60-90\%}}{dp_T^{avg}dy_b dy^*}}$$

Acceptance and Observables: p+Pb Dijets

$$p_T^{avg} = \frac{p_T^1 + p_T^2}{2} \qquad y^* = \frac{|y_1 - y_2|}{2} \qquad y_b = \frac{y_1 + y_2}{2}$$

$$x_p = \frac{2p_T^{avg}\cosh(y^*)e^{+y_b}}{\sqrt{s}} \qquad x_{Pb} = \frac{2p_T^{avg}\cosh(y^*)e^{-y_b}}{\sqrt{s}}$$

$$R_{CP}^{\frac{0-10\%}{60-90\%}}(p_T^{avg}, y_b, y^*) = \frac{\frac{1}{< T_{AB}^{0-10\%} >}\frac{1}{N_{evt}^{0-10\%}}\frac{dN_{dijet}^{0-10\%}}{dp_T^{avg}dy_b dy^*}}{\frac{1}{< T_{AB}^{60-90\%} >}\frac{1}{N_{evt}^{60-90\%}}\frac{dN_{dijet}^{60-90\%}}{dp_T^{avg}dy_b dy^*}}$$

Nuclear overlap function

Computed using Standard Glauber MC techniques to characterize the relationship between event geometry and mean number of participants

Acceptance and Observables: p+Pb Dijets

$$p_T^{avg} = \frac{p_T^1 + p_T^2}{2} \qquad y^* = \frac{|y_1 - y_2|}{2} \qquad y_b = \frac{y_1 + y_2}{2}$$

$$x_p = \frac{2p_T^{avg}\cosh(y^*)e^{+y_b}}{\sqrt{s}} \qquad x_{Pb} = \frac{2p_T^{avg}\cosh(y^*)e^{-y_b}}{\sqrt{s}}$$

$$R_{CP}^{\frac{0-10\%}{60-90\%}}(p_T^{avg}, y_b, y^*) = \frac{\frac{1}{< T_{AB}^{0-10\%} >}\frac{1}{N_{evt}^{0-10\%}}\frac{dN_{dijet}^{0-10\%}}{dp_T^{avg}dy_b dy^*}}{\frac{1}{< T_{AB}^{60-90\%} >}\frac{1}{N_{evt}^{60-90\%}}\frac{dN_{dijet}^{60-90\%}}{dp_T^{avg}dy_b dy^*}}$$

Nuclear overlap function

Computed using Standard Glauber MC techniques to characterize the relationship between event geometry and mean number of participants

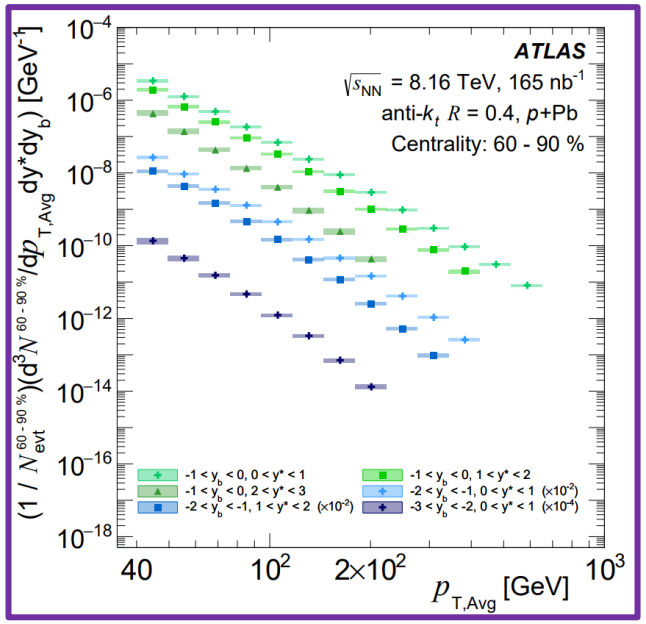

Peripheral dijet yield

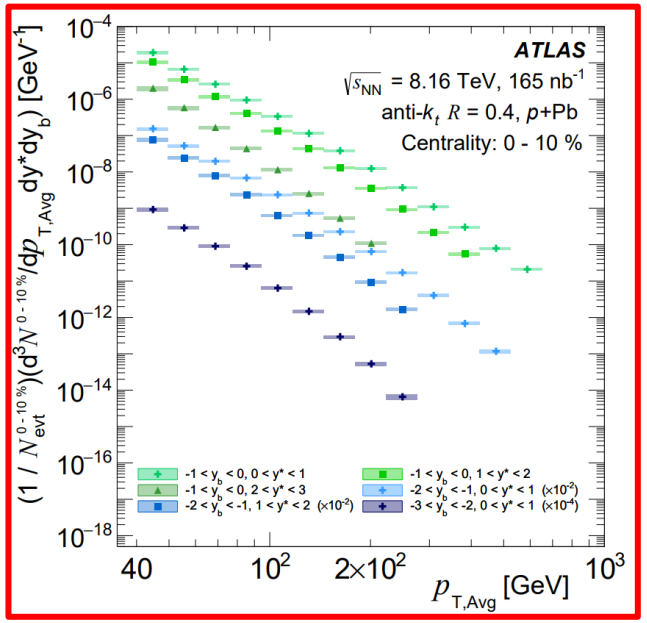

Central dijet yield